Available online at www.sciencedirect.com
ScienceDirect
Coordination Chemistry Reviews 251 (2007) 142–202
COORDINATION CHEMISTRY REVIEWS
www.elsevier.com/locate/ccr

Review

Lanthanides and actinides: Annual survey of their organometallic chemistry covering the year 2005

Jochen Gottfriedsen, Frank T. Edelmann *

Chemisches Institut der Otto-von-Guericke-Universität Magdeburg, D-39106 Magdeburg, Germany

Accepted 6 June 2006
Available online 29 June 2006

Contents

* Corresponding author. Tel.: +49 391 6718327; fax: +49 391 6712933.
E-mail address: frank.edelmann@vst.uni-magdeburg.de (F.T. Edelmann).

0010-8545/$ – see front matter
doi:10.1016/j.ccr.2006.06.011

Abstract

This article give a comprehensive overview of the chemistry of organolanthanide and organoactinide complexes published in the year 2005. Besides synthetic and structural aspects of all new compounds, the review also covers applications of organolanthanide and -actinide complexes in homogeneous catalysis, organic synthesis, and materials science.

Keywords: Lanthanides; Actinides; Cyclopentadienyl complexes; Cyclooctatetraenyl complexes; Organometallic chemistry

1. Introduction

This review summarizes the progress in organo-*f*-element chemistry during the year 2005. The year 2005 has witnessed a remarkable increase in research activities in this area.

2. Lanthanides

2.1. Lanthanide carbonyls

The electronic and geometric structure of scandium monocarbonyl ScCO has been investigated through coupled cluster (CC) and multireference variational methods (MRCI) combined with large basis sets. The bonding in this simple molecule is rather complicated and could be attributed mainly to π-conjugation effects between the Sc and CO π-electrons, along with weak σ-charge transfer from CO to the Sc atom [1]. Matrix-isolated $Sc_2[\eta^2(\mu_2\text{-CO})]$ molecules have been produced by co-deposition of laser-ablated Sc atoms with CO in excess argon at 7 K and investigated using FT-IR spectroscopy. It was shown that $Sc_2[\eta^2(\mu_2\text{-CO})]$ is an unprecedented homoleptic dinuclear metal carbonyl with an asymmetrically bridging and *side-on*-bonded CO. There is evidence that it is an intermediate to CO dissociation [2].

2.2. Lanthanide hydrocarbyls

2.2.1. Neutral homoleptic compounds

Ab initio and DFT calculations have been performed on a series of simple organometallic compounds of the formula MCH_n with $n = 1–3$. The main electronic characteristics of methylidynes, methylidenes, and methyl-metals have been described for first-row early transition metals, including the scandium species ScCH, $ScCH_2$, and $ScCH_3$. $ScCH_2$ exhibits a bent structure and therefore constitutes a candidate to present α-agostic bonds [3]. A major achievement in organolanthanide chemistry reported in 2005 was the synthesis of the elusive homoleptic alkyls trimethylyttrium and trimethyllutetium. The synthetic strategy employed involves donor-induced cleavage of the corresponding homoleptic lanthanide tetramethylaluminates as illustrated in Scheme 1. The elimination of trimethylaluminum could be achieved with the Lewis base donors THF or diethyl ether. Polymeric $[YMe_3]_n$ and $[LuMe_3]_n$ were isolated as white powders which are insoluble in aliphatic and aromatic solvents. The lutetium derivative detonates spontaneously when exposed to air. Preliminary investigations into the reaction behavior of $[LnMe_3]_n$ were performed using the yttrium derivative and are summarized in Scheme 1 [4].

Reaction of *o*-$Me_2NC_6H_4CH_2K$ with YCl_3 in THF yielded $(o\text{-}Me_2NC_6H_4CH_2)_3Y$ in the form of light yellow crystalline plates in 59% yield (Scheme 2, Ln = Y). The crystal structure shows three bidentate benzyl ligands bound to Y, which has a prismatic coordination sphere. The La analogue was prepared similarly (41% yield, Scheme 2, Ln = La) and is isostructural to the yttrium derivative, but shows more extensive multihapto bonding of the benzyl ligands to the larger metal atom (short aryl–La interactions) [5].

2.2.2. Heteroleptic compounds

Cationic yttrium methyl complexes have been prepared by protonation of formally trianionic precursors as illustrated in Scheme 3. The crystal structure of $[YMe_2(THF)_5][BPh_4]$ has been determined by X-ray diffraction. Fig. 1 shows the pentagonal-bipyramidally coordinated yttrium center with the methyl groups in the *trans*-positions [6].

A family of scandium and yttrium tris[(trimethylsilyl)methyl] complexes with neutral N_3 donor ligands has been reported. The synthetic routes are summarized in Scheme 4. Representatives of all three types of trialkyls have been structurally characterized by X-ray diffraction. As an example, the molecular structure of $[HC(Me_2pz)_3]Sc(CH_2SiMe_3)_3$ is shown in Fig. 2 [7].

X-ray crystallography and variable-temperature (VT) NMR spectroscopy revealed a structural diversity within the known series of neutral 12-crown-4 supported tris(trimethylsilylmethyl) complexes (12-crown-4)$Ln(CH_2SiMe_3)_3$ (Ln = Sc, Y, Sm, Gd–Lu) in the solid-state as well as in solution. VT NMR spectroscopy indicates fluxional 12-crown-4 coordination on the NMR time scale. The X-ray crystal structure determination of (12-crown-4)$Sc(CH_2SiMe_3)_3$ revealed incomplete 12-crown-4 coordination (Fig. 3). The molecule adopts a three-legged "piano-stool" geometry with the 12-crown-4 ligand bonded facially through only three oxygen atoms. Thus the coordination geometry around Sc is best described as distorted octahedral [8].

The neutral precursors of the type (12-crown-4)$Ln(CH_2SiMe_3)_3$ and $Ln(CH_2SiMe_3)_3(THF)_n$ ($n = 2,3$; Ln = Sc, Y, Lu) have been utilized in the preparation of a series of mono- and di-cationic trimethylsilylmethyl lanthanide complexes sup-

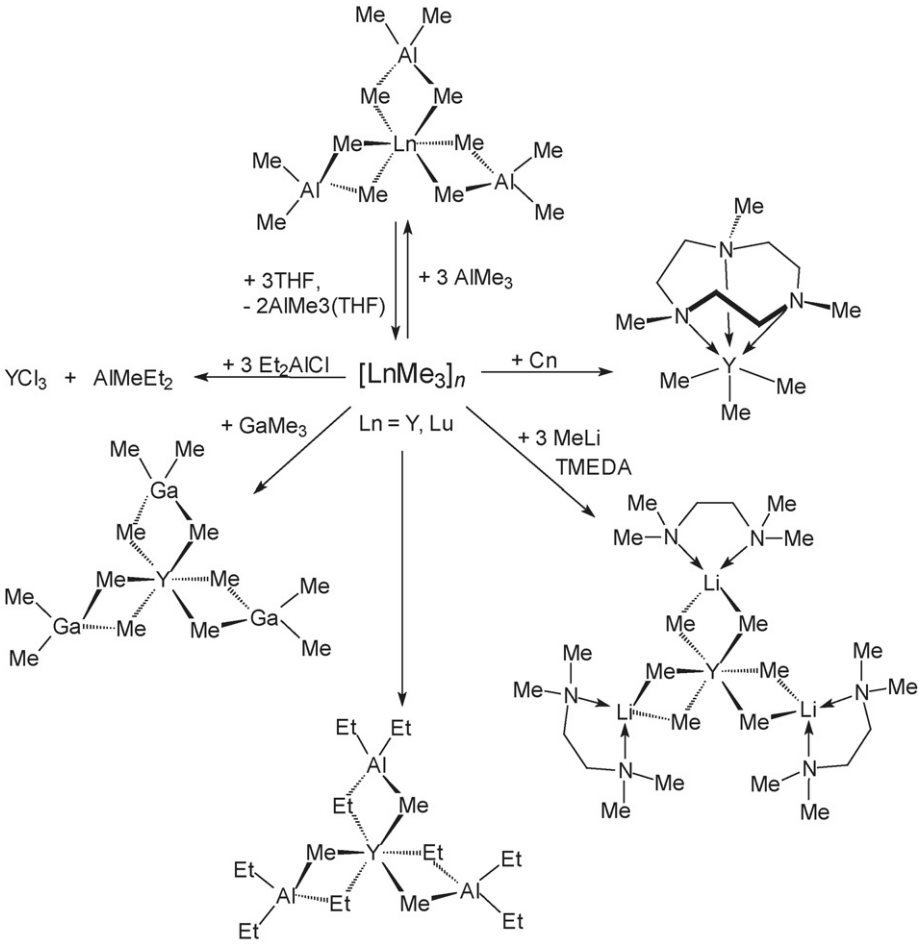

Scheme 1. (Cn = 1,4,7-trimethyl-1,4,7-triazacyclononane).

ported by THF and 12-crown-4 ligands as solvent-separated ion pairs with $[BPh_4]^-$, $[BPh_3(CH_2SiMe_3)]^-$, $[B(C_6F_5)_4]^-$, $[B(C_6F_5)_3(CH_2SiMe_3)]^-$, and $[Al(CH_2SiMe_3)_4]^-$ anions. X-ray crystallography of only the second structurally characterized dicationic rare-earth metal alkyl complex, $[Y(CH_2SiMe_3)(12\text{-crown-4})(THF)_3]^{2+}[BPh_4]^-{}_2$ showed exocyclic 12-crown-4 coordination at the 8-coordinate metal center with well separated counteranions (Fig. 4) [8].

Attempted synthesis of sterically demanding bis- or tris-β-diketiminato complexes of lanthanides resulted in ligand deprotonation and formation of complexes containing both a "normal" and a deprotonated ligand. As an example, a thulium derivative is shown in Scheme 5 [9].

A rare family of base-free organoscandium alkyl cations stabilized by β-diketiminato ligands (Ar)NC(R)CHC(R)NAr (Ar = 2,6-$Pr^iC_6H_3$; R = Me (L^{Me}), R = Bu^t (L^{Bu^t}) has been prepared by reaction of $LScR_2$ with the perfluorinated boranes $B(C_6F_5)_3$ and $(C_{12}F_8)B(C_6F_5)$. While the L^{Me} ancillary lig-

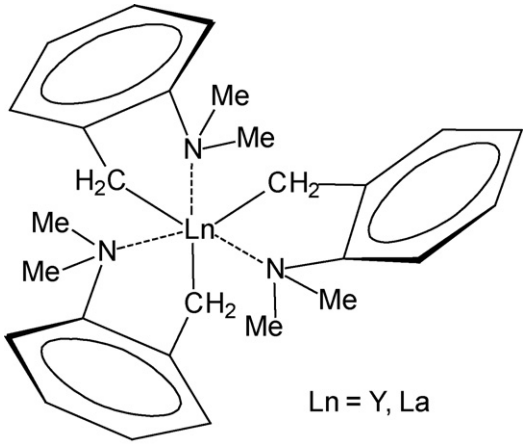

Scheme 2.

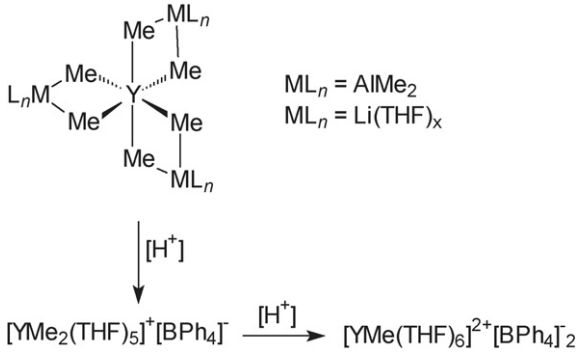

Scheme 3.

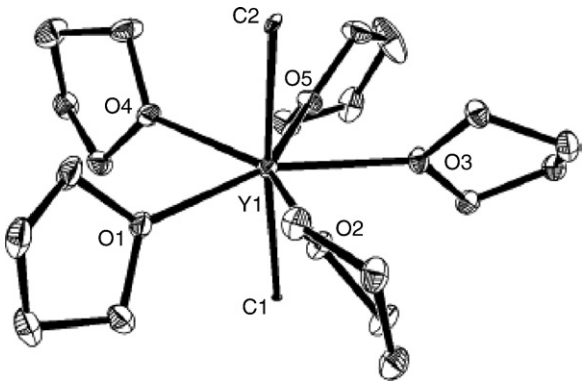

Fig. 1. Molecular structure of the cation in $[YMe_2(THF)_5][BPh_4]$ [6].

and lacked sufficient steric bulk to prevent C_6F_5 transfer to the metal center, the L^{Bu^t}-derivatives were found to be quite robust in solution. Fig. 5 depicts the molecular structure of the contact ion pair *endo*-$[L^{Me}Sc(C_6F_5)]^+[MeB(C_6F_5)_3]^-$ containing a bridging methyl group and a pentafluorophenyl unit transferred onto the scandium center [10]. Related chemistry has also been reported for samarium [11].

Various other nitrogen- and/or oxygen-coordinated polydentate ancillary ligands have been employed to stabilize heteroleptic lanthanide alkyls and aryls. For example, the two methyl complexes with Ln = Er, Yb shown in Scheme 6 have been prepared in moderate yields from the corresponding chloro precursors and methyllithium at low temperature. The crystal and molecular structure of the ytterbium derivative has been elucidated by X-ray diffraction, verifying its monomeric structure with and Yb–C distance of 2.441(4) Å (Fig. 6) [12].

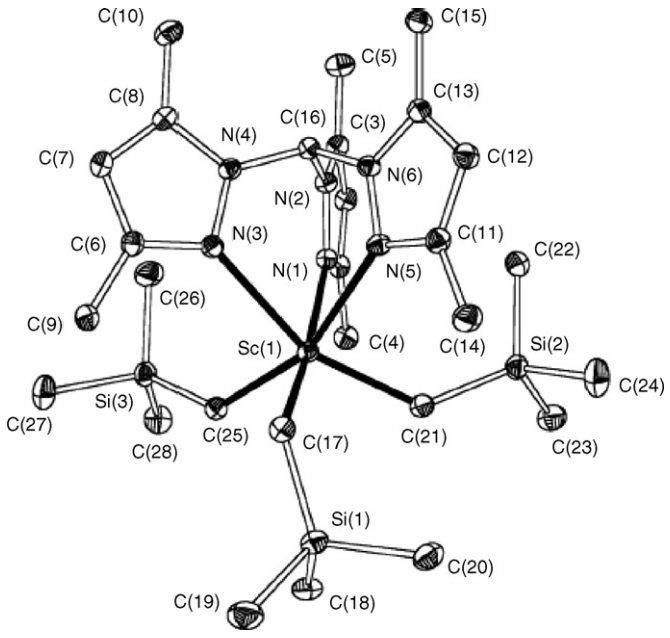

Fig. 2. Molecular structure of $[HC(Me_2pz)_3]Sc(CH_2SiMe_3)_3$ [7].

Other ligand systems which have been utilized to stabilize alkyl and aryl lanthanide complexes include diamidoamine, biphenolate and binaphtholate ligands. A typical example of a diamidoamine complex containing an additional chelating σ-aryl ligand is shown in Scheme 7. This compound is accessible by treatment of the homoleptic yttrium aryl complex $Y(o\text{-}C_6H_4NMe_2)_3$ with the free triamine under arene elimination [13].

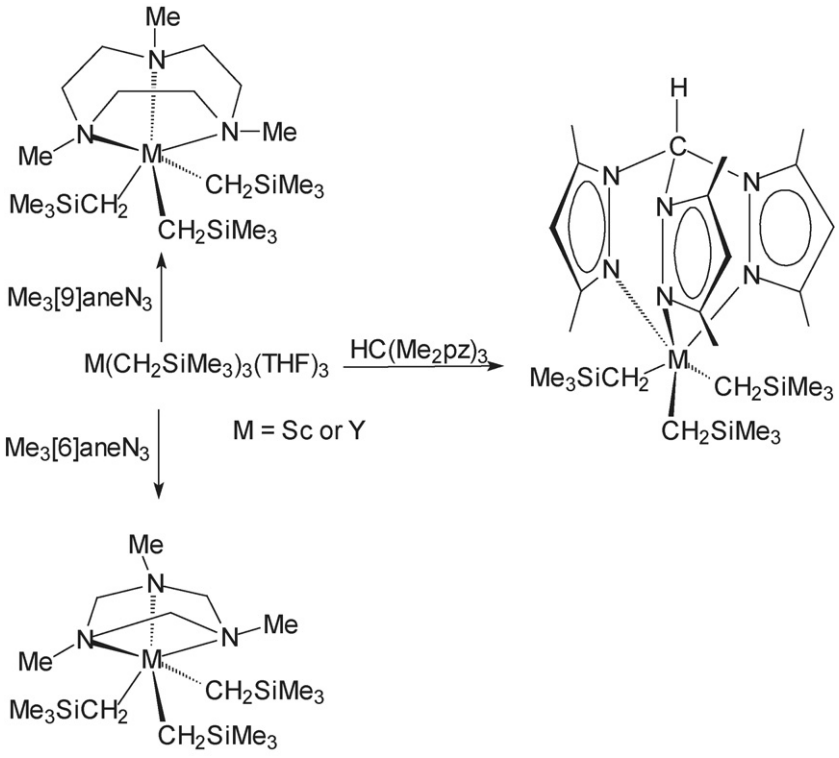

Scheme 4.

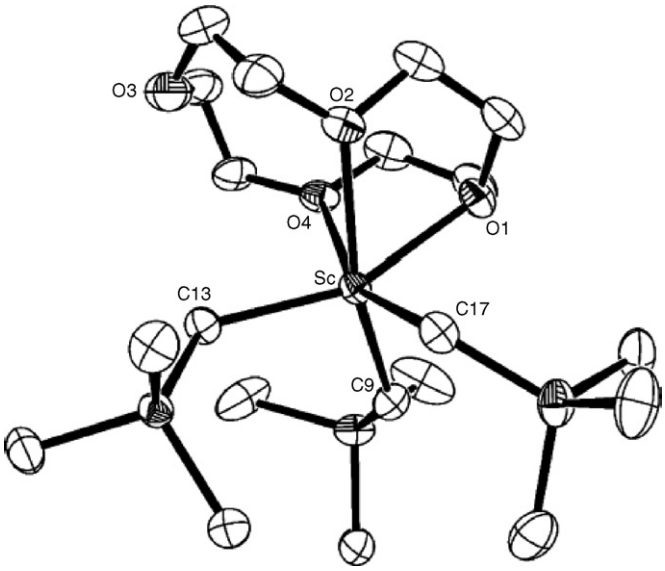

Fig. 3. Molecular structure of (12-crown-4)Sc(CH_2SiMe_3)$_3$ [8].

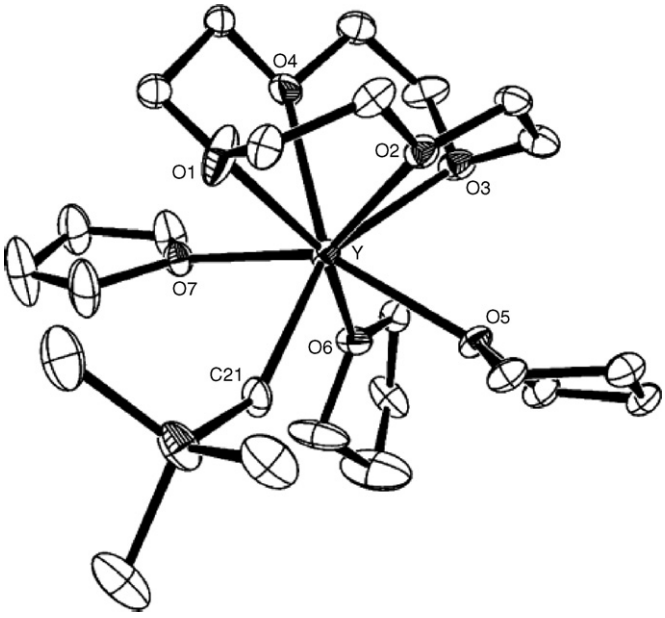

Fig. 4. Molecular structure of the dication in [Y(CH_2SiMe_3)(12-crown-4)(THF)$_3$]$^{2+}$[BPh_4]$^-{}_2$ [8].

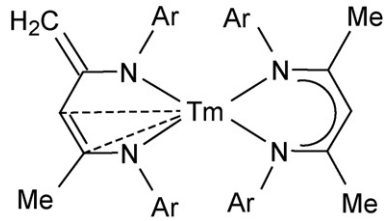

Scheme 5. (Ar = 2,6-$Pr_2^iC_6H_3$).

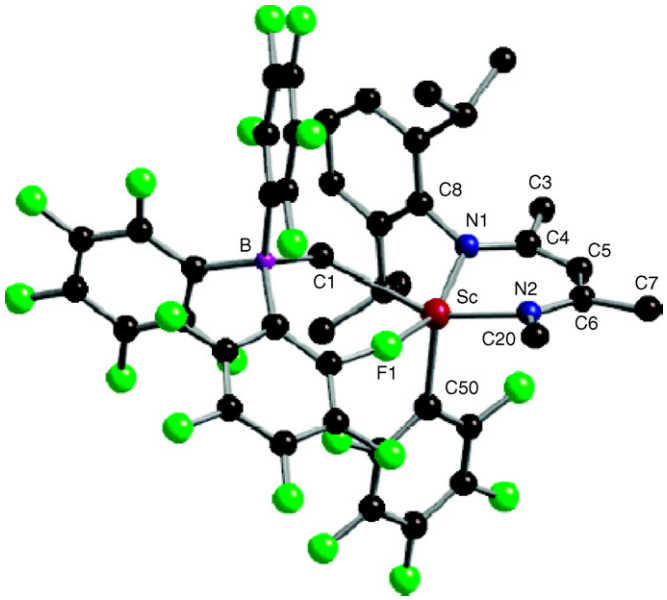

Fig. 5. Molecular structure of *endo*-[L^{Me}Sc(C_6F_5)]$^+$[MeB(C_6F_5)$_3$]$^-$ [10].

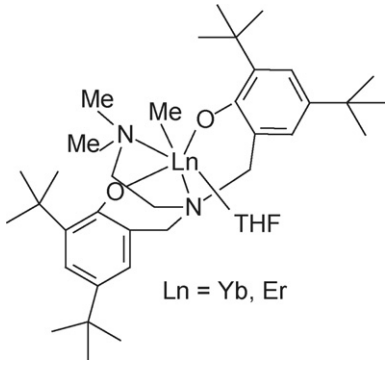

Scheme 6.

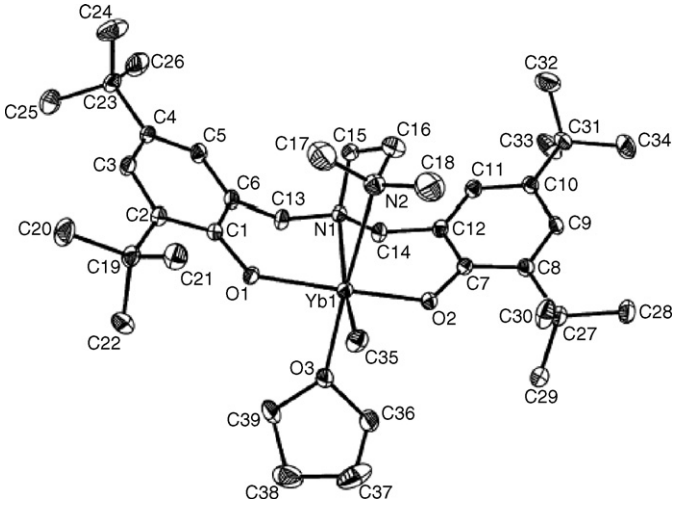

Fig. 6. Molecular structure of [$Me_2NCH_2CH_2N${CH_2(2-$OC_6H_2Bu^t_2$-3,5)}$_2$]-YbMe(THF) [12].

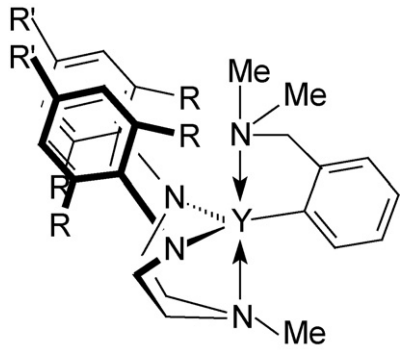

Scheme 7.

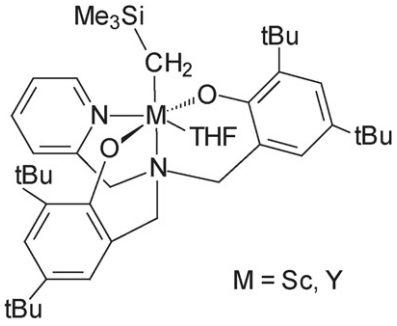

Scheme 8.

Yet another ligand systems which has been reported to afford stable mono(alkyl) lanthanide complexes involves diamino-bis(phenolate) ligands. The compounds shown in Scheme 8 have been isolated and characterized by spectroscopic methods and elemental analyses [14].

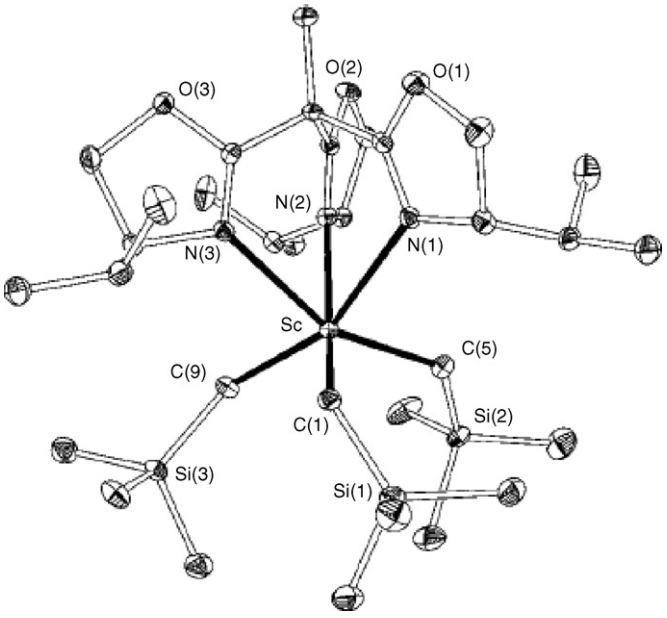

Fig. 7. Molecular structure of (^{i}Pr-trisox)Sc(CH_2SiMe_2)$_3$ [15].

Neutral, mono- and di-cationic scandium alkyls have been synthesized using a tridentate trisoxazoline ligand system. The trialkyl complex (^{i}Pr-trisox)Sc(CH_2SiMe_2)$_3$ was prepared by the reaction of the trialkyl precursor Sc(CH_2SiMe_3)$_3$(THF)$_2$ with an equimolar amount of ^{i}Pr-trisox according to Scheme 9. Fig. 7 shows the molecular structure of (^{i}Pr-trisox)Sc(CH_2SiMe_2)$_3$. By successive addition of 1 or 2 equiv. of [Ph_3C][$B(C_6F_5)_4$] the corresponding mono- and di-cationic species could be generated (Scheme 9) [15].

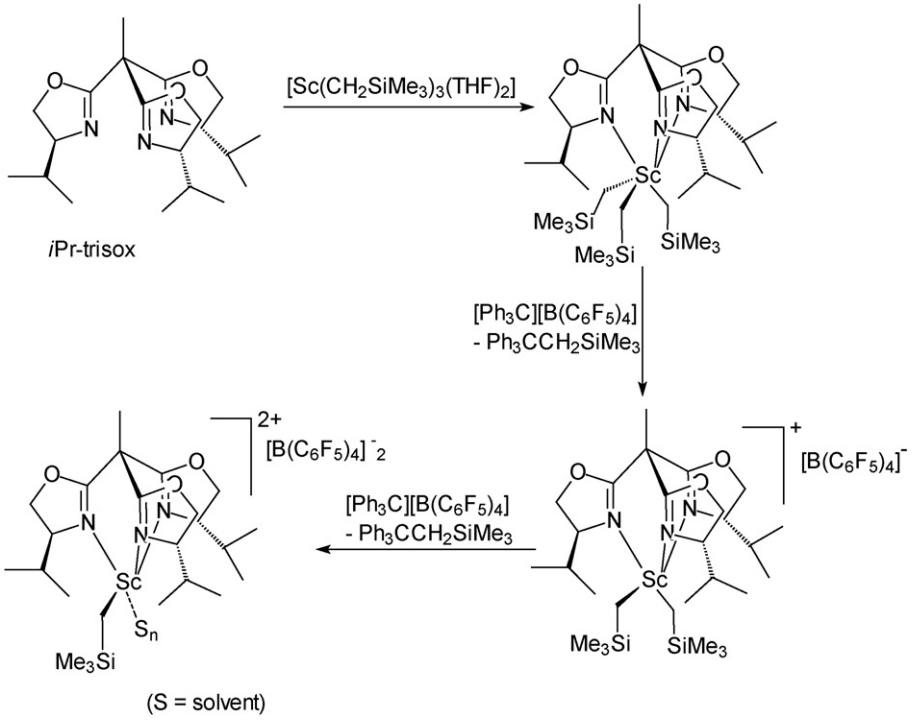

Scheme 9.

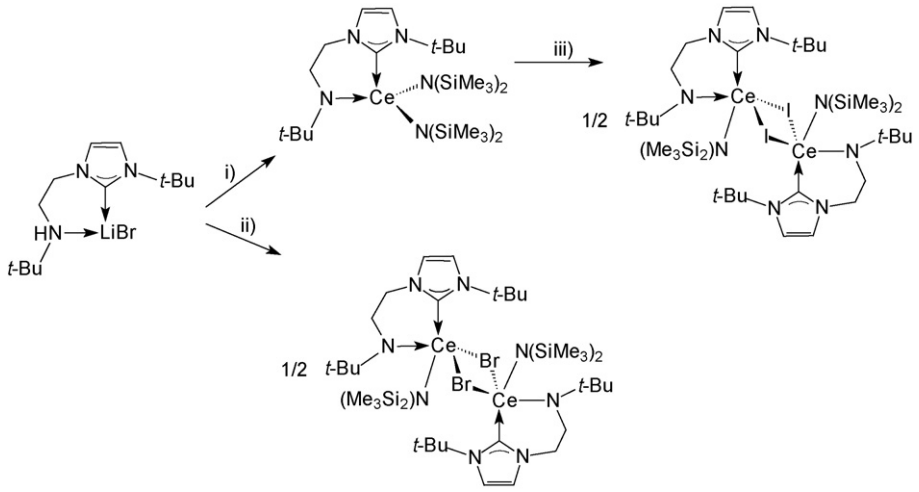

Scheme 10. (i) $Ce[N(SiMe_3)_2]_3$, toluene, –LiBr, $–HN(SiMe_3)_2$; (ii) $Ce[N(SiMe_3)_2]_3$, toluene, $–LiN(SiMe_3)_2$, $–HN(SiMe_3)_2$; (iii) LiI, 80 °C, $–LiN(SiMe_3)_2$.

Cerium(III) complexes containing an amido-tethered *N*-heterocyclic carbene ligand have been synthesized according to Scheme 10. All three products have been structurally characterized by X-ray diffraction. Figs. 8 and 9 depict the molecular structures of the bromo-bridged dimer and the bis(silylamide) derivative, respectively [16].

A regiospecific functionalization of the pendant-arm heterocyclic carbene ligand has been observed upon treatment of the neodymium complex $LNd[N(SiMe_3)_2]_2$ with trimethylsilyl iodide. In the course of this reaction a trimethylsilyl group is introduced at the C4-carbene ring position to afford the silylated complex $[L'Nd\{N(SiMe_3)_2\}(\mu\text{-}I)]_2$ ($L' = Bu^tC_3H(SiMe_3)N_2CH_2CH_2NBu^t$). An attempted reduction of this compound with potassium graphite led to formation of $L'Nd[N(SiMe_3)_2]_2$ (Scheme 11) [17].

Cerium–carbon bonds are involved in two novel cerium(III) complexes containing the C_1-symmetric bis(silyl)methyl ligand $[CH(SiMe_3)\{SiMe(OMe)_2\}]^-$ [18]. Weak Ln···C interactions have been detected in several lanthanide complexes containing bulky bis(phosphinimino)methanide ligands, which otherwise should not be considered *organo* lanthanide complexes in the strict sense [19,20].

2.3. Lanthanide alkenyl and alkynyl compounds

The nature of the chemical bonding in the 1:1 complexes formed by the first-row transition metals and C_2H_2, including $Sc(C_2H_2)$, has been investigated using an electron localization function (ELF) topological approach. The cyclic structure of $Sc(C_2H_2)$ possesses two covalent Sc–C bonds [21]. A theoretical study of the ScC_n, ScC_n^+, and ScC_n^- ($n = 1$–8) open-chain clusters has been carried out. Predictions for their electronic energies, rotational constants, dipole moments and vibrational frequencies have been made using the B3LYP method with different basis sets including effective core potentials, ECPs. For

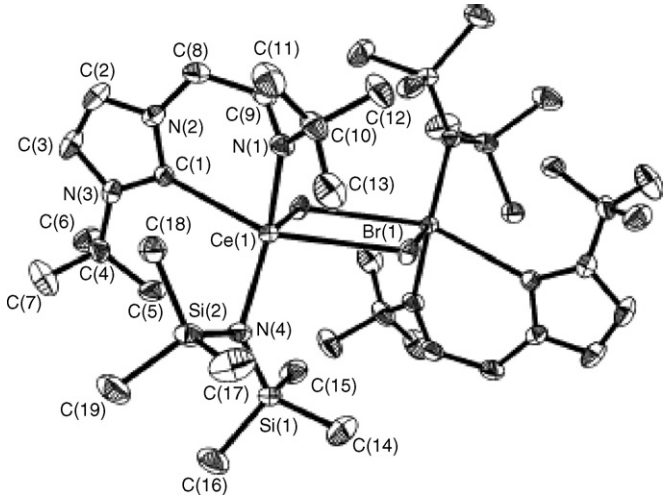

Fig. 8. Molecular structure of $[LCe(\mu\text{-}Br)\{N(SiMe_3)_2\}]_2$ ($L = Bu^tC_3H_2N_2CH_2CH_2NBu^t$) [16].

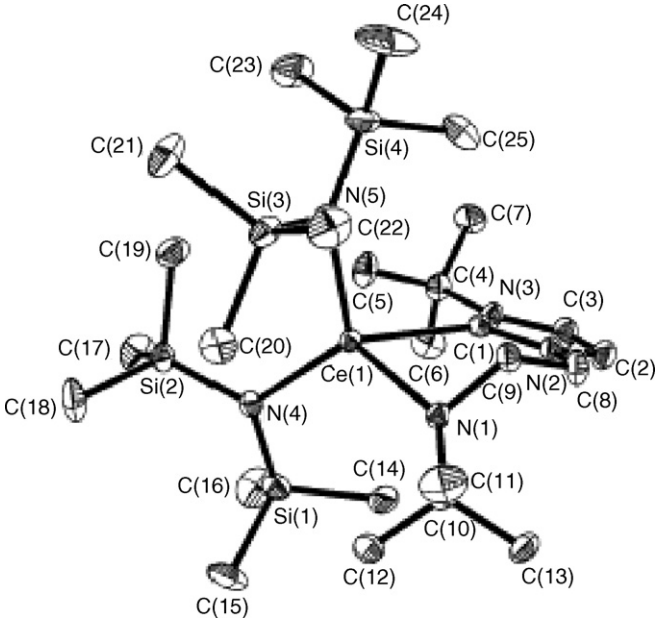

Fig. 9. Molecular structure of $LCe[N(SiMe_3)_2]_2$ ($L = Bu^tC_3H_2N_2CH_2CH_2NBu^t$) [16].

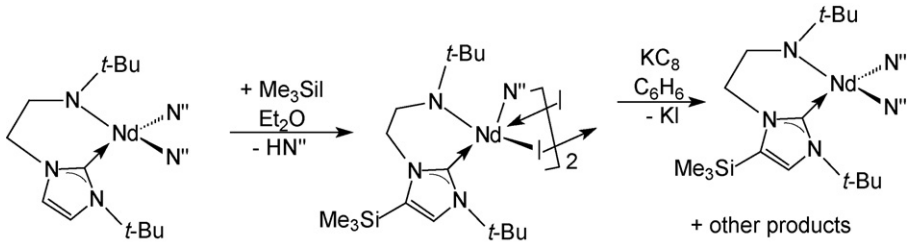

Scheme 11. ($N'' = N(SiMe_3)_2$).

the ScC_n open-chain clusters the lowest-lying states correspond to quartet states for *n*-odd members, whereas for *n*-even species the ground state is found to be a doublet. In the cationic and anionic species, the electronic ground state is found to be a singlet for even *n* and a triplet for odd *n*. An even-odd parity effect (*n*-even clusters being more stable than *n*-odd ones) was observed in neutral and charged clusters [22].

2.4. Lanthanide allyls

The divalent lanthanide allyl complexes $[1,3\text{-}(Me_3Si)_2C_3H_3]_2Ln(THF)_2$ (Ln = Sm, Eu, Yb) can be readily prepared from the bis(triflate) precursors (Scheme 12). The corresponding lanthanide diiodides can be used as well, and no difference was found when either precursor was used. If Yb(III) or Eu(III) triflate is treated with $K[1,3\text{-}(Me_3Si)_2C_3H_3]$(=K[A′]), reduction to the lanthanide(III) product is observed, but the yield of the allyl complex is reduced (<50%) [23].

All three lanthanide(II) allyls have been crystallographically characterized. Fig. 10 shows the europium derivative as a typical example. The monomeric complex comprises *trihapto* allyl ligands and *cis*-ligated THF molecules. The two allyl ligands are in *anti*-configuration and the angle between the C_3 planes is 118.3° [23].

In the same manner neutral tris(allyl)lanthanide complexes containing the 1,3-bis(trimethylsilyl)allyl ligand have been prepared according to Scheme 13. The crystal and molecular structures of all three representatives have been determined by X-ray diffraction. The molecules contain three *trihapto* allyl ligands and a single THF ligand [23].

Reactions of $LnCl_3(THF)_n$ (Ln = La, *n* = 4; Ln = Y, Sm, Nd, *n* = 3) with 3 equiv. of allylMgCl in THF/1,4-dioxane followed by crystallization from 1,4-dioxane/toluene was reported to proceed in very high yields to give the tris(η^3-allyl) complexes (μ-dioxane)[La(η^3-C_3H_5)$_3$(κ^1-dioxane)]$_2$ and [Ln(η^3-C_3H_5)$_3$(μ-dioxane)]$_\infty$ (Ln = Y, Sm, Nd) (Scheme 14). Improved one-pot syntheses for the tris(η^3-allyl) lanthanum and neodymium compounds have also been reported in this contribution. The crystal structures of the polymeric yttrium and samarium derivatives showed that the compounds consist of distorted square-pyramidal lanthanide centers in linear polymer chains as illustrated in Figs. 11 and 12. The latter shows a crystal structure packing diagram of the linear polymeric chains of [Y(η^3-C_3H_5)$_3$(μ-dioxane)]$_\infty$ with the η^3-allyl groups in alternating

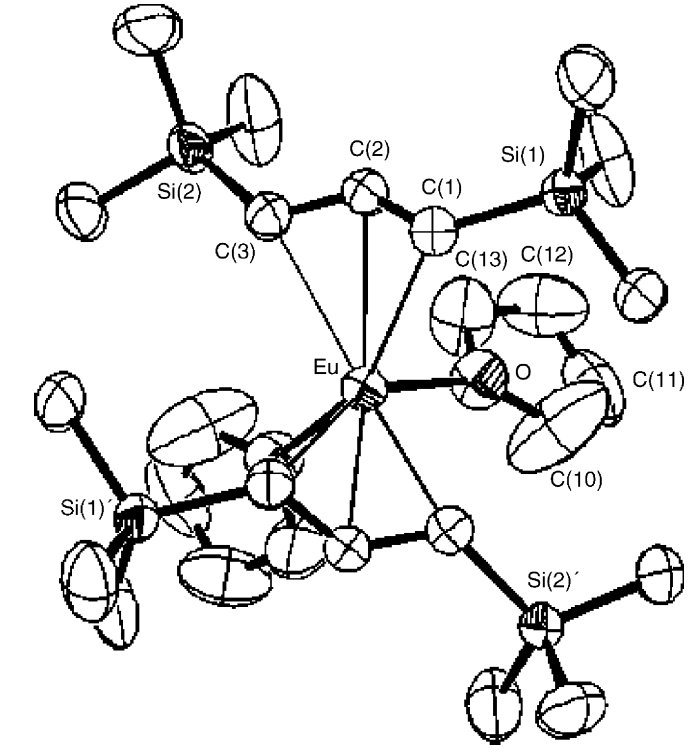

Fig. 10. Molecular structure of $[1,3\text{-}(Me_3Si)_2C_3H_3]Eu(THF)$ [23].

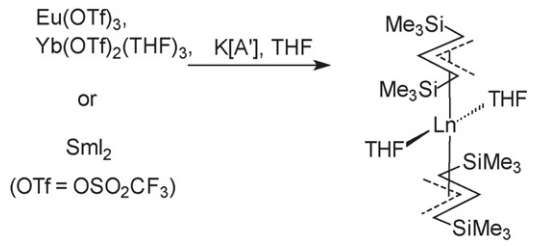

Scheme 12.

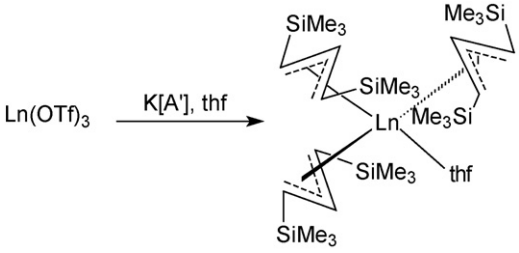

Scheme 13.

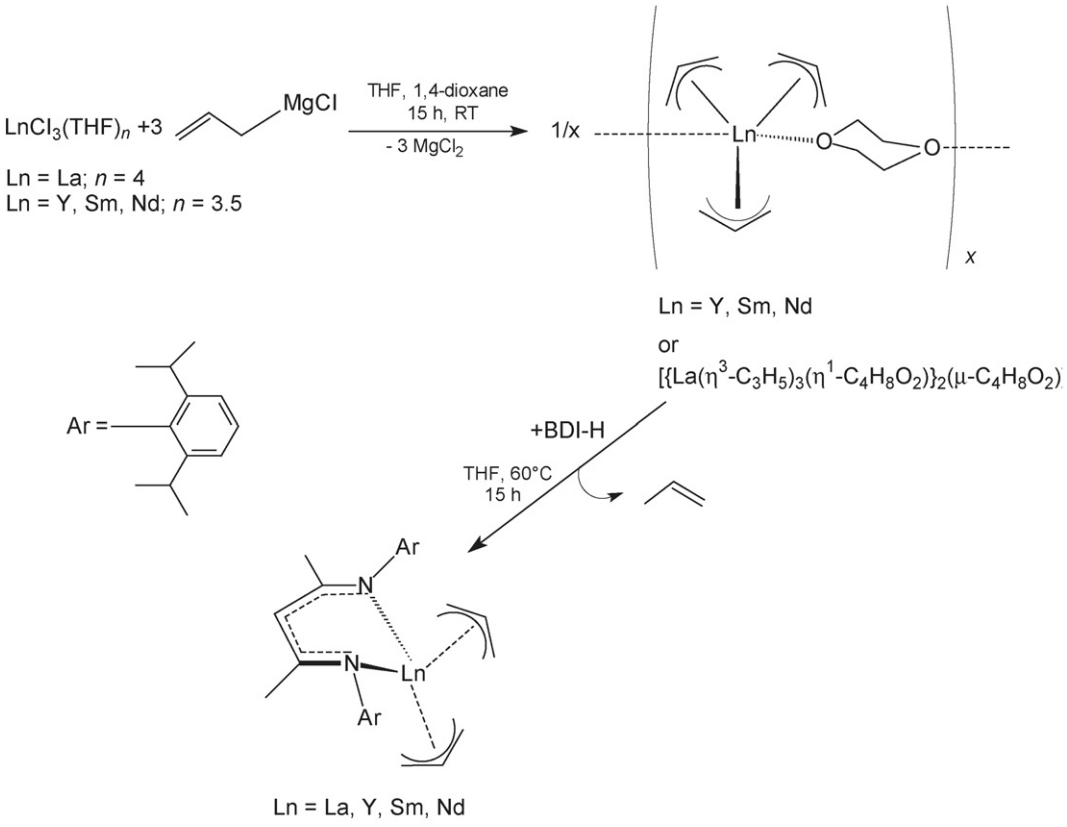

Scheme 14.

orientations and the bridging 1,4-dioxane ligands in chair conformation [24].

Reactions of (μ-dioxane)[La(η^3-C_3H_5)$_3$(κ^1-dioxane)]$_2$ and [Ln(η^3-C_3H_5)$_3$(μ-dioxane)]$_\infty$ (Ln = Y, Sm, Nd) with the diketimine ligand 2-(2,6-diisopropylphenyl)amino-4-(2,6-diisopropylphenyl)imino-2-pentene (BDI-H) in THF at 60 °C cleanly generated the β-diketiminato complexes Ln(η^3-C_3H_5)$_2$[κ^2-HC(MeCNAr)$_2$] (Ar = 2,6-$C_6H_3Pr_2^i$; Ln = La, Y, Sm, Nd) with propene elimination (Scheme 14). The crystal structure of the samarium complex showed a distorted *pseudo*-tetrahedral $SmN_2(allyl)_2$ core, with the samarium positioned 1.438(4) Å out of the C_3N_2 ligand plane (Fig. 13) [24].

Novel types of hexa-1,5-diene-1,6-diamide neodymium complexes have been prepared from the THF adduct of neodymium bromide, $NdBr_3(THF)_{3.5}$, and the appropriate dilithium hexa-1,5-diene-1,6-diamide reagent. The initially formed product, shown in the center of Scheme 15, undergoes dimerizaion upon repeated crystallization from 1,2-dimethoxyethane (DME) (Scheme 15 top). When $NdBr_3(THF)_{3.5}$ was treated with 2 equiv. of the dilithium reagent, a nearly colorless anionic complex was produced (Scheme 15 bottom). The molecular structures of the new complexes revealed that the chelating hexa-1,5-diene-1,6-diamide can be bound either as an enamide or as an azaallyl-type ligand [25].

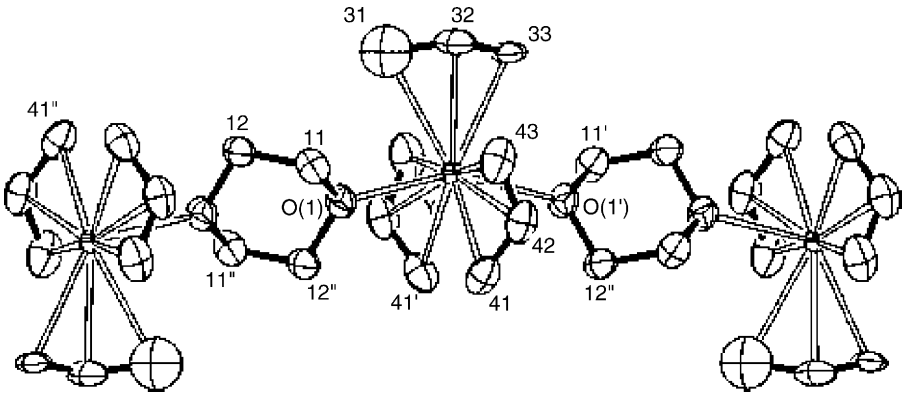

Fig. 11. View of a fragment of the polymeric complex [Y(η^3-C_3H_5)$_3$(μ-dioxane)]$_\infty$ [24].

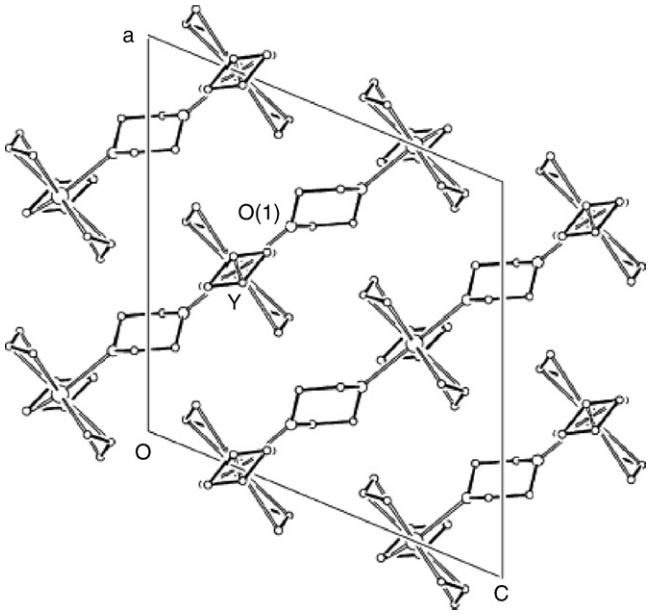

Fig. 12. Crystal structure of polymeric $[Y(\eta^3\text{-}C_3H_5)_3(\mu\text{-dioxane})]_\infty$. Projection of the linear polymer chains down the *b*-axis [24].

2.5. Lanthanide cyclopentadienyl complexes

2.5.1. Cp_2Ln compounds

A thulium(II) metallocene complex, $(C_5H_3Bu^t_2\text{-}1,3)_2Tm(THF)$, has been synthesized from $TmI_2(THF)_3$ and 2 equiv. of $Na(C_5H_3Bu^t_2\text{-}1,3)$ and isolated as a dark reddish-purple solid (Scheme 16) [26].

2.5.2. $CpLnX_2$ compounds

The mono(cyclopentadienyl) compounds $(C_5H_4Bu^t)LnI_2$ (Ln = La, Ce, Nd) were formed in THF by comproportionation reactions of $Ln(C_5H_4Bu^t)_3$ and LnI_3 in the molar ratio of 1:2. Reactions of LnI_3 (Ln = La, Ce, Nd) with one molar equivalent of $Li(C_5H_4Bu^t)$ in THF also afforded the $(C_5H_4Bu^t)LnI_2$ complexes. The X-ray crystal structures of $(C_5H_4Bu^t)LnI_2(py)_3$ (Ln = La, Ce, Nd) have been determined [27]. The reaction of Cp_3Nd with the bis(phenolate) ligand 2,2′-methylenebis(6-*tert*-butyl-4-methylphenoxo) ($MBMP^{2-}$) in a 1:1 molar ratio in THF according to Scheme 17 produced the bis(phenolato)lanthanide complex CpNd(MBMP)$(THF)_2$ as pale blue microcrystals in nearly quantitative yield [28].

The acid–base reactions between the scandium-tris(alkyl) complex $Sc(CH_2SiMe_3)_3(THF)_2$ and silyl-substituted cyclo-

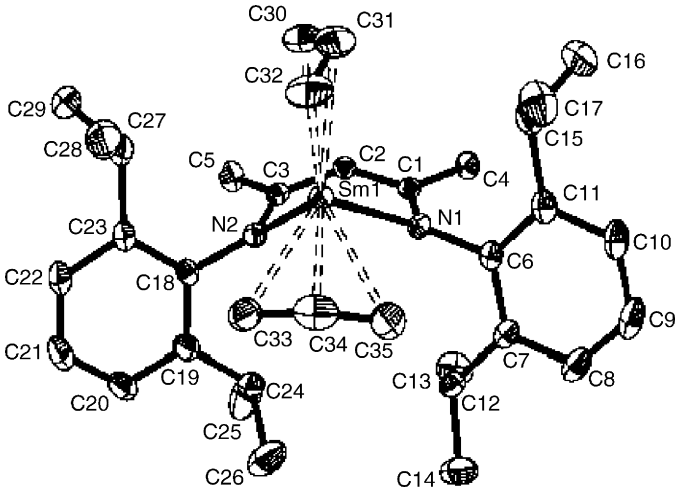

Fig. 13. Molecular structure of $Sm(\eta^3\text{-}C_3H_5)_2[\kappa^2\text{-}HC(MeCNAr)_2]$ (Ar = 2,6-$C_6H_3Pr^i_2$) [24].

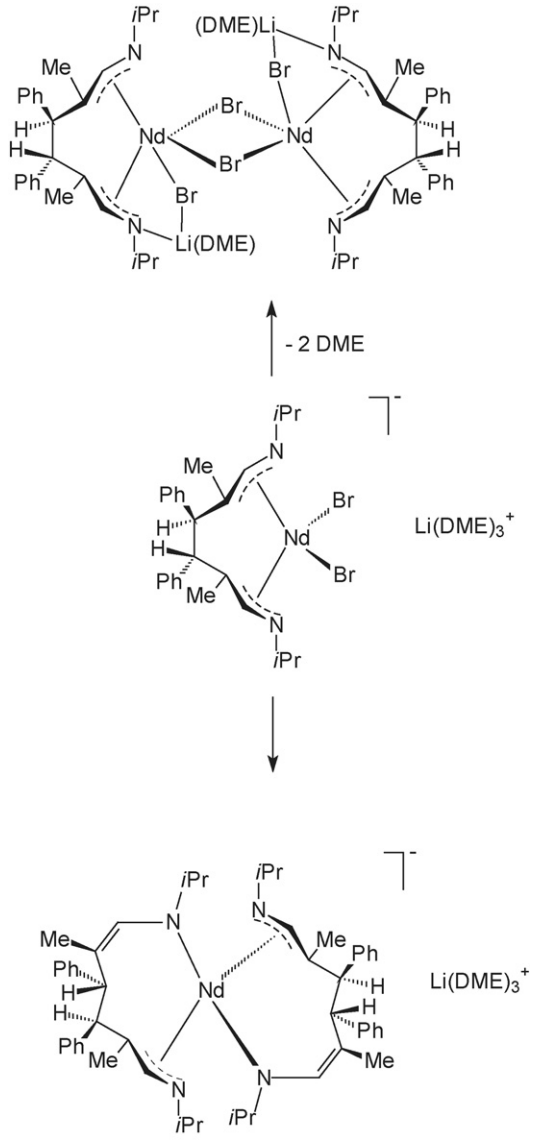

Scheme 15.

Scheme 16.

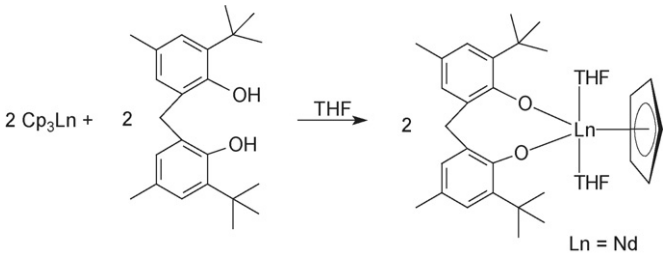

Scheme 17.

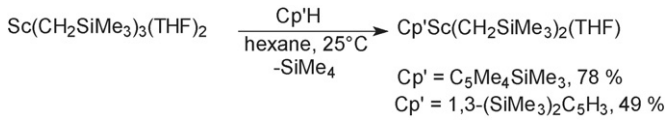

Scheme 18.

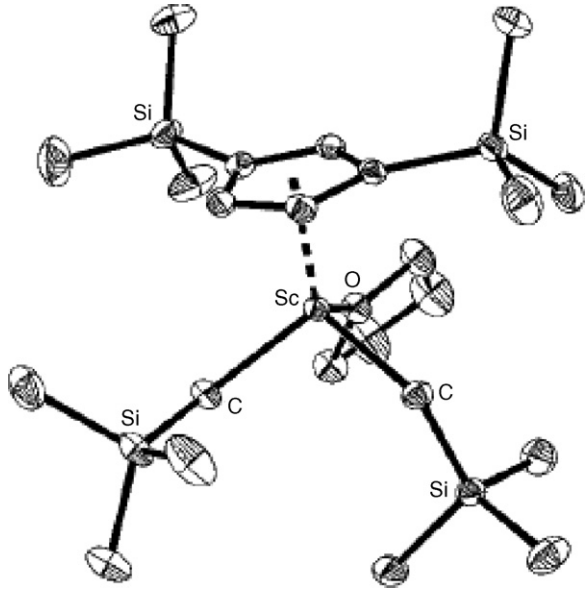

Fig. 14. Molecular structure of $[C_5H_3(SiMe_3)_2\text{-}1,3]Sc(CH_2SiMe_3)_2(THF)$ [29].

pentadienyl ligands Cp′H easily afford the corresponding mono(cyclopentadienyl)scandium-bis(alkyl) complexes Cp′Sc-$(CH_2SiMe_3)_2(THF)$ (Scheme 18, Cp′ = $C_5Me_4SiMe_3$, C_5H_3-$(SiMe_3)_2$-1,3). The molecular structure of $[C_5H_3(SiMe_3)_2$-1,3]$Sc(CH_2SiMe_3)_2(THF)$ is shown in Fig. 14. The monomeric

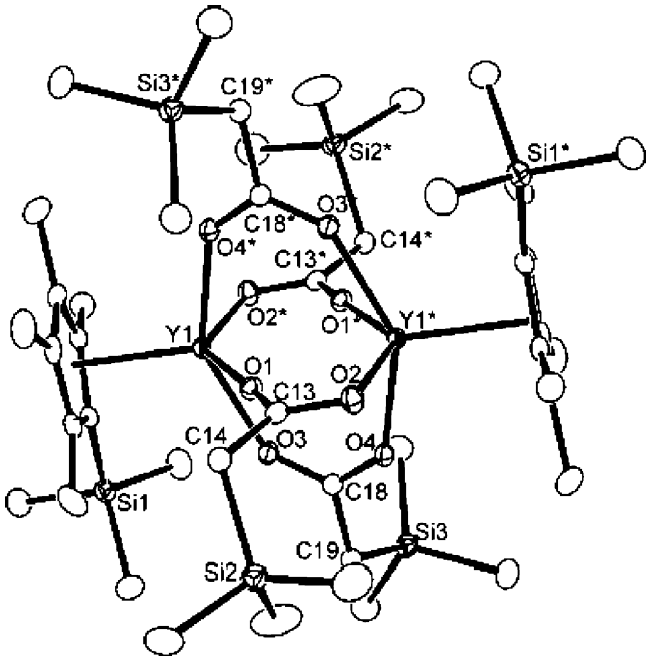

Fig. 15. Molecular structure of $[(C_5Me_4SiMe_3)Y(\mu\text{-}\eta^1\text{:}\eta^1\text{-}O_2CCH_2SiMe_3)_2]_2$ [30].

compound adopts the typical three-legged piano-stool geometry in the solid state [29].

The mono(cyclopentadienyl)lanthanide bis(alkyl) complexes have been investigated as single-component catalysts for the alternating copolymerization of cyclohexene oxide and carbon dioxide. In the course of this study, the stoichiometric reaction of the bis(alkyl) complexes $(C_5Me_4SiMe_3)Ln(CH_2SiMe_3)_2$ (Ln = Sc, Y, Lu) with CO_2 were found to quantitatively afford the corresponding bis(carboxylate) complexes $[(C_5Me_4SiMe_3)Ln(\mu\text{-}\eta^1\text{:}\eta^1\text{-}O_2CCH_2SiMe_3)_2]_2$, which adopt a dimeric structure through the carboxylate bridges (Scheme 19, Fig. 15) [30].

The chemistry of organolanthanide imido complexes still awaits exploration, and the reactions of lanthanide-imido complexes have remained almost unexplored to date. In 2005 it was found that compounds containing the novel Ln_4N_4 cubane core structure exhibit unprecedented reactivity (Scheme 20) [31]. The starting materials $[(C_5H_4SiMe_3)Ln(\mu_3\text{-}NCH_2R)]_4$ (Ln = Y, Lu) were made by allowing the tetranuclear lanthanide polyhydrido complexes $[(C_5H_4SiMe_3)Ln(\mu\text{-}H)_2]_4(THF)$ to react with

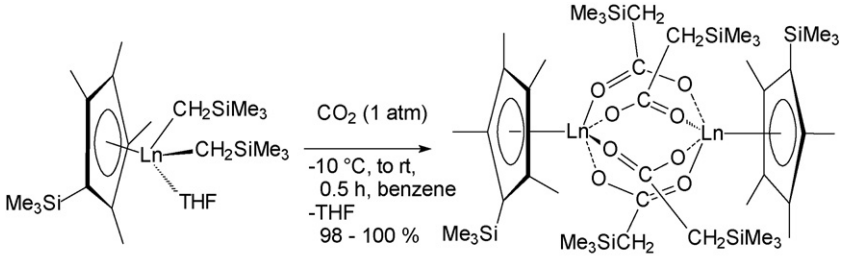

Ln = Y, Lu, Sc

Scheme 19.

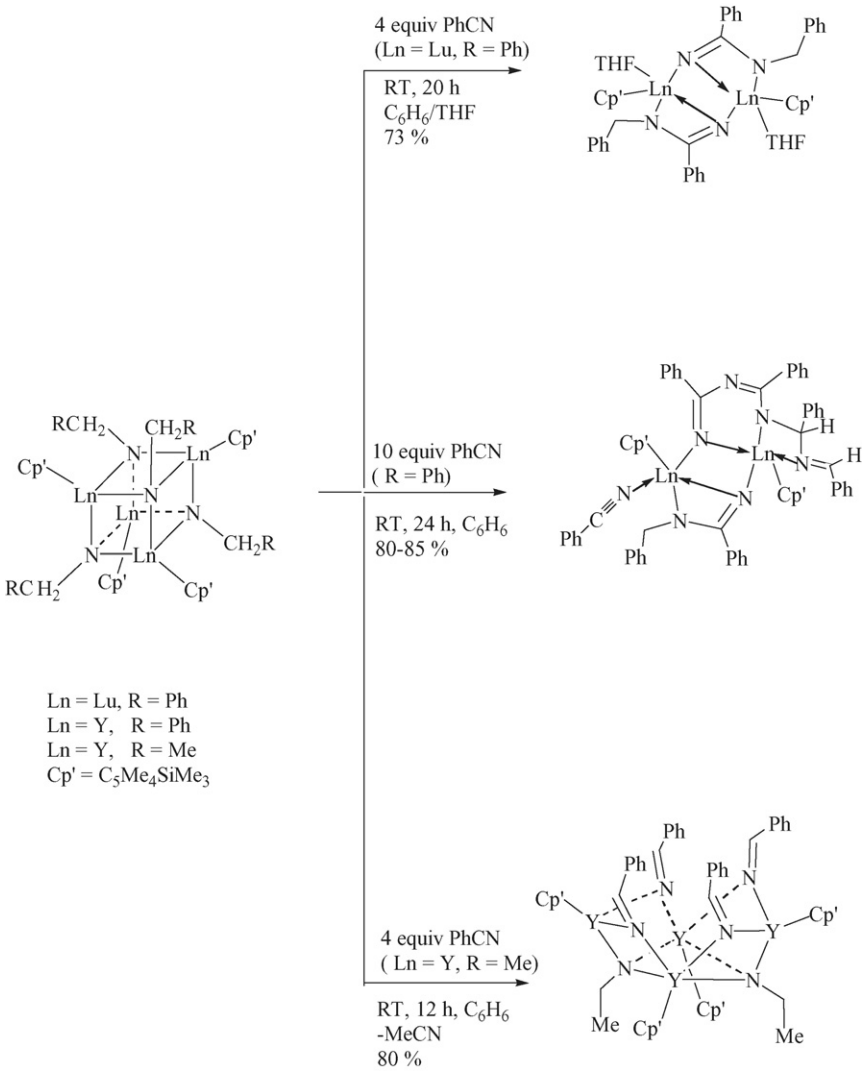

Scheme 20.

nitriles RCN. This reaction involves double addition of the Ln–H units across the C≡N bond. In their high reactivity the lanthanide-imido complexes differ from their d-transition metal counterparts. Depending on the stoichiometries of the starting materials, the cubane clusters add different amounts of benzonitrile (Scheme 20). The products catalyze the trimerization of benzonitrile [31].

The reaction of $[Me_2Si(C_5Me_4)(NPh)]Y(CH_2SiMe_3)(THF)$ with 1 equiv. of phenylacetylene yielded quantitatively the corresponding phenylacetylide as illustrated in Scheme 21. Nucleophilic addition of the latter to 1,3-di-*tert*-butylcarbodiimide took place rapidly at 80 °C to give the corresponding propiolamidinate complex [32].

A mono(cyclopentadienyl) ytterbium complex containing a linked bis(amidinate) dianionic ligand, CpYbL(DME) [L = $Me_3SiNC(Ph)N(CH_2)_3NC(Ph)NSiMe_3$] has been prepared by allowing $LYbCl(THF)_2$ to react with 1 equiv. of NaCp in DME [33].

DFT calculations revealed some unprecedented aspects of the structure of the tetranuclear lutetium and yttrium polyhydride complexes $(C_5H_4SiMe_3)_4Ln_4H_8$ (Ln = Lu, Y). In contrast with the previously described X-ray analysis of $(C_5H_4SiMe_3)_4Lu_4H_8$, which suffered from a serious disorder problem and showed a C_{2v}-symmetrical structure with one body-centered μ_4-H, two face-capping μ_3-H, and five edge-bridging μ_2-H atoms, the DFT studies indicated that the optimized Ln_4H_8 core prefers a *pseudo*-C_{3v}-symmetrical structure with one body-centered μ_4-H, one face-capping μ_3-H, and six edge-bridging μ_2-H atoms. Metal–metal orbital interactions *via* the hydride bridges were also observed in these complexes. The μ_4-H bonding fashion, a new bonding mode for hydrogen, was well proved by the Wiberg bond indexes and linear overlap bond orders. The X-ray crystal structure of $(C_5H_4SiMe_3)_4Y_4H_8$ (Fig. 16), which was solved without disorder problems, showed excellent agreement with the theoretical calculations [34].

2.5.3. Cp_2LnX compounds

The stability and nature of metal–ligand multiple bonding between the tetravalent lanthanide element cerium and a number of different ligand sets that commonly form metal–ligand multiple bonds in transition element chemistry have been investigated theoretically. A comparison of electronic structure and bonding

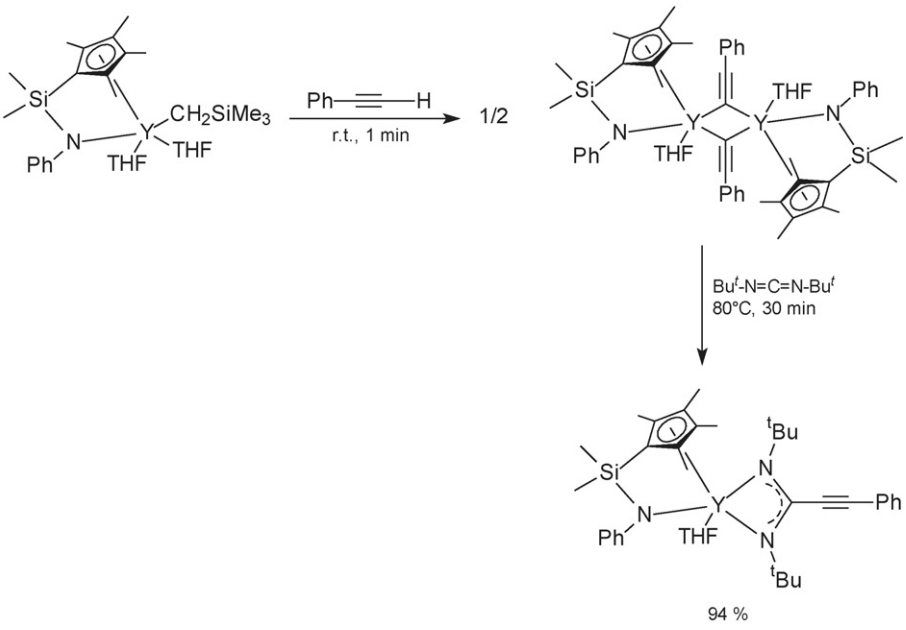

Scheme 21.

in a homologous series of bent metallocene complexes Cp_2CeF^+, Cp_2CeO, $Cp_2Ce(NH)$, $Cp_2Ce(CH_2)$, and $Cp_2Ce(CH)^-$ and the Lewis base adduct $Cp_2Ce(CH_2)(NH_3)$ has been presented. A direct comparison of bonding between Cp_2CeO and the transition element analogue Cp_2HfO was also discussed. The main result of this computational study was the recognition that species with terminal multiple bonds between lanthanide ions (such as tetravalent cerium) and main group elements appear to be legitimate synthetic targets [35].

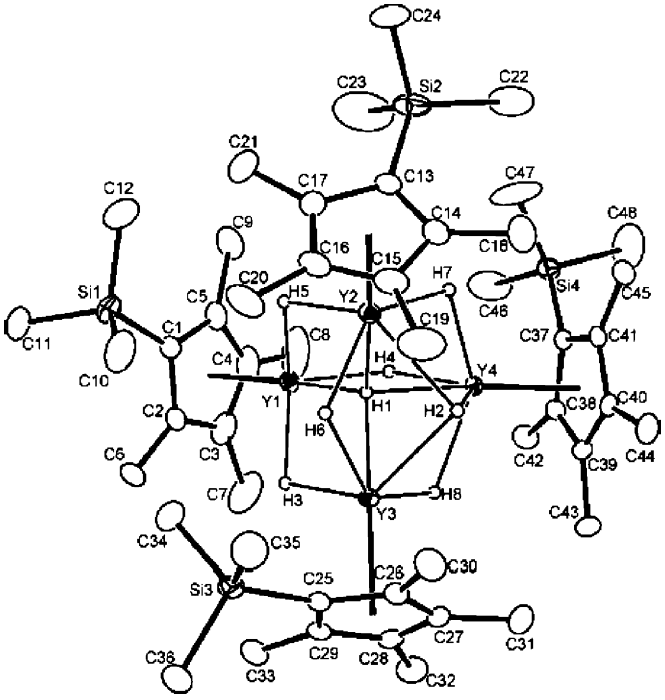

Fig. 16. Molecular structure of $(C_5H_4SiMe_3)_4Y_4H_8$ [34].

The bis(cyclopentadienyl) compounds $(C_5H_4Bu^t)_2LnI$ (Ln = La, Ce, Nd) were formed in THF by comproportionation reactions of $Ln(C_5H_4Bu^t)_3$ and LnI_3 in the molar ratio of 2:1. Reactions of LnI_3 (Ln = La, Ce, Nd) with two molar equivalents of $Li(C_5H_4Bu^t)$ in THF afforded the anionic $[(C_5H_4Bu^t)_2LnI_2]^-$ complexes. The X-ray crystal structures of $[(C_5H_4Bu^t)_2Ce(\mu\text{-}I)]_2$ and $(C_5H_4Bu^t)_2NdI(py)_2$ have been determined [27]. The crystal and molecular structure of the chloro-bridged dimer di-μ-chloro-bis[bis(cumylcyclopentadienyl)yttrium(III)] have been determined by X-ray diffraction [36]. Reactions of the yttrium metallocene allyl complex $[(C_5H_4)SiMe_2(CH_2CH{=}CH_2)]_2Y(C_3H_5)$ with ethylene, trimethylaluminum, and hydrogen have been examined to determine how the olefins tethered to the cyclopentadienyl ligands interact with these species that are typically present in olefin polymerizations. The starting material $[(C_5H_4)SiMe_2(CH_2CH{=}CH_2)]_2Y(C_3H_5)$ was prepared from allylmagnesium chloride and $[(C_5H_4)\text{-}SiMe_2(CH_2CH{=}CH_2)]_2YCl$ and isolated in the form of bright yellow crystals in 72% yield (Scheme 22). An X-ray structure analysis of $[(C_5H_4)SiMe_2(CH_2CH{=}CH_2)]_2Y(C_3H_5)$ revealed that the alkenes are oriented away from the yttrium metal center (Fig. 17) [37].

Hydrogen for fluorine exchange in C_6F_6 and C_6F_5H by the monomeric organocerium hydride $(C_5H_2Bu_3{}^t\text{-}1,3,4)_2CeH$ has been thoroughly investigated in experimental and computational studies. The synthetic sequence begins with the synthesis of the bis(1,3,4-tri-*tert*-butylcyclopentadienyl) cerium triflate, $(C_5H_2Bu_3{}^t\text{-}1,3,4)_2CeOTf$ (Tf = OSO_2CF_3), then replacing the triflate by a benzyl group with the use of the Grignard reagent $PhCH_2MgCl$. Addition of H_2 to the benzyl derivative in pentane produced the deep purple hydride $(C_5H_2Bu^t_3\text{-}1,3,4)_2CeH$, which may be crystallized from pentane. The solid-state structure clearly revealed that the hydride is a monomer (Fig. 18) [38].

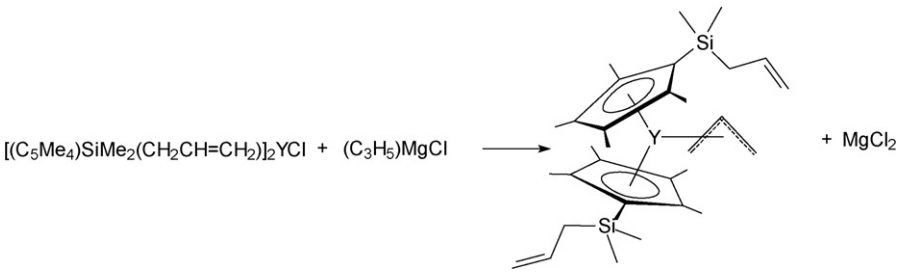

Scheme 22.

The corresponding fluoride was prepared by allowing $(C_5H_2Bu^t_3\text{-}1,3,4)_2Ce(CH_2Ph)$ to react with $BF_3(OEt_2)$ in pentane. According to an X-ray diffraction analysis, the fluoride complex too is a monomer in the solid-state [38].

The net reaction of monomeric $(C_5H_2Bu^t_3\text{-}1,3,4)_2CeH$ with C_6F_6 in C_6D_6 was shown to afford $(C_5H_2Bu^t_3\text{-}1,3,4)_2CeF$, H_2, and tetrafluorobenzyne. The pentafluorophenylmetallocene $(C_5H_2Bu^t_3\text{-}1,3,4)_2Ce(C_6F_5)$ is formed as an intermediate that decomposes slowly to $(C_5H_2Bu^t_3\text{-}1,3,4)_2CeF$ (orange crystals) and C_6F_4 (tetrafluorobenzyne), and the latter is trapped by the solvent C_6D_6 as a [2 + 4] cycloadduct. Fig. 19 illustrates the molecular structure of the pentafluorophenyl complex [38].

Hydrogen for fluorine exchange in $CH_{4-x}F_x$ by the monomeric hydride $(C_5H_2Bu^t_3\text{-}1,3,4)_2CeH$ has also been investigated by experimental and computational methods. The metallocene cerium hydride reacts instantaneously with CH_3F, but slower with CH_2F_2, to give $(C_5H_2Bu^t_3\text{-}1,3,4)_2CeF$ and CH_4 in each case, a net H for F exchange reaction. The hydride reacts very slowly with CHF_3, and not at all with CF_4, to give $(C_5H_2Bu^t_3\text{-}1,3,4)_2CeF$, H_2 and 1,2,4- and 1,3,5-tri-*tert*-butylbenzene. The substituted benzenes are postulated to

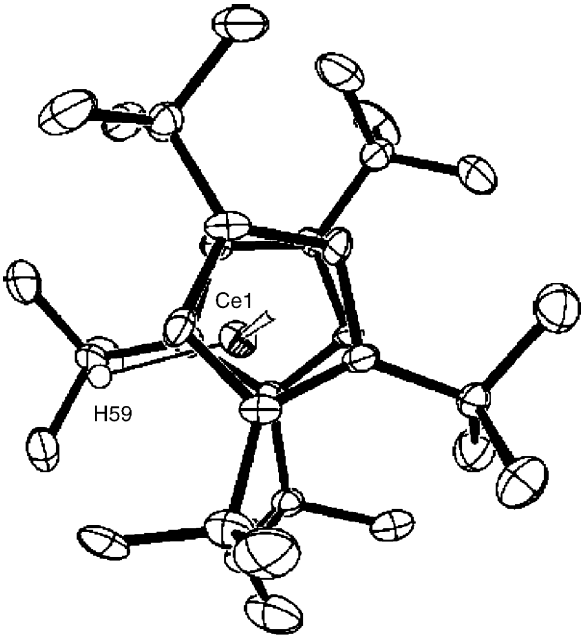

Fig. 18. Molecular structure of $(C_5H_2Bu_3{}^t\text{-}1,3,4)_2CeH$ [38].

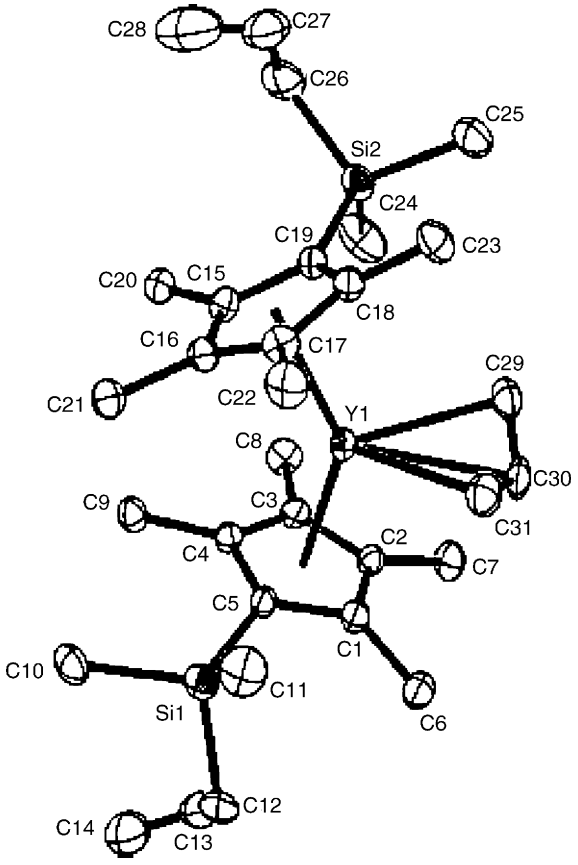

Fig. 17. Molecular structure of $[(C_5H_4)SiMe_2(CH_2CH{=}CH_2)]_2Y(C_3H_5)$ [37].

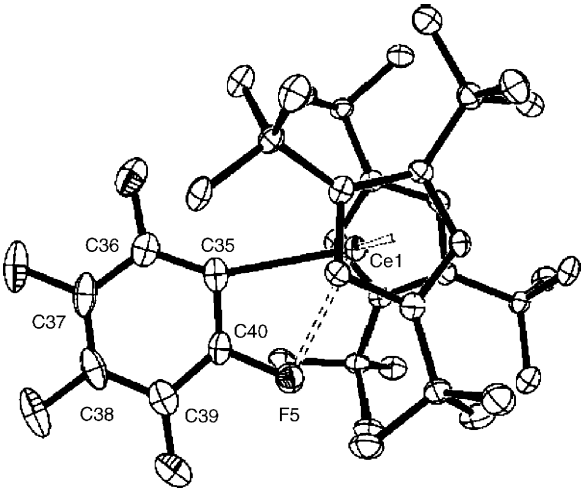

Fig. 19. Molecular structure of $(C_5H_2Bu_3{}^t\text{-}1,3,4)_2Ce(C_6F_5)$ [38].

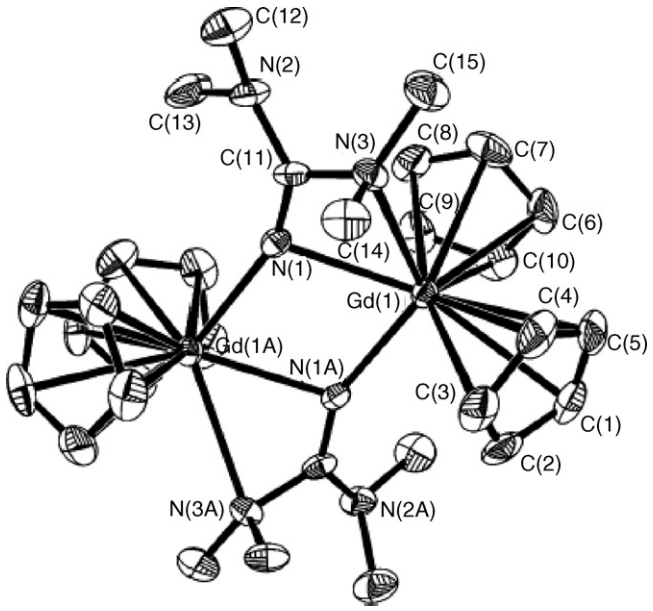

Fig. 20. Molecular structure of $[Cp_2Gd\{\mu\text{-}\eta^1\text{:}\eta^2\text{-}N{=}C(NMe_2)_2\}]_2$ [40].

result from trapping of a fluorocarbene fragment derived by α-fluoride abstraction from an intermediate fluoroalkyl complex, $(C_5H_2Bu^t_3\text{-}1,3,4)_2CeCF_3$ [39].

Reactions of $[Cp_2Ln(\mu\text{-}Cl)]_2$ with $LiN{=}C(NMe_2)_2$ proceeded at room temperature in THF to yield the lanthanocene guanidinate complexes $[Cp_2Ln\{\mu\text{-}\eta^1\text{:}\eta^2\text{-}N{=}C(NMe_2)_2\}]_2$ (Ln = Gd, Er). Fig. 20 shows the molecular structure of the gadolinium derivative. The X-ray analysis showed an unusual bonding mode of the guanidinate ligand $N{=}C(NMe_2)_2^-$, which acts both as a bridging and a chelating group. Each gadolinium atom is coordinated by two η^5-cyclopentadienyl groups, one chelating η^2-guanidinate ligand and one bridging nitrogen atom from another guanidinate ligand, to form a distorted octahedral geometry. Treatment of these complexes with phenylisocyanate resulted in monoinsertion of PhNCO into the Ln–N bond to yield the corresponding insertion products $[Cp_2Ln\{\mu\text{-}\eta^1\text{:}\eta^2\text{-}OC(N{=}C(NMe_2)_2)NPh\}]_2$. Fig. 21 depicts the bridging coordination mode of the resulting new ligand in the case of the gadolinium derivative. Monomeric guanidinoacetimidinate complexes of the type $Cp_2Ln[(Pr^iN)_2C(N{=}C(NMe_2)_2)]$ (Ln = Dy, Er, Yb) were obtained by treatment of $[Cp_2Ln(\mu\text{-}Cl)]_2$ with $Li[(Pr^iN)_2C(N{=}C(NMe_2)_2)]$. The molecular structure of the ytterbium complex is illustrated in Fig. 22. The complex forms a solvent-free monomer with the ytterbium atom bonded to two η^5-cyclopentadienyl rings and one chelating guanidinoacetamidinate ligand $[(Pr^iN)_2C(N{=}C(NMe_2)_2)]^-$ to form a distorted *pseudo*-tetrahedral coordination geometry [40].

Similar insertion reactions of phenyl isocyanate into lanthanide-sulfur bonds have been investigated [41]. In a related study the synthesis and reactivity of new lanthanocene complexes incorporating a phenothiazine ligand have been described. The reaction of phenothiazine (HPtz) with Bu^nLi in THF and subsequently with 1 equiv. of $Cp_2LnCl(THF)$ gave the starting materials $Cp_2LnPtz(THF)$ (Ln = Y, Dy, Er, Yb). Treatment of these complexes with *N*,*N*′-diisopropylcarbodiimide according to Scheme 23 resulted in mono-insertion of carbodiimide into the Ln–N(Ptz) bond to yield the corresponding guanidinates $Cp_2Ln[(Pr^iN)_2C(Ptz)]$. Analogous insertion reactions have been carried out with phenyl isothiocyanate. Fig. 23 shows the molecular structure of the ytterbium guanidinate derivative $Cp_2Yb[(Pr^iN)_2C(Ptz)]$ [42].

The organosamarium thiolate complex $[(MeC_5H_4)_2Sm(\mu\text{-}SPh)(THF)]_2$ has been synthesized in high yield as yellow crystals by treatment of $(MeC_5H_4)_3Sm$ with PhSH in a 1:1 molar ratio in THF solution [43]. Reaction of $[Cp_2Ln(\mu\text{-}Me)]_2$ with 2 equiv. of elemental sulfur in toluene at room temperature led to formation of the methylthiolate complexes $[Cp_2Ln(\mu\text{-}SMe)]_2$ (Ln = Yb, Y, Er, Dy) in good yields. While reaction of

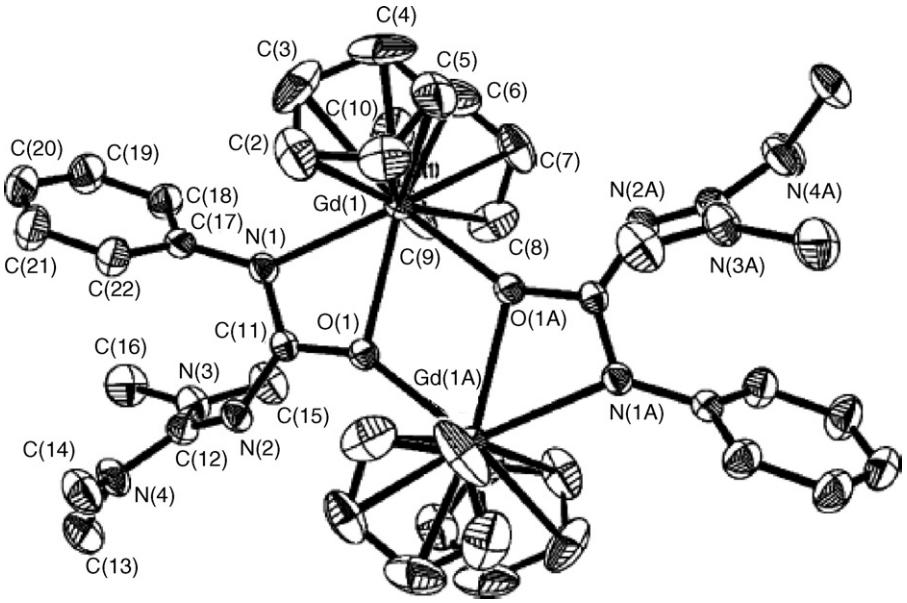

Fig. 21. Molecular structure of $[Cp_2Gd\{\mu\text{-}\eta^1\text{:}\eta^2\text{-}OC(N{=}C(NMe_2)_2)NPh\}]_2$ [40].

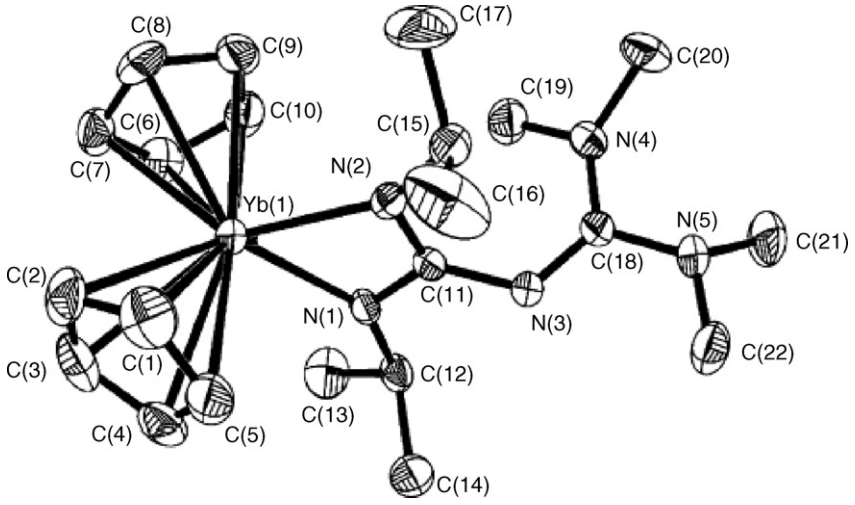

Fig. 22. Molecular structure of $Cp_2Yb[(Pr^iN)_2C(N{=}C(NMe_2)_2)]$ [40].

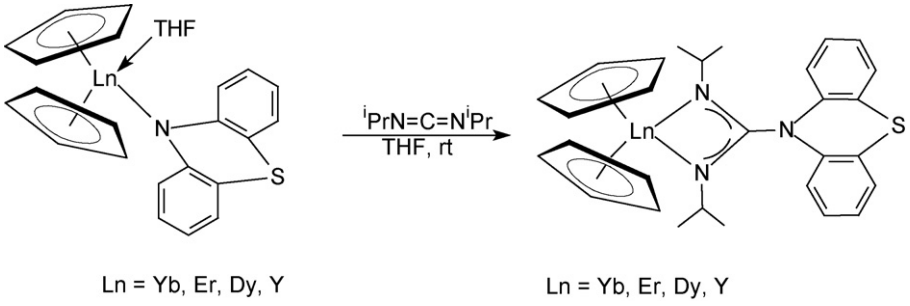

Scheme 23.

$Cp_2Y(Bu^n)$ with elemental sulfur in a 1:1 stoichiometric ratio under the same conditions afforded $[(Cp_2Y)_2(\mu_3\text{-}S)(THF)]_2$ as the metal-containing product accompanied by the extrusion of Bu^n_2S and $Bu^n_2S_2$, the corresponding insertion intermediate $[Cp_2Y(\mu\text{-}SBu^n)]_2$ could be isolated only by decreasing the relative amount of S_8 under more mild reaction conditions. Furthermore, $[Cp_2Yb(\mu\text{-}SEt)]_2$ was found to react with 2 equiv. of sulfur to give a mixture of $[(Cp_2Yb)_2(\mu_3\text{-}S)(THF)]_2$ and $(\mu\text{-}\eta^2{:}\eta^2\text{-}S_2)[Cp_2Yb(THF)]_2$. Fig. 24 shows the molecular structure of $[Cp_2Yb(\mu\text{-}SMe)]_2$ (orange-red crystals), while the solid-state structure of $[(Cp_2Yb)_2(\mu_3\text{-}S)(THF)]_2$ (red crystals) is depicted in Fig. 25. The latter is a centrosymmetric square-planar tetrametallic structure, in which each S^{2-} ligand bridges three metal atoms [44].

The molecular structure of the disulfide-bridged dinuclear ytterbium complex $(\mu\text{-}\eta^2{:}\eta^2\text{-}S_2)[Cp_2Yb(THF)]_2$ (dark green crystals) has also been determined by X-ray diffraction. The formal coordination number in this complex is 9, and the S–S bond length is 2.115(4) Å (Fig. 26) [44].

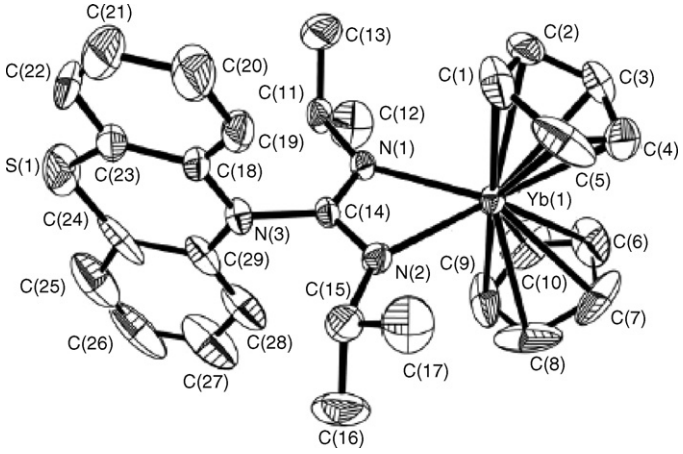

Fig. 23. Molecular structure of $Cp_2Yb[(Pr^iN)_2C(Ptz)]$ [42].

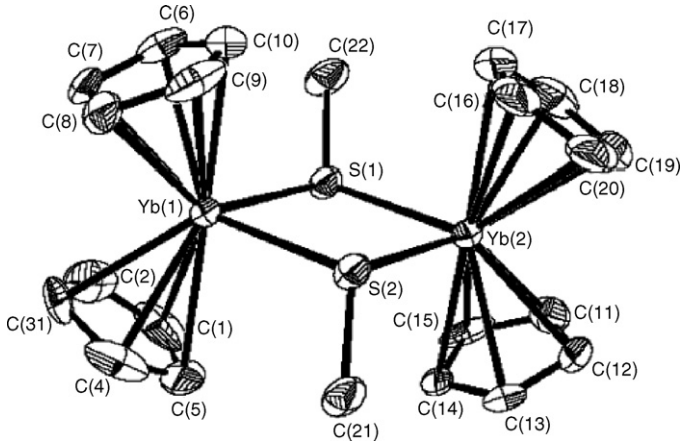

Fig. 24. Molecular structure of $[Cp_2Yb(\mu\text{-}SMe)]_2$ [44].

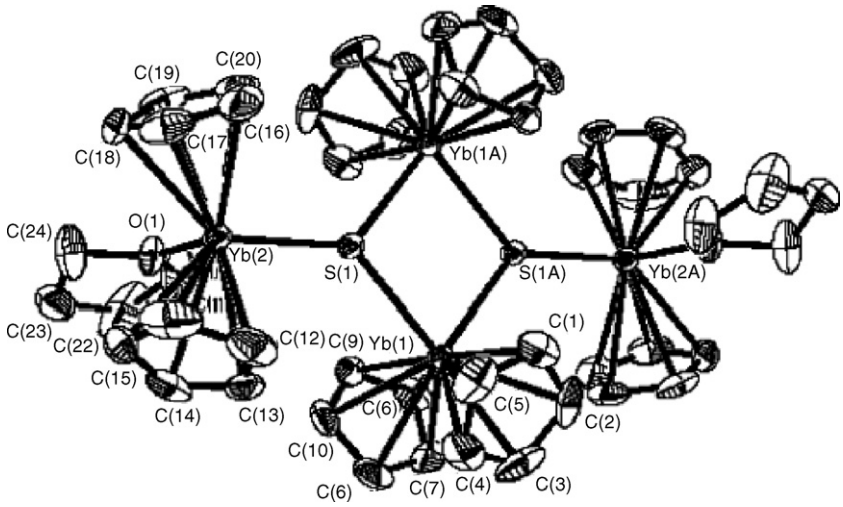

Fig. 25. Molecular structure of $[(Cp_2Yb)_2(\mu_3\text{-}S)(THF)]_2$ [44].

An unusual regioselective O_2 oxidation reaction of air-sensitive lanthanocene thiolates has been reported, revealing a novel oxygenation pattern of thiolate ligands. Complexes $[Cp_2Ln\{SC(Bu^n)NPh\}]_2$ (Ln = Y, Gd) were prepared in good yields by the reaction of PhNCS with Bu^nLi and subsequently with Cp_2LnCl in toluene. When solution of these complexes in THF/toluene were exposed to an N_2 atmosphere with limited amounts of dried air at ambient temperature (*ca.* 12 h), both were converted into O-bound sulfenate complexes $[Cp_2Ln\{OSC(Bu^n)NPh\}]_2$ (Ln = Y, 35% yield; Ln = Gd, 41% yield) (Scheme 24). The samarium analogue $[Cp_2Sm\{OSC(Bu^n)NPh\}]_2$ was obtained in 44% yield by reaction of $Cp_2SmCl(THF)$ with $PhNC(Bu^n)SLi$ in toluene, followed by slow diffusion of trace O_2 into the reaction flask. The molecular structures of the Y and Sm derivatives have been confirmed by X-ray diffraction analyses [45].

$(C_5Me_4H)_3Lu$ or $(C_5Me_4H)_2Lu[(\mu\text{-}Ph)_2BPh_2]$ were reduced with potassium graphite under dinitrogen in THF to afford in both cases the bridging dinitrogen complex $(\mu\text{-}\eta^2\text{:}\eta^2\text{-}N_2)[(C_5Me_4H)_2Lu(THF)]$ (Scheme 25). The highest yields (80%) were obtained when $(C_5Me_4H)_2Lu[(\mu\text{-}Ph)_2BPh_2]$ was used as precursor [46].

2.5.4. Cp_3Ln compounds

Tris(cyclopentadienyl)scandium, Cp_3Sc, has been isolated in Ar-matrices (20 K) and the structure of monomeric Cp_3Sc has been studied using infrared spectroscopy. When compared with the spectra and results of density functional calculations, the matrix-isolated Cp_3Sc was found to have a structure where all three of the cyclopentadienyl rings coordinate to scandium in η^5 fashion, $(\eta^5\text{-}Cp)_3Sc$, which is different from the structure in the solid-state. Moreover, a stable dimeric structure was estimated

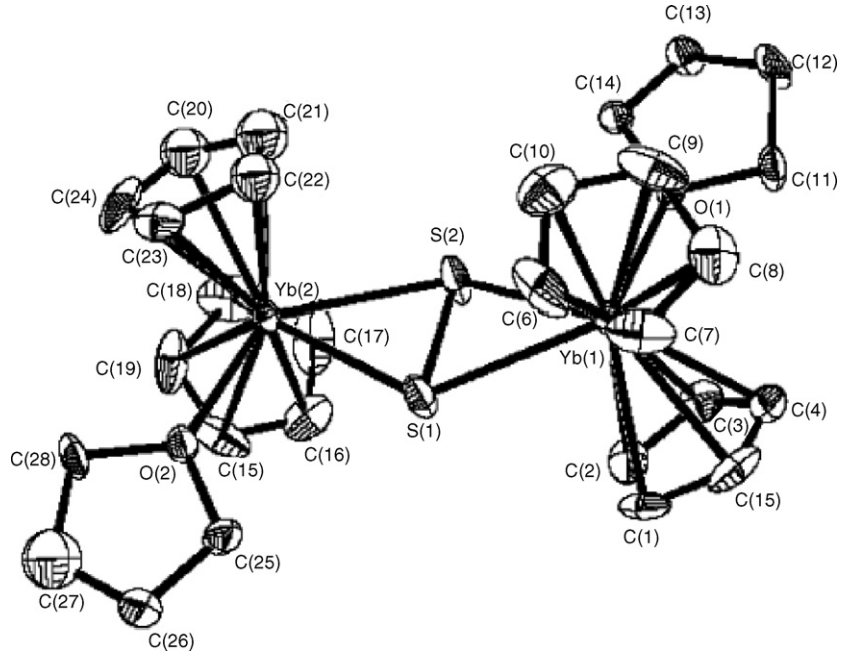

Fig. 26. Molecular structure of $(\mu\text{-}\eta^2\text{:}\eta^2\text{-}S_2)[Cp_2Yb(THF)]_2$ [44].

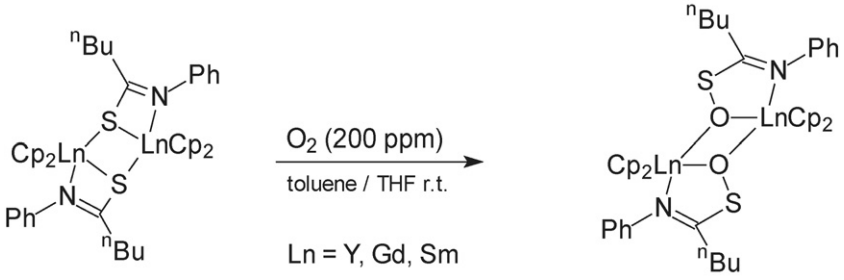

Scheme 24.

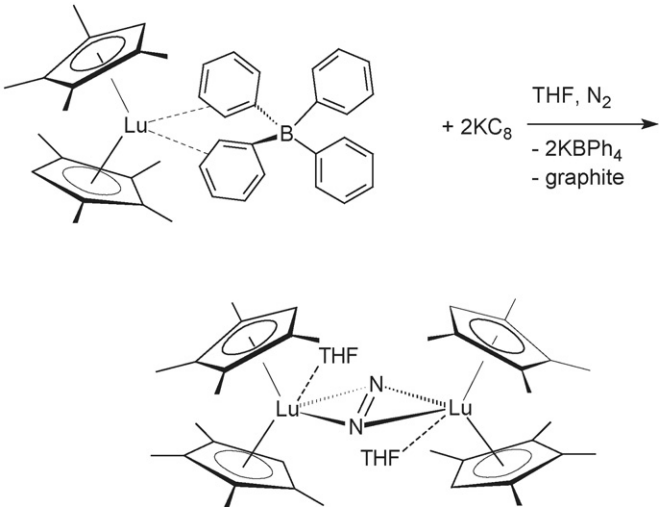

Scheme 25.

to be $[(\eta^5\text{-Cp})_2\text{Sc}(\mu\text{-}\eta^1\text{-Cp}{:}\eta^1\text{-Cp})]_2$, using density functional calculations [47].

Selective O_2 oxidation of a chelating thioether group in a Cp_3Ln-type complex has been reported. The starting material, $(EtSCH_2CH_2C_5H_4)_3Sm$ was prepared in 54% yield by the reaction of anhydrous $SmCl_3$ with 3 equiv. of $NaC_5H_4CH_2CH_2SEt$ in THF. Treatment of a solution of $(EtSCH_2CH_2C_5H_4)_3Sm$ in THF with trace O_2, added intermittently over several days at ambient temperature under an atmosphere of nitrogen, gave the unusual side-chain oxidation product $(EtSCH_2CH_2C_5H_4)_2[EtS(O)C_2H_4C_5H_4]Sm$ in 43% yield (Scheme 26) [45].

The previously inaccessible smallest member of the $(C_5Me_4H)_3Ln$ series, $(C_5Me_4H)_3Lu$, has been synthesized from $(C_5Me_4H)_2Lu[(\mu\text{-Ph})_2BPh_2]$ and KC_5Me_4H and isolated as a yellow powder in 90% yield [46].

2.5.5. Cp_3LnL and Cp_3LnL_2 compounds

$Cp_3Ln(THF)$-type complexes containing 1,2-phenylenedioxoborylcyclopentadienyl ligands have been reported for Ln = La, Ce, and Yb in the form of colorless, pale yellow and pink crystals, respectively (Scheme 27) [48].

2.5.6. Pentamethylcyclopentadienyl compounds

2.5.6.1. Cp^*_2M compounds. A new *N*-heterocyclic complex of decamethylytterbocene, Cp^*_2Yb, has been prepared by the addition of 4′-cyano-2,2′:6′,2″-terpyridine (terpyCN) to $Cp^*_2Yb^{II}(OEt_2)$ in toluene to give a dark blue species designated as Cp^*_2Yb(terpyCN) (Scheme 28). The compound undergoes oxidation with ferrocinium hexafluorophosphate in THF to give an Yb^{III} complex with a neutral terpyCN ligand as the major product (80% isolated yield) of the reaction. An unusual side product (<5% yield) was also formed during this oxidation reac-

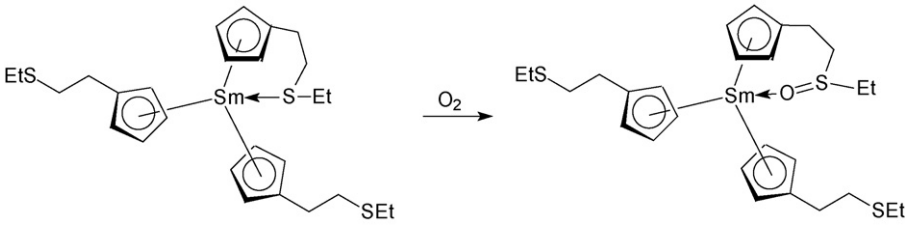

Scheme 26.

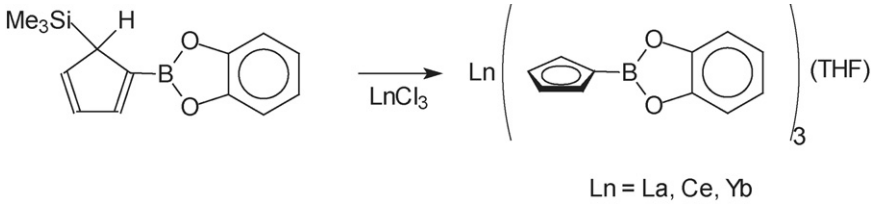

Scheme 27.

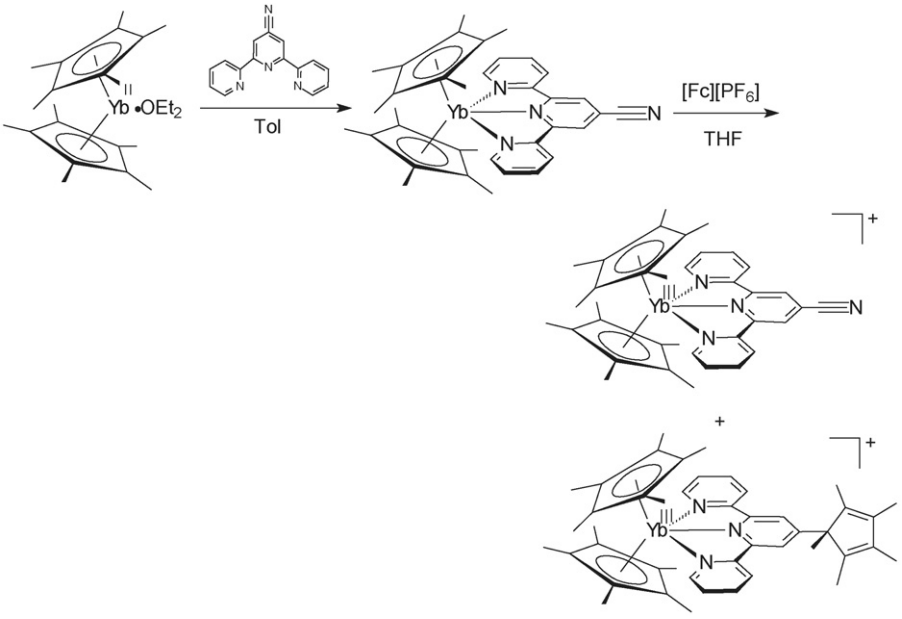

Scheme 28.

tion in which the nitrile group is cleaved from the terpyridine and a new C–C bond is formed between the terpyridine and a Cp^* ligand (Scheme 28) [49].

2.5.6.2. Mono(pentamethylcyclopentadienyl)lanthanide(III) compounds. The synthesis and characterization of complexes containing a $Cp^*Sc(R_2bipy)$ motif (R_2bipy = 4,4′-R,R-2,2′-bipyridine, R = H, Me) have been described. The starting material, bright yellow Cp^*ScI_2, was prepared from $Cp^*Sc(acac)_2$ (acac = acetylacetonato) and AlI_3 (2 equiv.) in pentane (63% yield). In the solid-state, Cp^*ScI_2 forms an inversion-symmetric, cyclic tetramer as shown in Fig. 27 [50].

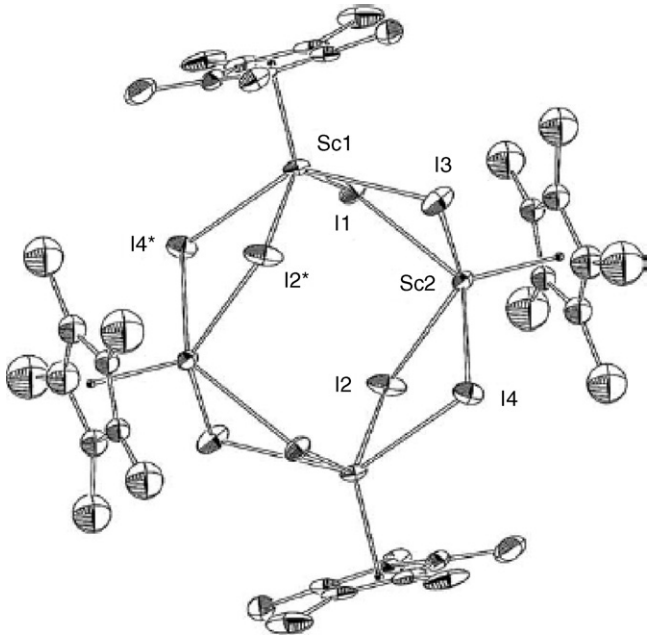

Fig. 27. Molecular structure of $[Cp^*ScI_2]_4$ [50].

Attempts to prepare phosphine derivatives of Cp^*ScI_2 were largely unsuccessful, although it did react cleanly with bis(dimethylphosphino)ethane (dmpe) in toluene according to Scheme 29 to precipitate colorless crystals of $[Cp^*ScI_2(\mu\text{-dmpe})]_2$, isolated in 24% yield [50].

Cp^*ScI_2 was also found to react with bipyridine (bipy) and 4,4′-dimethyl-2,2′-bipyridine (dmb) in benzene to yield Cp^*ScI_2(bipy) (bright orange) and Cp^*ScI_2(dmb) (bright yellow), respectively. Cp^*ScI_2(bipy) was reduced by alkali metal reductants such as Na/Hg, NaK_2, and K in aromatic solvents to yield $[Cp^*ScI(bipy)]_2$, which was isolated in the form of large black crystals (Scheme 30). As shown in Figs. 28 and 29, $[Cp^*ScI(bipy)]_2$ has a dimeric structure in which the two scandium centers are bridged by the two iodide ligands. A Cp^* and a bipyridine ligand complete the coordination sphere of each scandium. Each scandium center is thus in a square pyramidal coordination environment with the Cp^* centroid occupying the apical position. The two bipyridine ligands

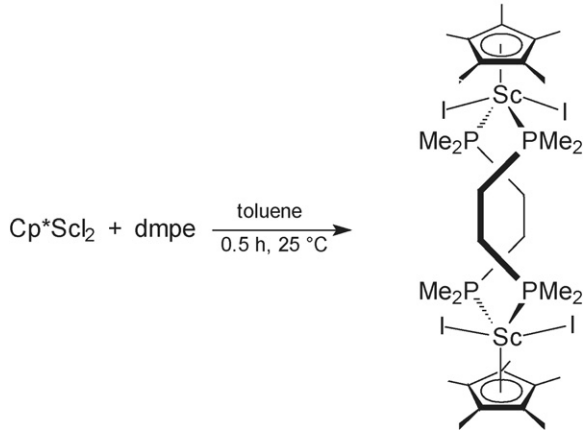

Scheme 29.

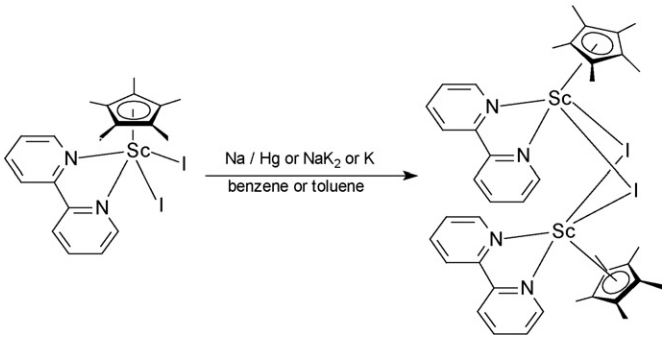

Scheme 30.

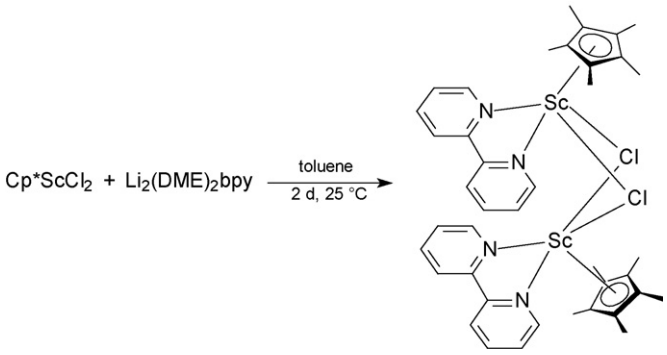

Scheme 31.

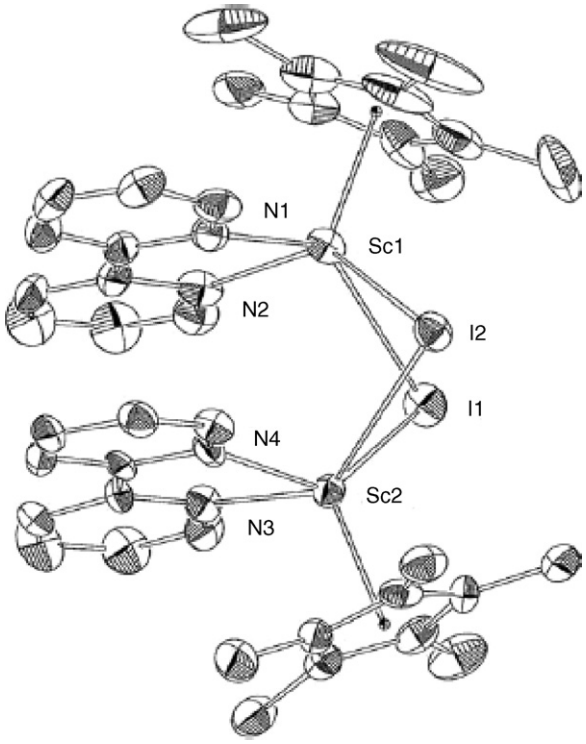

Fig. 28. Molecular structure of $[Cp^*ScI(bipy)]_2$ [50].

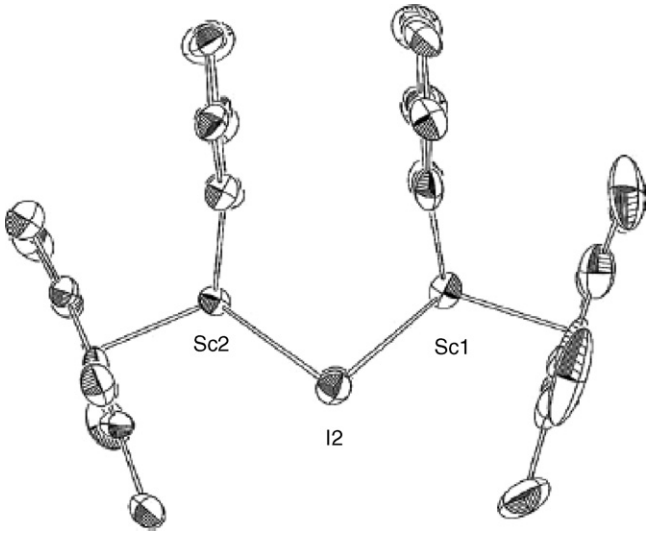

Fig. 29. Side view of $[Cp^*ScI(bipy)]_2$ [50].

are arranged in a *cis*-orientation and are coplanar (Fig. 29) [50].

The chloride analogue, $[Cp^*ScCl(bipy)]_2$, was prepared from Cp^*ScCl_2 by salt metathesis with $Li(DME)_2bipy$ (DME = 1,2-dimethoxyethane) in toluene according to Scheme 31. This compound too forms black crystals [50].

Reaction of $SmCl_3$ with 1 equiv. of the β-diketiminato precursor KL (L = [DippNC(Me)CHC(Me)NDipp; Dipp = 2,6-$Pr_2^iC_6H_3$) in THF afforded the dimeric samarium dichloride $LSmCl_2(THF)Cl_2SmL$. Reaction of this complex with KCp^* afforded the mono(pentamethylcyclopentadienyl) derivative $LSmCp^*Cl$ as orange crystals in 76% yield [11]. The acid–base reactions between the scandium-tris(alkyl) complex $Sc(CH_2SiMe_3)_3(THF)_2$ and pentamethylcyclopentadiene easily afforded the corresponding mono(pentamethylcyclopentadienyl)scandium-bis(alkyl) complex $Cp^*Sc(CH_2SiMe_3)_2$-(THF) in 65% yield (Scheme 32) [29].

2.5.6.3. Bis(pentamethylcyclopentadienyl)lanthanide(III) compounds. To compare the ligand-based reduction chemistry of $(EPh)^-$ ligands (E = S, Se, Te) in a metallocene environment to the sterically induced reduction chemistry of the Cp^*-ligands in Cp^*_3Sm, $Cp^*_2Sm(EPh)$ complexes have been synthesized and treated with substrates reduced by Cp^*_3Sm: cyclooctatetraene; azobenzene; phenazine. Reactions of PhEEPh with $Cp^*_2Sm(THF)_2$ and Cp^*_2Sm produced THF-solvated monometallic complexes, $Cp^*_2Sm(EPh)(THF)$, and their unsolvated dimeric analogues, $[Cp^*_2Sm(\mu\text{-}EPh)]_2$, respectively. Both sets of the paramagnetic benzene chalcogenolate complexes were definitively identified by X-ray crystallography and form a homologous series. Only the $(TePh)^-$ complexes show reduction reactivity and only upon heating to 65 °C [51]. The dimeric lanthanide complexes $[Cp^*_2Ln(dddt)K(THF)_2]_2$ (Ln = Ce, Nd; dddt = 5,6-dihydro-1,4-dithiin-2,3-dithiolate) have been prepared by reaction of $Cp^*_2Ln(\mu\text{-}Cl)_2K$ with K_2dddt. In the presence of 15-crown-5, they are transformed into the cation–anion pairs $[K(15\text{-crown-}5)_2][Cp^*_2Ln(dddt)]$ [52].

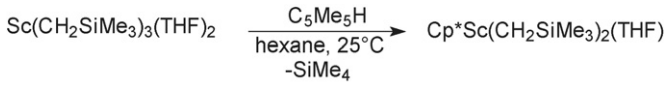

Scheme 32.

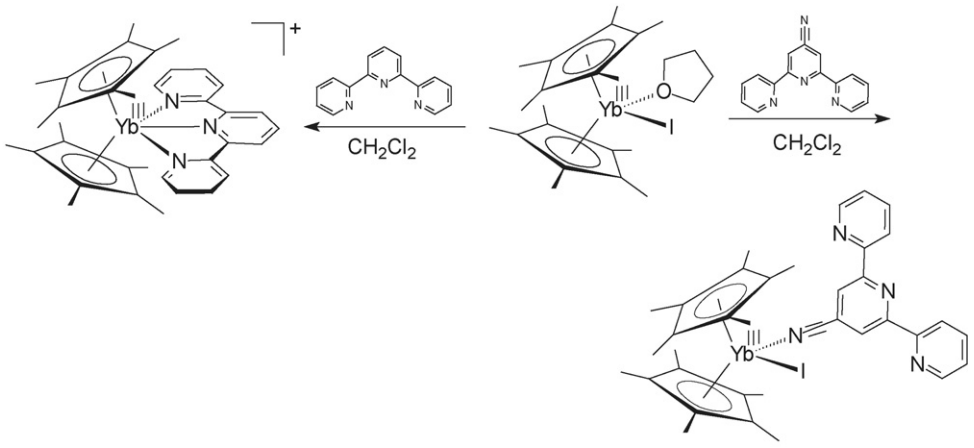

Scheme 33.

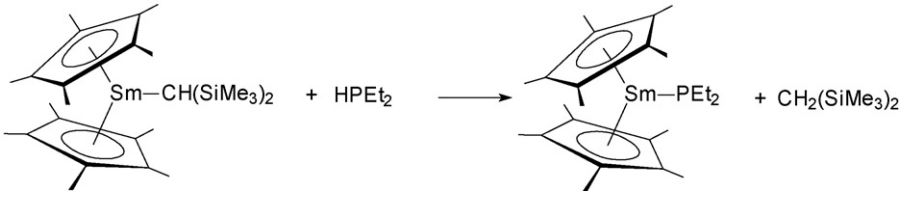

Scheme 34.

Treatment of Cp^*_2CeI with one mole equivalent of 2,2′-bipyridine (=bipy) in THF gave the adduct $Cp^*_2CeI(bipy)$, which was transformed into $Cp^*_2Ce(bipy)$ by Na(Hg) reduction. Similar reaction of Cp^*_2CeI with one mole equivalent 2,2′:6′,2″-terpyridine (=terpy) afforded the ionic adduct $[Cp^*_2Ce(terpy)]I$, which could also be reduced to the neutral complex $Cp^*_2Ce(terpy)$ by sodium amalgam [53]. Different coordination modes of the heterocyclic ligand 4′-cyano-2,2′:6′,2″-terpyridine (=terpyCN) to decamethylytterbocene(III), $Cp^*_2Yb^{III}$, units have been confirmed by isolation and X-ray crystallographic characterization of complexes binding through either the cyano nitrogen of terpyCN or the three terpyridyl nitrogen atoms of terpyCN. The synthetic routes are outlined in Scheme 33 [49].

A series of bis(pentamethylcyclopentadienyl)lanthanide phosphido complexes has been obtained by protonolysis reactions between $Cp^*_2LnCH(SiMe_3)_2$ (Ln = La, Sm) and secondary phosphines as exemplified in Scheme 34 [54].

The allyl metallocenes $Cp^*_2Ln(C_3H_5)$ (Ln = Y, Lu) have been synthesized from the corresponding chloro precursors by treatment with allylmagnesium chloride. Fig. 30 depicts the molecular structure of the yttrium derivative showing the *trihapto*-coordination of the allyl ligand [37].

The loosely ligated $[BPh_4]^-$ anion in $[Cp^*_2Ln][(\mu\text{-}Ph)_2BPh_2]$ has been reported to be readily displaced by alkyllithium or potassium reagents to provide access to unsolvated alkyl lanthanide metallocenes, $[Cp^*_2LnR]_x$, which display high C–H activation reactivity. The compounds $[Cp^*_2SmMe]_3$, $[Cp^*_2LuMe]_2$, $[Cp^*_2LaMe]_x$, $Cp^*_2Sm(CH_2Ph)$, $[Cp^*_2Sm(CH_2SiMe_3)]_x$, and $[Cp^*_2SmPh]_2$ were prepared in this way. The synthetic route leading to the precursor complexes $[Cp^*_2Ln][(\mu\text{-}Ph)_2BPh_2]$ is outlined in Scheme 35 [55].

Initial studies showed that $[Cp^*_2Sm][(\mu\text{-}Ph)_2BPh_2]$ reacts readily with alkyllithium reagents LiR in arene solvents, but the reaction is not useful for the synthesis of $[Cp^*_2SmR]_x$ products because they immediately metalate the arene solvent. To avoid metalation of the solvent, reactions must be conducted in cyclohexane or methylcyclohexane. Although $[Cp^*_2Sm][(\mu\text{-}Ph)_2BPh_2]$ has lower solubility in cyclohexanes, reaction with MeLi occurs according to Scheme 36 under formation of the desired product, $[Cp^*_2SmMe]_3$ (orange solid, 83% yield) [55].

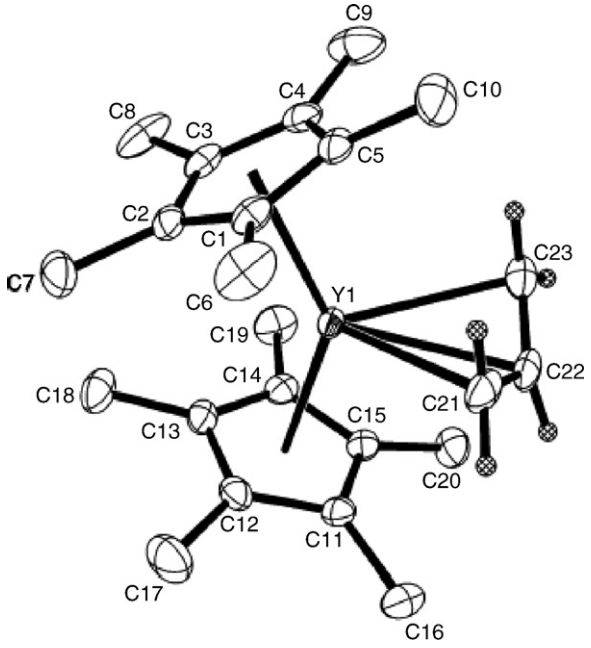

Fig. 30. Molecular structure of $Cp^*_2Ln(C_3H_5)$ [37].

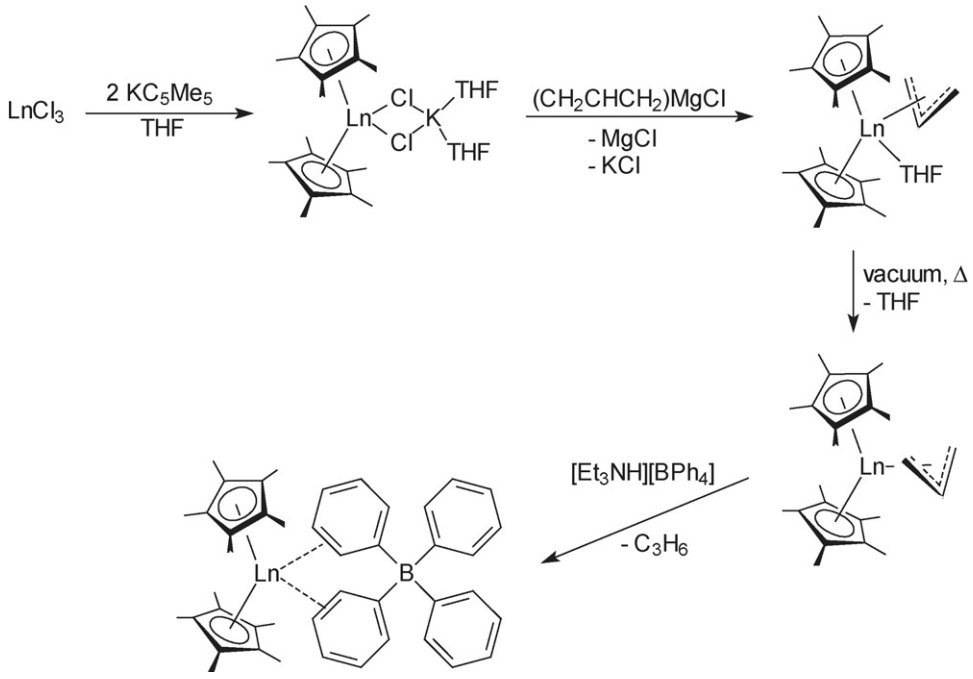

Scheme 35.

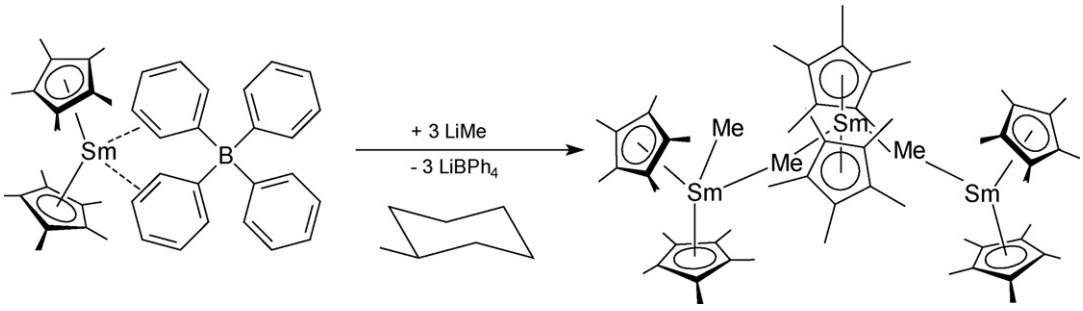

Scheme 36.

The analogous reaction conducted with $[Cp^*_2Lu][(\mu\text{-}Ph)_2BPh_2]$ and MeLi in methylcyclohexane led to the unsolvated dimer $[Cp^*_2LuMe]_2$, which was isolated as colorless crystals in 75% yield (Scheme 37). Its asymmetric, methyl-bridged structure has been determined by X-ray diffraction. Fig. 31 clearly shows the presence of both formally seven- and eight-coordinate lutetium centers [55].

Using the tetraphenylborate alkali metal alkyl reaction method, the benzyl complex $Cp^*_2Sm(CH_2Ph)$ was synthesized in 80% yield from $[Cp^*_2Sm][(\mu\text{-}Ph)_2BPh_2]$ and KCH_2Ph (Scheme 38). A crystal structure analysis revealed the presence of a monomeric *trihapto*-benzyl complex in the solid-state (Fig. 32) [55].

The benzyl complex $Cp^*_2Sm(CH_2Ph)$ was also found to be the primary product in the metalation of toluene by $[Cp^*_2SmMe]_3$ as illustrated in Scheme 39 [55].

Reaction of neopentyllithium, $LiCH_2Bu^t$, with $[Cp^*_2Sm][(\mu\text{-}Ph)_2BPh_2]$ in methylcyclohexane did not lead to the isolation of the expected $[Cp^*_2Sm(CH_2Bu^t)]_x$ but instead generated the trimethylenemethane dianion complex $[\mu\text{-}\eta^3\text{:}\eta^3\text{-}$

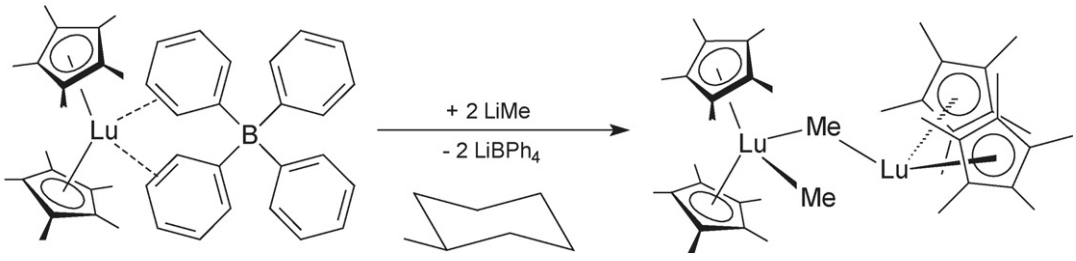

Scheme 37.

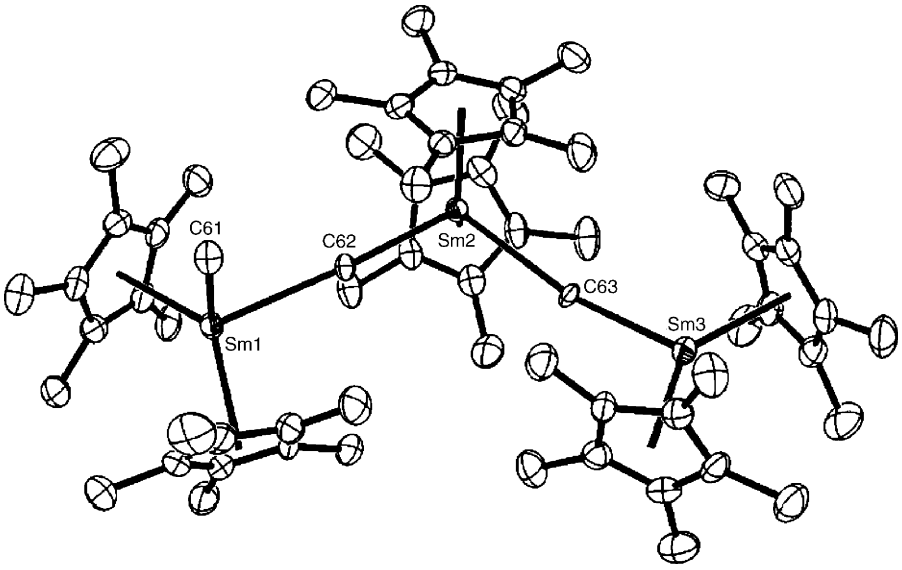

Fig. 31. Molecular structure of $[Cp^*_2LuMe]_2$ [55].

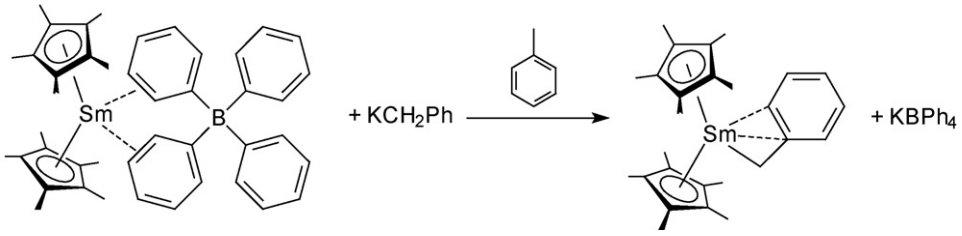

Scheme 38.

$C(CH_2)_3][Cp^*_2Sm]_2$ according to Scheme 40. Fig. 33 depicts the molecular structure of this interesting binuclear complex. The trimethylenemethane ligand in $[\mu\text{-}\eta^3\text{:}\eta^3\text{-}C(CH_2)_3][Cp^*_2Sm]_2$ is unusual in several ways as compared to previously reported transition metal trimethylenemethane complexes. It is the first bridging ligand of this type to be reported in the literature. It is also unusual in that the four carbon atoms are planar within 0.01 Å, which matches calculations for the free trimethylenemethane dianion [56].

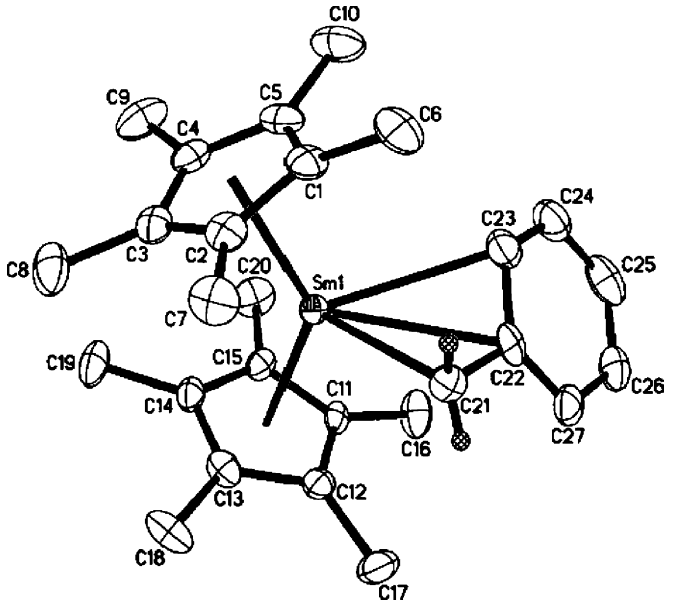

Fig. 32.

A plausible route by which $[\mu\text{-}\eta^3\text{:}\eta^3\text{-}C(CH_2)_3][Cp^*_2Sm]_2$ could be formed from "$[Cp^*_2Sm(CH_2Bu^t)]_x$", the likely initial product of the $LiCH_2Bu^t/[Cp^*_2Sm][(\mu\text{-}Ph)_2BPh_2]$ reaction, involves β-methyl elimination to make $[Cp^*_2SmMe]_3$ and isobutene, $CH_2{=}CMe_2$, as shown in Scheme 41. Subsequent C–H activation of the isobutene by $[Cp^*_2SmMe]_3$ could generate a 2-methylallyl complex, $Cp^*_2Sm[CH_2C(Me)CH_2]$, which could be metalated again by $[Cp^*_2SmMe]_3$ to form $[\mu\text{-}\eta^3\text{:}\eta^3\text{-}C(CH_2)_3][Cp^*_2Sm]_2$ [56].

Addition of one molar equivalent of the heterocyclic carbene $C_3Me_4N_2$ (=tetramethylimidazolylidene) to Cp^*_2CeI in toluene

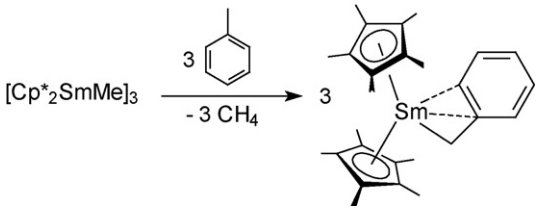

Scheme 39.

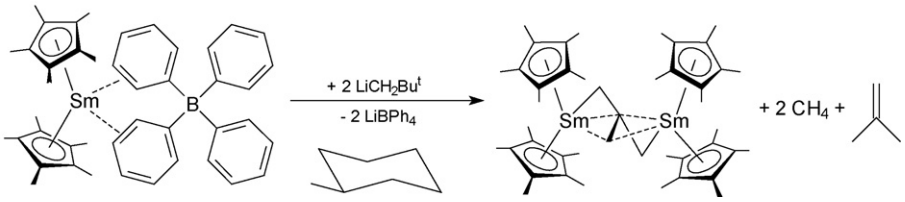

Scheme 40.

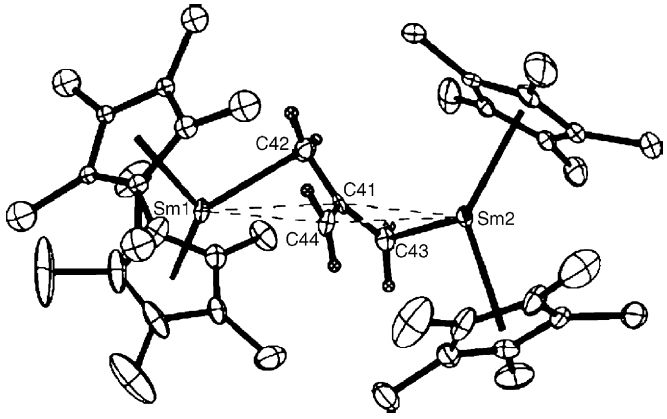

Fig. 33. Molecular structure of $[\mu\text{-}\eta^3{:}\eta^3\text{-}C(CH_2)_3][Cp^*_2Sm]_2$ [56].

led to immediate formation of the first carbene complex of cerium, $Cp^*_2CeI(C_3Me_4N_2)$, which was isolated as orange crystals in 70% yield [57].

The ionic scandium metallocene complex $[Cp^*_2Sc][BPh_4]$ was obtained as a yellow solid in 67% yield by allowing Cp^*_2ScMe to react with $[PhNMe_2H][BPh_4]$ in toluene. In the unsolvated salt the anion interacts weakly with the scandium center through one of the phenyl groups (Fig. 34) [58].

The strongly Lewis acidic species $[Cp^*_2Sc][BPh_4]$ was found to react with fluorobenzene and 1,2-difluorobenzene to yield $[Cp^*_2Sc(\kappa F\text{-}FC_6H_5)_2][BPh_4]$ and $[Cp^*_2Sc(\kappa^2F\text{-}1,2\text{-}F_2C_6H_4)][BPh_4]$, the first examples of κF-fluorobenzene and κ^2F-1,2-difluorobenzene adducts of transition metals. Fig. 35 depicts the molecular structures of these fluoroarene scandium complexes [58].

Treatment of Cp^*_2ScMe with $[PhNMe_2H][B(C_6F_5)_4]$ instead of $[PhNMe_2H][BPh_4]$ resulted in formation of $[Cp^*_2Sc(\kappa^2F\text{-}C_6F_5)B(C_6F_5)_3]$, which was isolated in 62% yield. In the solid-state structure of $[Cp^*_2Sc(\kappa^2\textit{F}\text{-}C_6F_5)B(C_6F_5)_3]$ (Fig. 36) the anions are coordinated to the scandium center in a κ^2F-fashion with two adjacent C–F bonds, comparable to the 1,2-difluorobenzene adducts. The nature of the scandium–fluoroarene interaction was studied by density functional theory (DFT) calculations and by comparison with the corresponding THF adducts and was found to be predominantly electrostatic [58].

The scandium dihydrosilyl complexes $Cp^*_2ScSiH_2R$ (R = Mes, Trip, $SiPh_3$, $Si(SiMe_3)_3$; Trip = 2,4,6-$Pr^i_3C_6H_2$) have been synthesized by addition of the appropriate hydrosilane to Cp^*_2ScMe. Studies of these complexes in the context of hydrocarbon activation led to discovery of catalytic processes for the dehydrogenative silylation of hydrocarbons (including methane, isobutene and cyclopropane) with Ph_2SiH_2 *via* σ-bond metathesis. In the course of this investigation, the molecular structures of $Cp^*_2ScSiH_2SiPh_3$ (Fig. 37) and $Cp^*_2ScSiH(SiMe_3)_2$ (Fig. 38) have been determined by single-crystal X-ray diffraction [59].

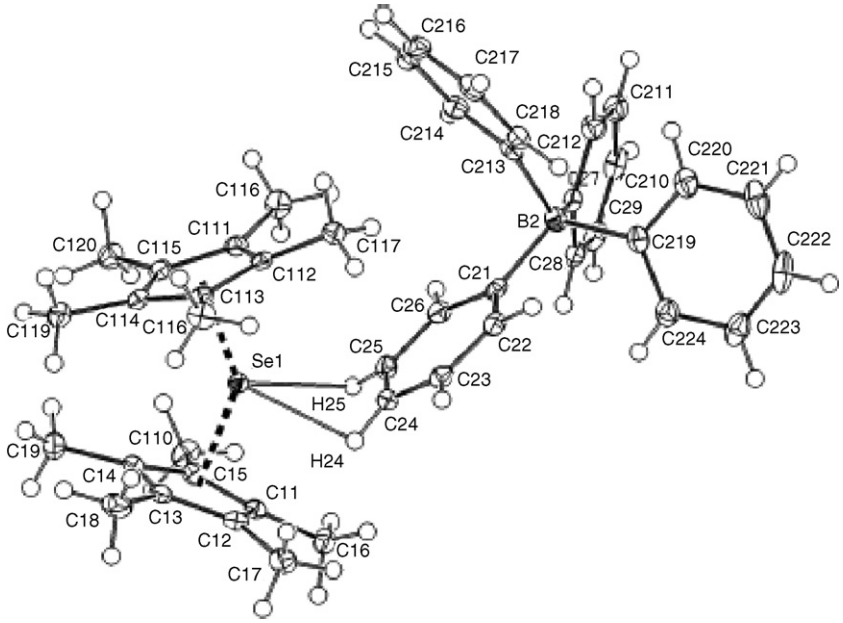

Fig. 34. Molecular structure of $[Cp^*_2Sc][BPh_4]$ [58].

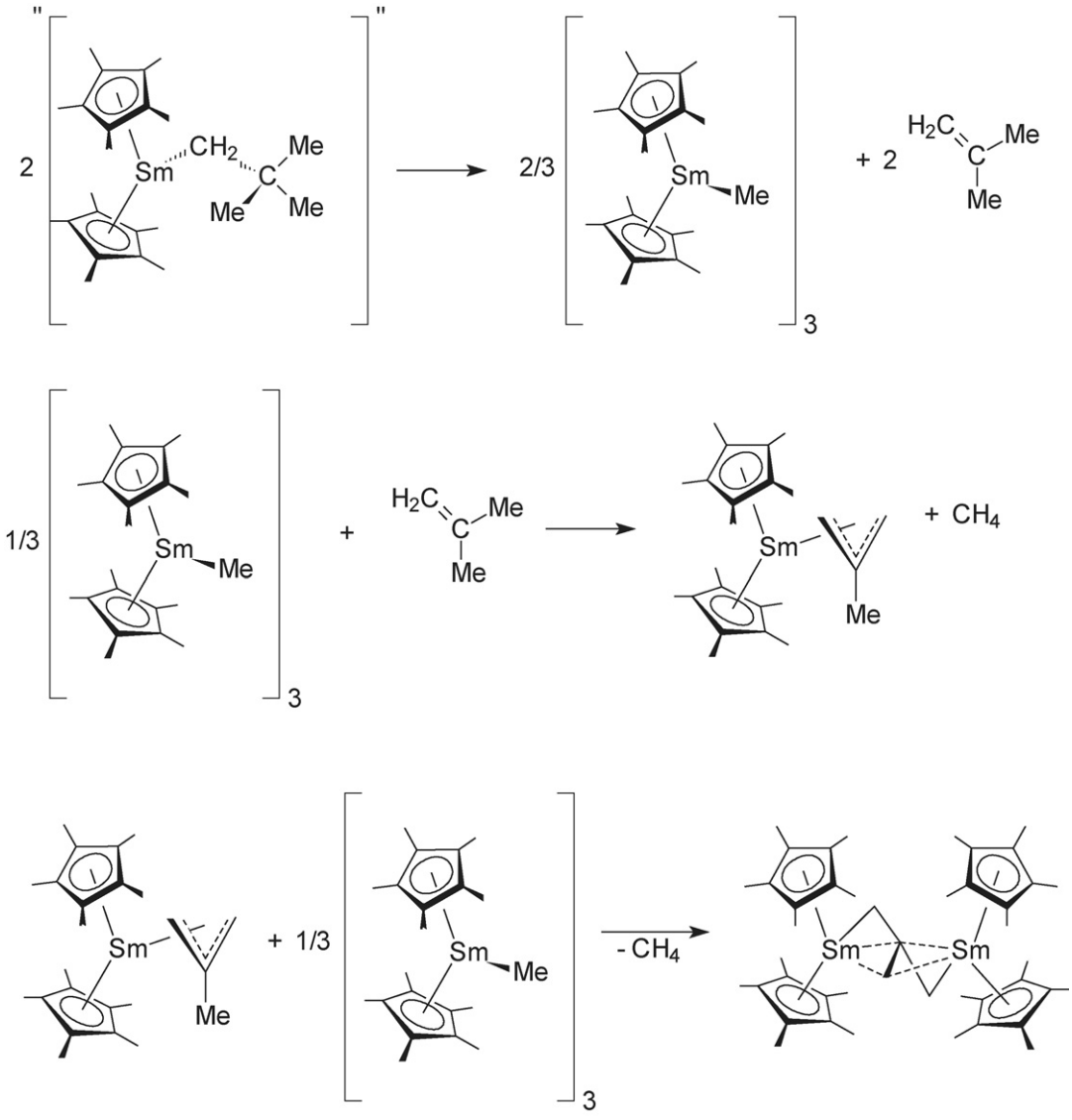

Scheme 41.

$[Cp^*_2LaH]_x$ reacts with BEt_3 to afford a product of composition $Cp^*_2La(HBEt_3)$ according to Scheme 42. X-ray crystallography revealed a structure in which the $(HBEt_3)^-$ ligand approaches the trivalent $[Cp^*_2La]^+$ unit not only with the hydride attached to boron, but also with two of the ethyl groups. Since the hydrogen positions could be located and refined, closer inspection showed that one hydrogen substituent from each bridging ethyl group is oriented toward lanthanum (Fig. 39) [60].

Crystallization of $Cp^*_2La(HBEt_3)$ from toluene-d_8 in the presence of 1 equiv. of THF led to a THF adduct of the formula $Cp^*_2La(HBEt_3)(THF)$ (Scheme 43) [60].

In this complex the $(HBEt_3)^-$ ligand also ligates the lanthanum center with the hydride attached to boron, but in this case only one ethyl group is oriented toward the lanthanide. Once again the bridging hydrogen positions could be located and refined (Fig. 40) [60].

In the course of working with $[Cp^*_2LaH]_x$ the hydride-bridged "tuckover" complex $Cp^*_2La(\mu\text{-}H)(\mu\text{-}\eta^1{:}\eta^5\text{-}CH_2C_5Me_4)LaCp^*$ was also isolated (Scheme 44) and the structure of this internal C–H activation product determined (Fig. 41) [60].

2.5.6.4. Tris(pentamethylcyclopentadienyl)lanthanide(III) compounds. The displacements of the methyl substituents away from the metal and out of the cyclopentadienyl ring plane have been compared in sterically crowded Cp^*_3M (M = Ln, Ac) complexes *versus* sterically normal *f*-element complexes in an attempt to evaluate the utility of this parameter in predicting unusual Cp^* ring reactivity. The out-of-plane displacements of 16 sterically crowded tris(cyclopentadienyl) complexes of the general formulas Cp^*_3M, $(C_5Me_4R)_3M$ (R = Et, Pr^i, Bu^t, $SiMe_3$), Cp^*_3MX (X = anionic ligand), and Cp^*_3ML (L = neutral ligand) were compared with $(\mu\text{-}C_6H_6)[Cp^*_2U]_2$, $Cp^*_2Sm(PC_4H_2Bu^t_2)$, and 33 representative examples of *f*-element bis(cyclopentadienyl) complexes with normal cyclopentadienyl behavior and coordination numbers ranging from 6 to 10. In general, the methyl displacement values

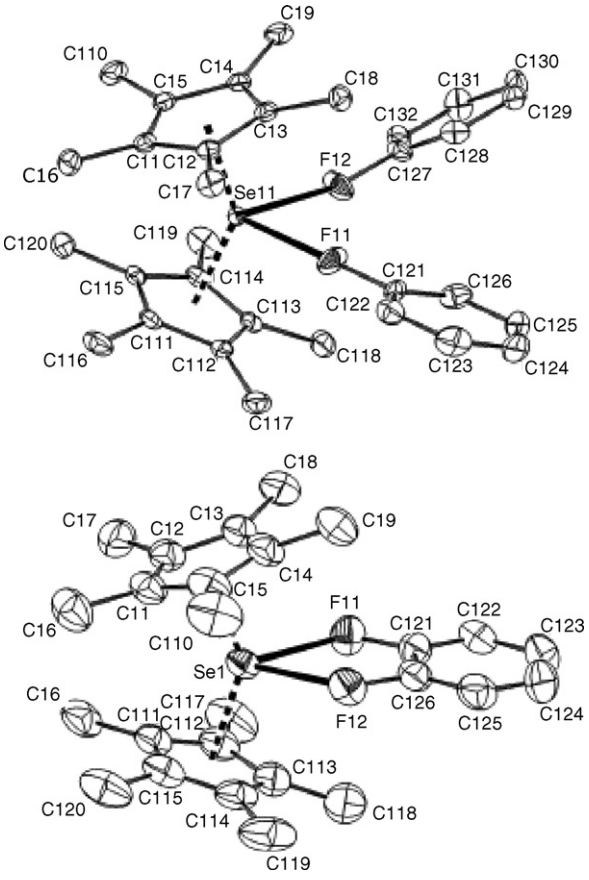

Fig. 35. Molecular structures of the cations in $[Cp^*_2Sc(\kappa F\text{-}FC_6H_5)_2][BPh_4]$ and $[Cp^*_2Sc(\kappa^2F\text{-}1,2\text{-}F_2C_6H_4)][BPh_4]$ [58].

of sterically crowded complexes overlap with those in the other complexes, which demonstrates that the basis of the structural distortions is complex. However, if the most extreme out-of-plane displacement in each of the sterically crowded

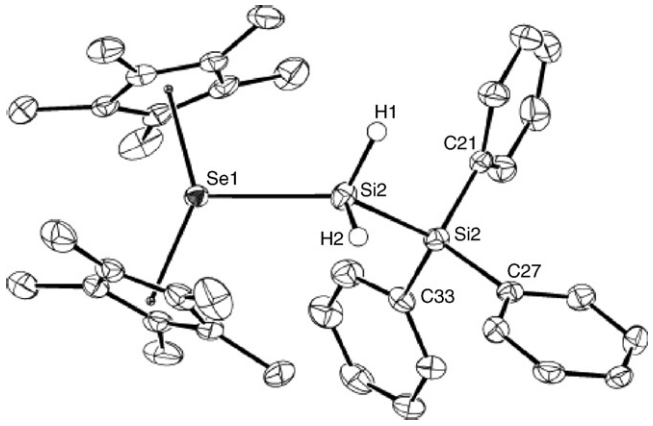

Fig. 37. Molecular structure of $Cp^*_2ScSiH_2SiPh_3$ [59].

complexes is examined versus the analogous maximum out-of-plane displacement in less crowded systems, there appears to be a basis for predicting cyclopentadienyl reactivity. Representations of (a) Cp^*_3Sm and (b) $Cp^*_2Sm[N(SiMe_3)_2]$ that highlight the out-of-plane methyl substituent displacements are shown in Fig. 42 [61].

The series of sterically crowded Cp^*_3Ln complexes has been completed for the larger lanthanides La–Nd and Sm by the synthesis of Cp^*_3Ce and Cp^*_3Pr from $[Cp^*_2Ln][(\mu\text{-}Ph)_2BPh_2]$ and KCp^*. Synthesis of these new Cp^*_3Ln complexes required silylated glassware, which surprisingly was not necessary for the more sterically crowded analogues. Cp^*_3Ce and Cp^*_3Pr display longer Ln–C(Cp^*) distances than any previously described Ce or Pr complexes containing the Cp^* ligand. The η^1-Cp^* alkyl-like reactivity of the Cp^*_3Ln complexes was investigated with CO, ethylene, THF, and H_2. The sterically induced reduction (SIR) reactivity of the Cp^*_3Ln complexes was examined with $Se{=}PPh_3$, $AgBPh_4$, C_8H_8, and phenazine. The reactivity of Cp^*_3Ln with CO_2 and with $[Et_3NH][BPh_4]$ was examined since each sub-

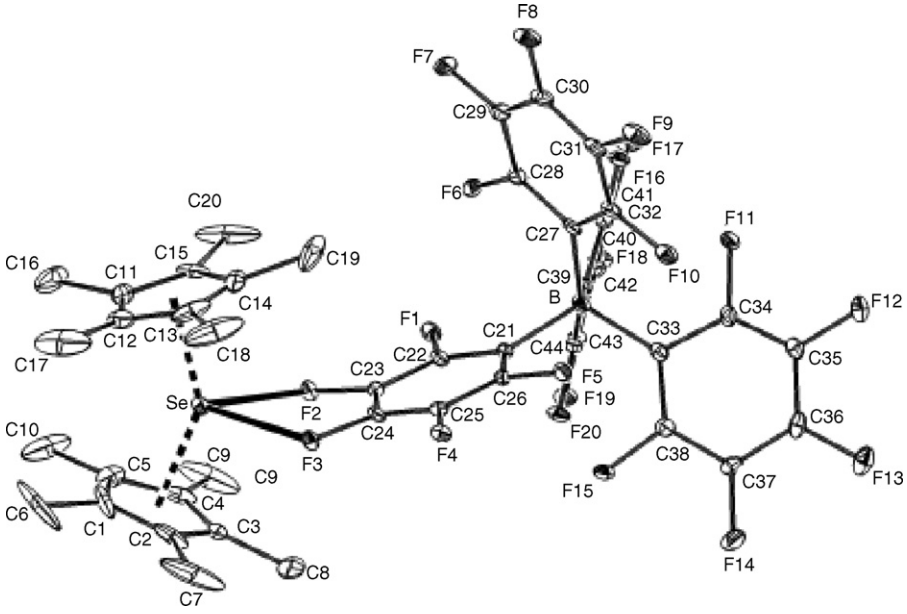

Fig. 36. Molecular structure of $[Cp^*_2Sc(\kappa^2F\text{-}C_6F_5)B(C_6F_5)_3]$ [58].

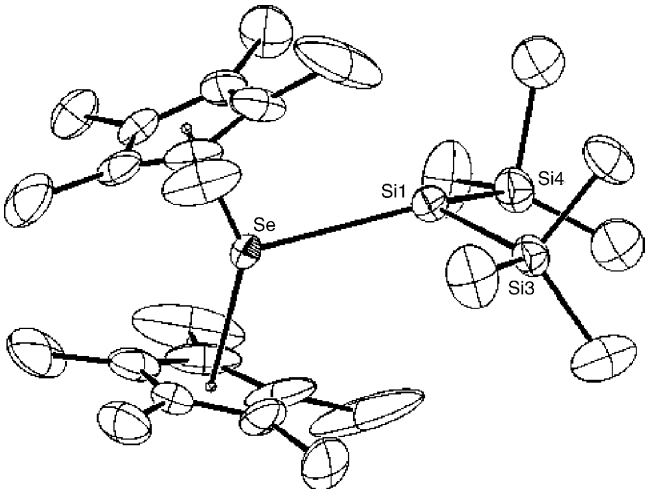

Fig. 38. Molecular structure of $Cp^*_2ScSiH(SiMe_3)_2$ [59].

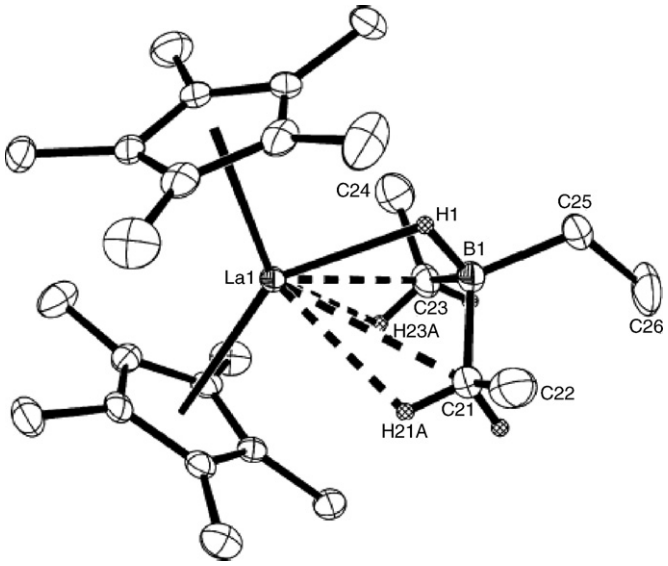

Fig. 39. Molecular structure of $Cp^*_2La(HBEt_3)$ [60].

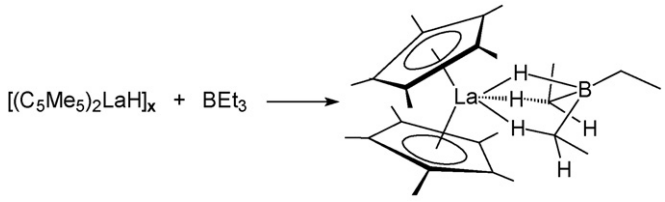

Scheme 42.

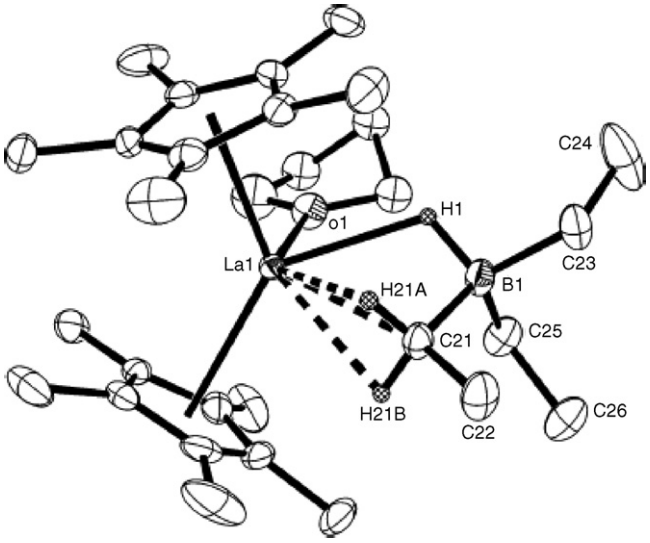

Fig. 40. Molecular structure of $Cp^*_2La(HBEt_3)(THF)$ [60].

strate could react by either the η^1-Cp^* alkyl or SIR pathways. In both cases, alkyl-like reactivity was observed: CO_2 forms the insertion product $Cp^*_2Ln(O_2CCp^*)$, containing a carboxylate with a pentamethylcyclopentadienyl substituent (Scheme 45), and $[Et_3NH][BPh_4]$ forms $[Cp^*_2Ln][(\mu\text{-}Ph)_2BPh_2]$ and Cp^*H. Fig. 43 depicts the molecular structure of the samarium carboxylate derivative $Cp^*_2Sm(O_2CCp^*)$ [62].

2.5.7. *Compounds with ring-bridged cyclopentadienyl ligands*

A series of *ansa*-lanthanocene complexes containing the dimethyl-bis(3-(1-methyl-1-phenylethyl)-2, 4 - cyclopentadien-1-yl]silane ligand have been prepared [63]. The dimethylsilyl-bridged bis(cyclopentadienyl) ligands $[Me_2Si(C_5H_2Bu^t_2\text{-}2,4)_2]^{2-}$ and $[Me_2Si\{C_5H_2(SiMe_3)_2\}_2]^{2-}$ have been prepared and used for the preparation of divalent ytterbium *ansa*-metallocene complexes. The molecular structures of *ansa*-$[Me_2Si(C_5H_2Bu^t_2\text{-}2,4)_2]Yb(OEt_2)$ and an analogous isocyanide complex have been determined [64]. The *ansa*-complex $[Me_2Si(C_5Me_4)_2]ScMe$ was isolated in 45% yield from the reaction of $[Me_2Si(C_5Me_4)_2]ScCH_2CCH(CH_2CH_3)_2$ with methane according to Scheme 46. The rate of the C–H bond activation of methane by $[Me_2Si(C_5Me_4)_2]ScMe$ was found to be 2 orders of magnitude greater than that by Cp^*_2ScMe. Compound $[Me_2Si(C_5Me_4)_2]ScMe$ is a catalyst for the addition of methane across the double bond of secondary terminal olefins [65].

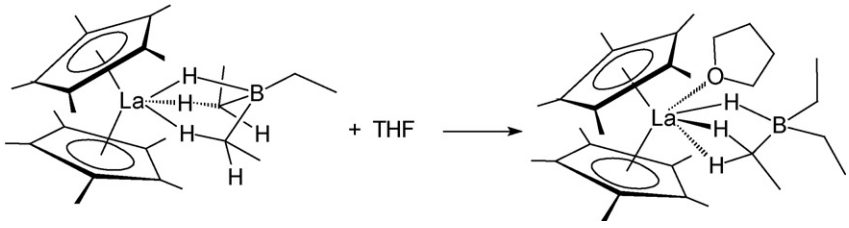

Scheme 43.

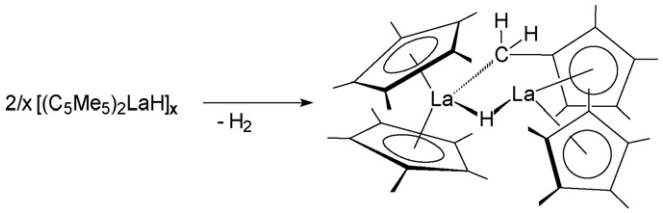

Scheme 44.

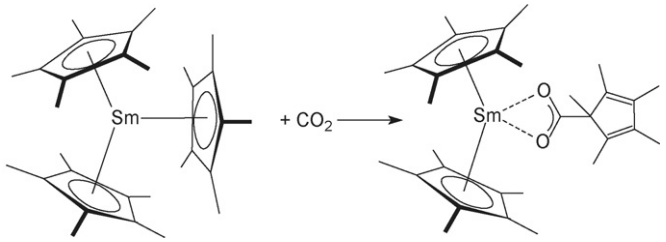

Scheme 45.

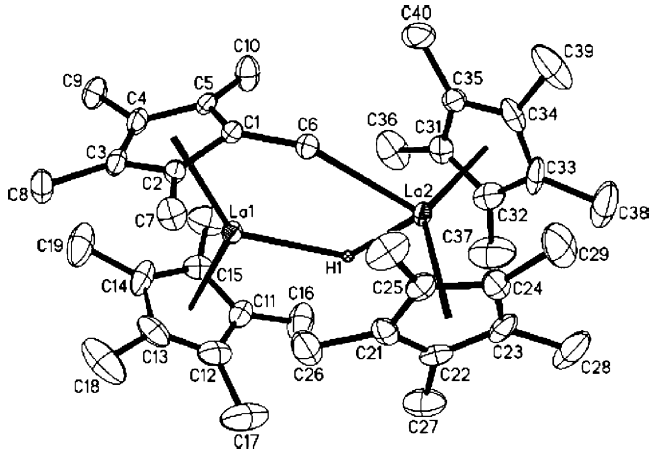

Fig. 41. Molecular structure of $Cp^*_2La(\mu\text{-}H)(\mu\text{-}\eta^1{:}\eta^5\text{-}CH_2C_5Me_4)LaCp^*$ [60].

An yttrium allyl complex containing a dimethylsilyl-bridged *ansa*-cyclopentadienyl ligand has been prepared according to Scheme 47. The molecular structure of the THF-free product has been determined by X-ray diffraction (Fig. 44) [37].

2.5.8. Indenyl and fluorenyl compounds

A review article entitled "Groups 2 and 3 metal complexes incorporating fluorenyl ligands" has been published by Carpentier et al [66]. It covers fluorenyl complexes of di- and trivalent lanthanides and related group 3 metals as well as their applications in catalysis.

2.5.8.1. Lanthanide(II) compounds. Several organolanthanide(II) complexes containing furfuryl- and tetrahydrofurfuryl-functionalized indenyl ligands have been prepared and structurally characterized. The molecular structure of the tetrahydrofurfuryl-substituted derivative $[\eta^5{:}\eta^1\text{-}(C_4H_7OCH_2C_9H_5SiMe_3)]_2Yb$ (Fig. 45) clearly shows the participation of the tetrahydrofurfuryl oxygen donor atoms in the coordination to ytterbium(II) [67].

2.5.8.2. Lanthanide(III) compounds. The molecular structure of two monomeric lanthanide mono(fluorenyl) complexes, $(\eta^5\text{-fluorenyl})LnI_2(py)_3$ (Ln = La, Nd) have been determined by X-ray diffraction. Both contain two *trans*-disposed iodides and three meridionally oriented pyridine molecules in addition to the

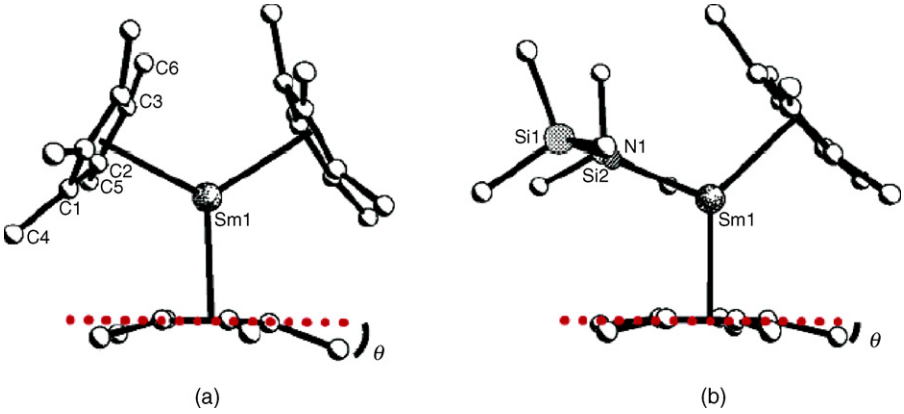

Fig. 42. Molecular structures of (a) Cp^*_3Sm and (b) $Cp^*_2Sm[N(SiMe_3)_2]$ [61].

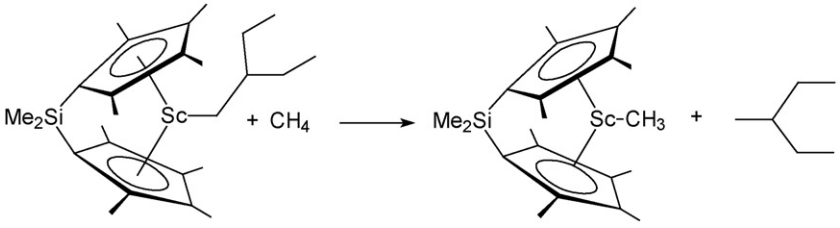

Scheme 46.

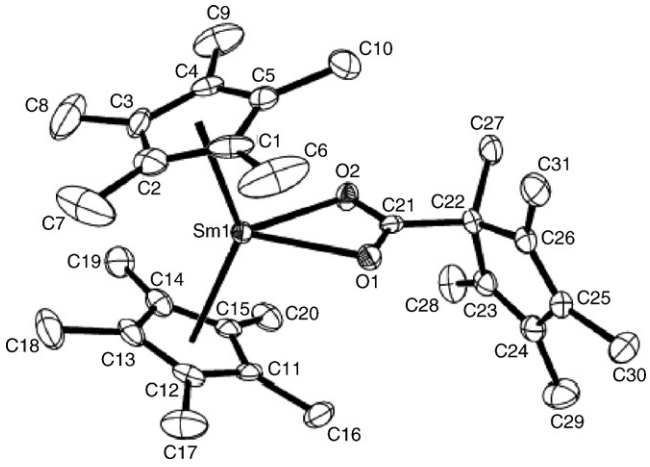

Fig. 43. Molecular structure of $Cp^*_2Sm(O_2CCp^*)$ [62].

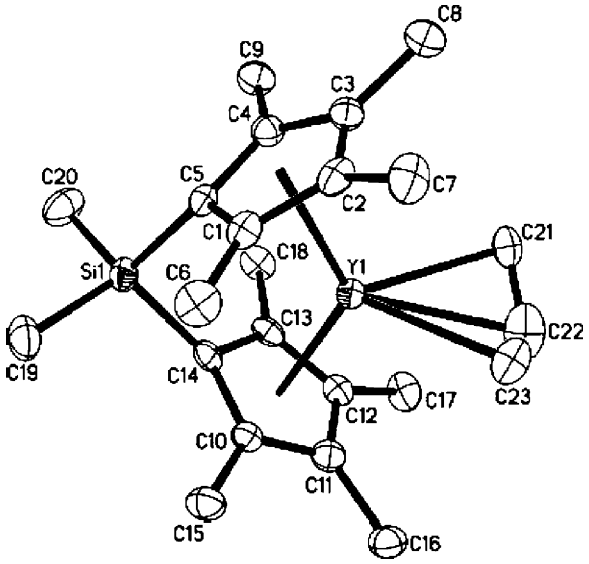

Fig. 44. Molecular structure of $[Me_2Si(C_5Me_4)_2]Y(C_3H_5)$ [37].

pentahapto-coordinated fluorenyl ligand [68]. The homoleptic lanthanide tris(aryls) (o-$Me_2NC_6H_4CH_2)_3Ln$ (Ln = Y, La) have been shown to deprotonate fluorenes and alkylamines. They could thus serve as interesting precursors in the synthesis of constrained-geometry catalysts based on lanthanides. Reaction of the yttrium derivative with the ligand 9-*t*-BuN(H)$SiMe_2$-fluorene in THF to give the heteroleptic benzylyttrium complex (9-*t*-BuN(H)$SiMe_2$-fluorene)(o-$Me_2NC_6H_4CH_2$)Y(THF) in the form of orange crystals in 85% yield (Scheme 48). The crystal structure revealed an allylic coordination mode for the fluorenyl ligand [5].

The heteroleptic benzylyttrium complex (9-*t*-BuN(H)$SiMe_2$-fluorene)(o-$Me_2NC_6H_4CH_2$)Y(THF) can easily be converted into an yttrium hydride complex. Hydrogenation with molecular hydrogen (10 bar) gave crystals of the dimeric yttrium hydride species in 84% isolated yield (Scheme 49) [5].

2.6. Organolanthanide complexes with cyclopentadienyl-like ligands

2.6.1. Compounds with heteroatom five-membered ring ligands

Thulium(II) phospholyl sandwich complexes containing the 2,5-di-*t*-butyl-3,4-dimethylphospholide (=dtp) or 2,5-bis(trimethylsilyl)-3,4-dimethylphospholide (=dsp) ligand have been synthesized from thulium diiodide according to Scheme 50 and structurally characterized. X-ray studies revealed that they are both monomeric in the solid-state [26].

The C–H activation (γ-deprotonation of a methyl group) of a samarium(III) bis(trimethylsilyl)amide complex has been reported for a samarium complex stabilized by a macrocyclic dimetallated *trans*-dioxaporphyrinogen ligand [69]. η^5–π-Interactions between europium centers and pyrrolate and pyrrole ligands have been detected in the crystal structure of a polymeric europium pyrrolate, [70] while η^2-agostic C–H interactions to Er and Yb have been found in the first lanthanide complexes

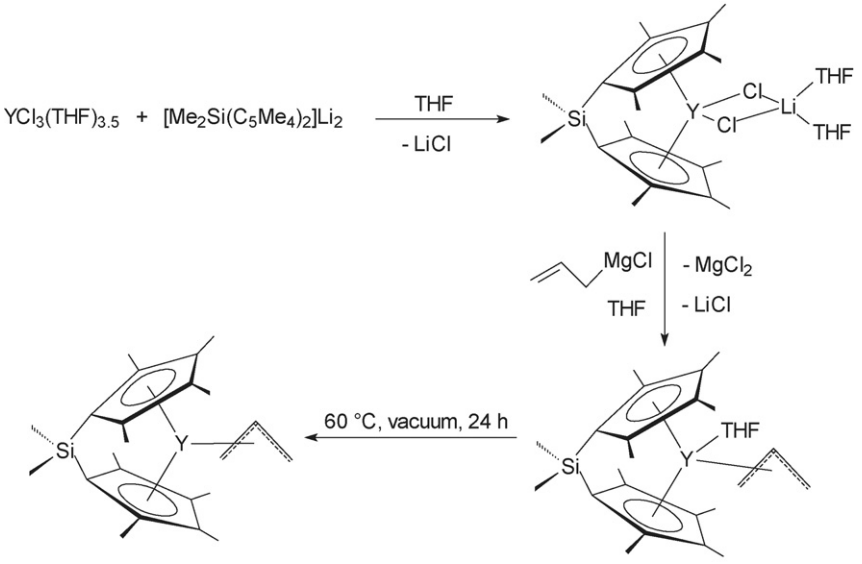

Scheme 47.

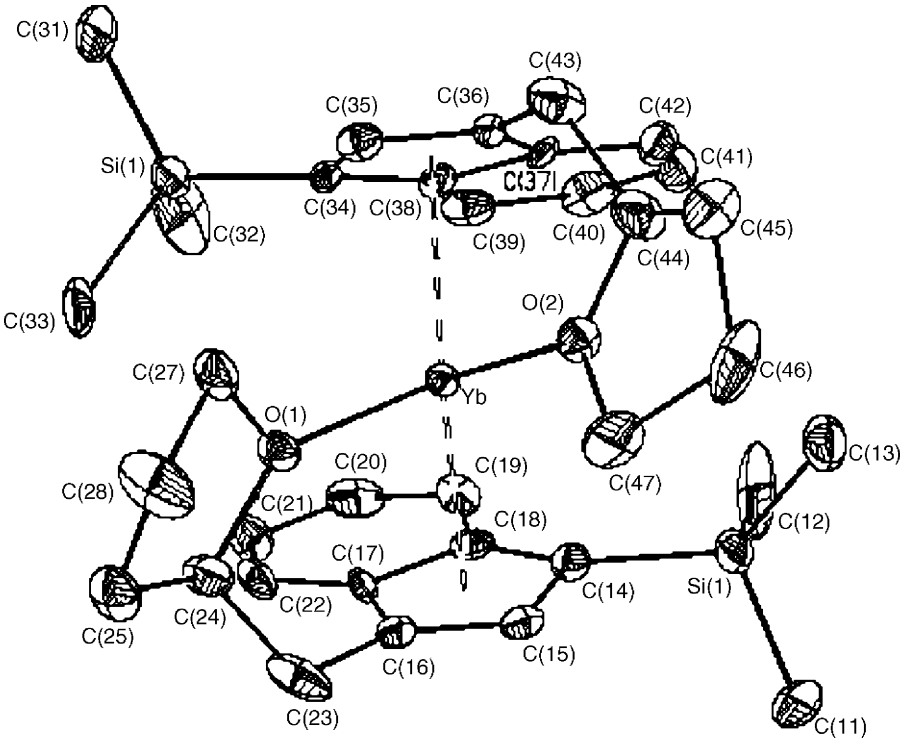

Fig. 45. Molecular structure of $[\eta^5{:}\eta^1\text{-}(C_4H_7OCH_2C_9H_5SiMe_3)]_2Yb$ [67].

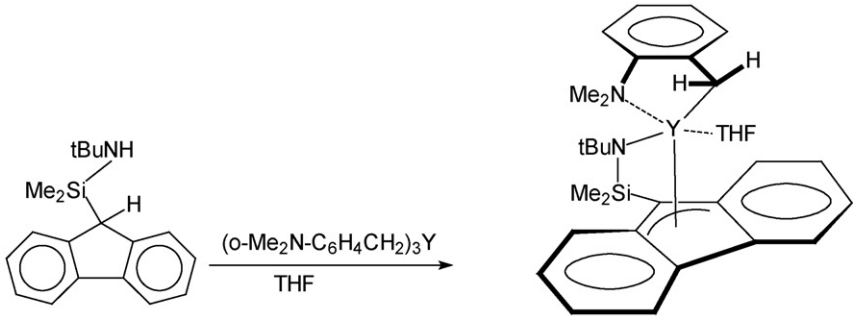

Scheme 48.

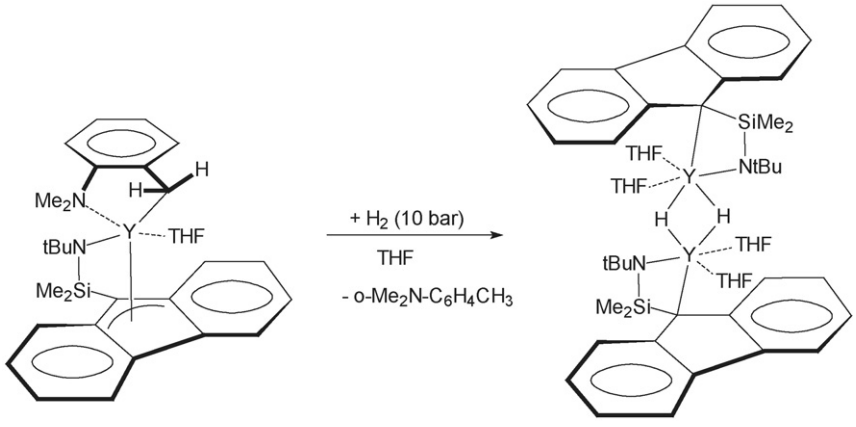

Scheme 49.

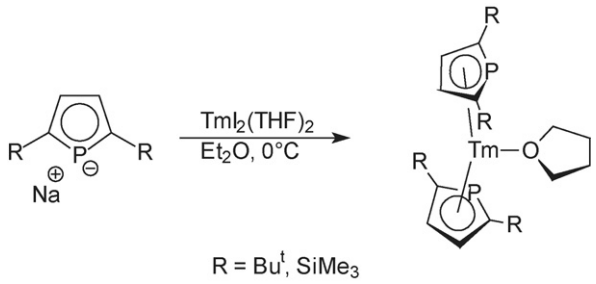

Scheme 50.

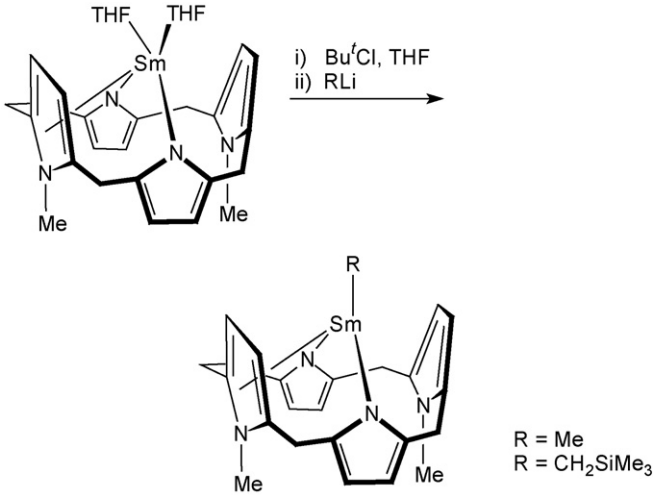

Scheme 51.

of an N-confused porphyrin ligand [71]. Alkylsamarium(III) complexes of a dimetalated porphyrinogen have been synthesized that have strong resemblance to samarocene(III) alkyl complexes (Scheme 51). The monomeric complexes are free of alkali metals, halides, and coordinating solvent. The methyl and (trimethylsilyl)methyl complexes have been fully characterized, including X-ray structural analyses. Fig. 46 highlights the molecular structure of the methyl derivative. Initial reactivity studies indicated a low reactivity of these lanthanide alkyls [72].

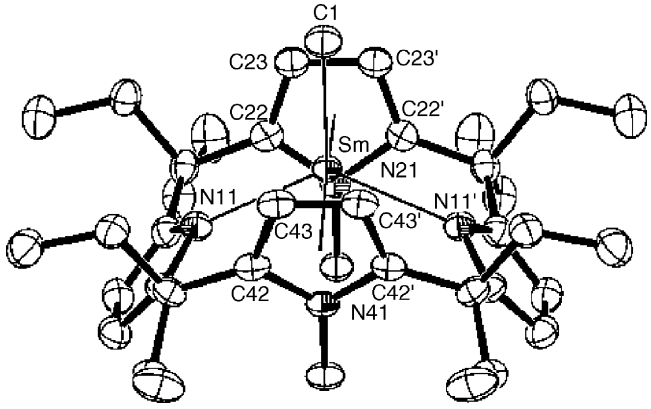

Fig. 46. Molecular structure of (porphyrinogen)SmMe [72].

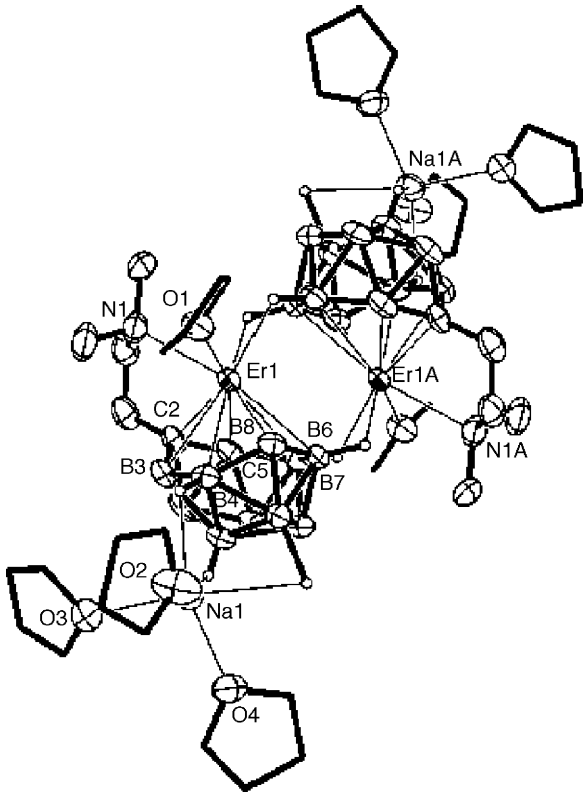

Fig. 47. Molecular structure of $[\{\eta^1{:}\eta^7\text{-}[(Me_2NCH_2CH_2)C_2B_{10}H_{11}]Er(THF)\}\{Na(THF)_3\}]_2$ [73].

2.6.2. Compounds with carboranyl ligands

The synthesis, structural characterization, and reactivity of 13-vertex lanthanacarboranes bearing η^7-*arachno*-carboranyl ligands have been reported. Treatment of 1-$Me_2NCH_2CH_2$-1,2-$C_2B_{10}H_{11}$ with $LnCl_3$ in the presence of excess Na metal gave, after recrystallization from a combination of solvents, the 13-vertex-lanthanacarboranes shown in Scheme 52. Various complexes in this system have been structurally characterized by X-ray diffraction. As a typical example, the molecular structure of $[\{\eta^1{:}\eta^7\text{-}[(Me_2NCH_2CH_2)C_2B_{10}H_{11}]Er(THF)\}\{Na(THF)_3\}]_2$ is depicted in Fig. 47 [73].

Reactions of $Na_2[nido\text{-}(Me_2NCH_2CH_2)RC_2B_{10}H_{10}]$ (R = H, $MeOCH_2CH_2$, $Me_2NCH_2CH_2$) with $SmI_2(THF)_x$ also gave unprecedented metallacarboranes with η^7-*arachno*-carboranyl ligands, in which the heteroatom-containing pendant sidearms are involved in the coordination to samarium [74]. In a similar manner the Lewis base-appended carborane derivatives 1-$Me_2NCH_2CH_2$-1,2-$C_2B_{10}H_{11}$ and 7-$Me_2NHCH_2CH_2$-7,8-$C_2B_9H_{11}$ have been employed as starting materials in the synthesis of various organolanthanide complexes incorporating the corresponding anions [75].

2.7. Lanthanide arene complexes

The low lying electronic states of the scandium–benzene complex $Sc(C_6H_6)$ have been investigated by performing complete active-space self-consistent field and multireference configuration interaction calculations. Geometries, energetics, and electronic structure have been presented and discussed [76]. In

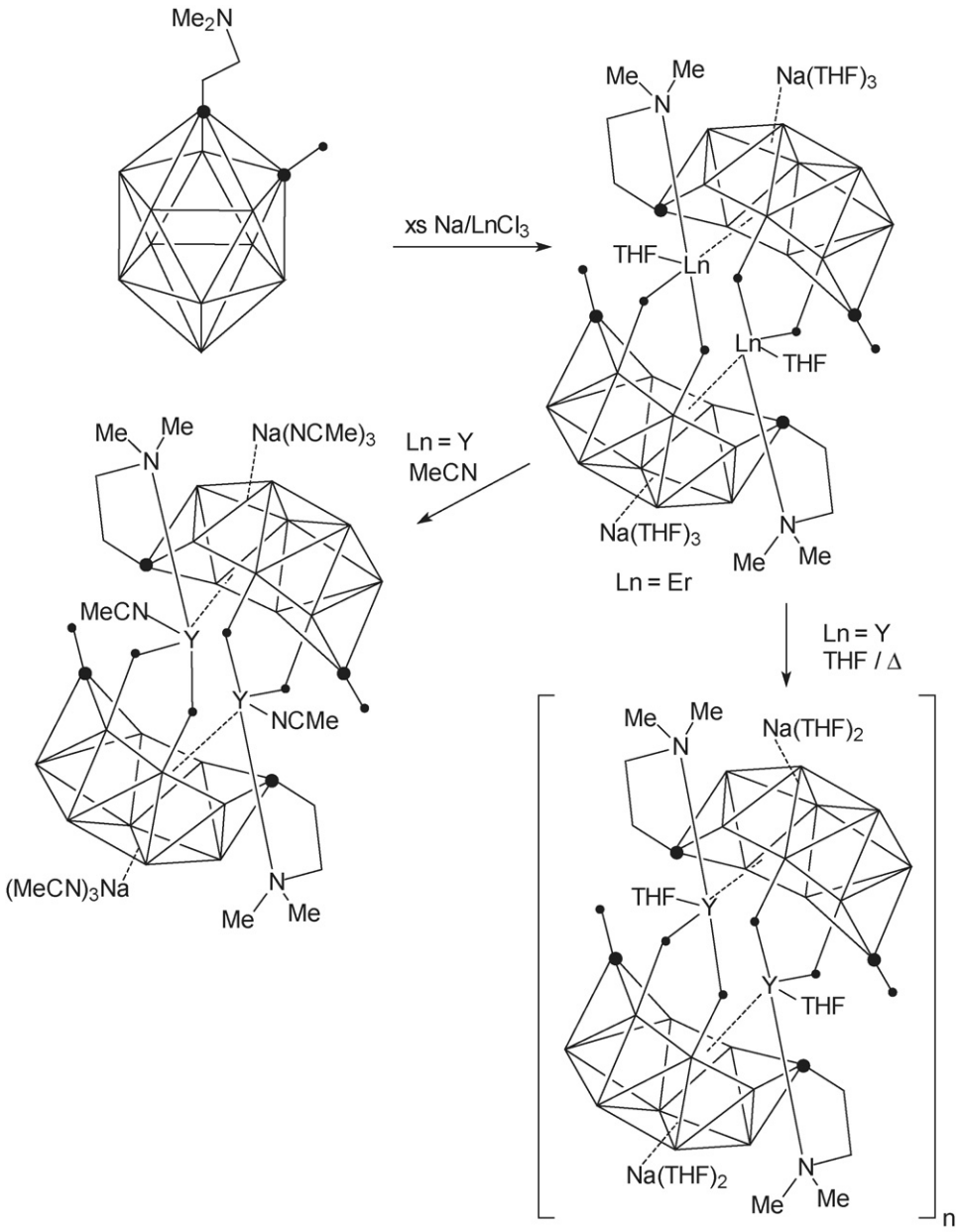

Scheme 52.

a related study, the electronic and magnetic properties of the proposed one-dimensional scandium–benzene sandwich polymer $[Sc(C_6H_6)]_\infty$ has been investigated by means of density functional calculations. It was demonstrated that stretching the $[M(C_6H_6)]_\infty$ (M = transition metal) polymers could have dramatic effects on their electronic and magnetic properties [77]. The formation of lanthanide–benzene complexes $Ln(C_6H_6)_n^+$ (Ln = Y, La; n = 1–3) and $LnC_n(C_6H_6)_m^+$ (Ln = Y, La; n = 4, 6; m = 1, 2) in gas-phase ion-molecule reactions of lanthanide carbide cations MC_n^+ (Ln = Y, La; n = 2, 4, 6) with benzene and cyclohexane has been investigated by FTICR mass spectrometry and DFT calculations [78].

The *p*-benzosemiquinone radical anion ($Q^{\bullet-}$) forms a 2:2 π-dimer radical anion complex ($Q^{\bullet-}$-$(Sc^{3+})_2$-Q) with Q and Sc^{3+} ions at 25 °C (yellow color), which is converted to a 2:3 π-dimer radical anion complex ($Q^{\bullet-}$-$(Sc^{3+})_3$-Q) with a strong absorption band at λ_{max} = 604 nm (blue color) when the temperature is lowered to −70 °C. The change in the number of binding Sc^{3+} ions depending on temperature also results in the remarkable color change, associated with a change in the ESR spectra. The central Sc^{3+} ion in ($Q^{\bullet-}$-$(Sc^{3+})_3$-Q) was proposed to be sandwiched between the two η^6-coordinated benzene rings [79]. π-Arene interactions have been detected in the solid-state structures of a series of ionic lanthanide complexes derived from chiral, substituted (*R*)-binaphthylamine ligands, $[Li(THF)_4][Ln\{(R)\text{-}C_{20}H_{12}(NR)_2\}_2]$ (Ln = Nd, Sm, Yb, Lu; R = Pr^i, CH_2Pr^i, CH_2Ph), [80], in low-temperature condensates formed from lanthanide atoms and 4-pentyl-4′-cyanobiphenyl, [81] in samarium and ytterbium complexes formed with carbazol and *N*-phenylpiperazine, [82] and in dysprosium aryloxides [83].

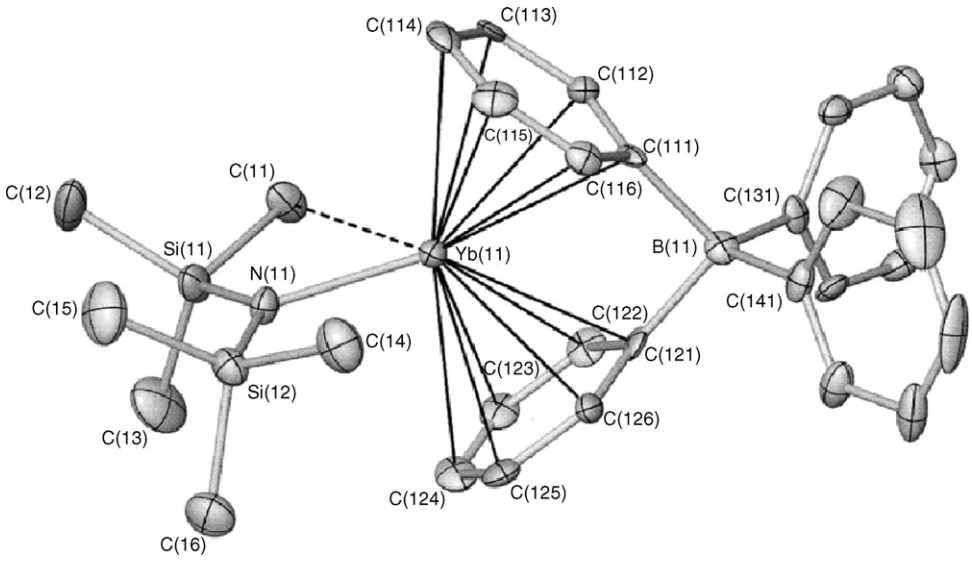

Fig. 48. Molecular structure of $Yb[N(SiMe_3)_2]BPh_4$ [84].

The ytterbium(II) complexes $Yb(Bu_2^tpz)(THF)BPh_4$ (Bu_2^t-pz = 3,5-di-*tert*-butylpyrazole) and $Yb[N(SiMe_3)_2]BPh_4$ have been synthesized by reaction of $Yb[N(SiMe_3)_2](THF)BPh_4$ with Bu_2^tpz or by *in situ* desolvation of the THF complex $Yb[N(SiMe_3)_2](THF)BPh_4$. X-ray analyses of these complexes revealed η^6:η^6-binding of chelating BPh_4^- to ytterbium in both cases, generating true metallocene structures. The silylamide $Yb[N(SiMe_3)_2]BPh_4$ is distingushed by a very short Yb–N bond and an agostic Yb–Me interaction, both indicative of a highly Lewis acidic metal center (Fig. 48) [84].

The stabilization of unsolvated europium and ytterbium pentafluorophenyls by π-bonding encapsulation through a sterically crowded triazenido ligand has been reported. The one-pot transmetalation/deprotonation reaction of the bulky triazene

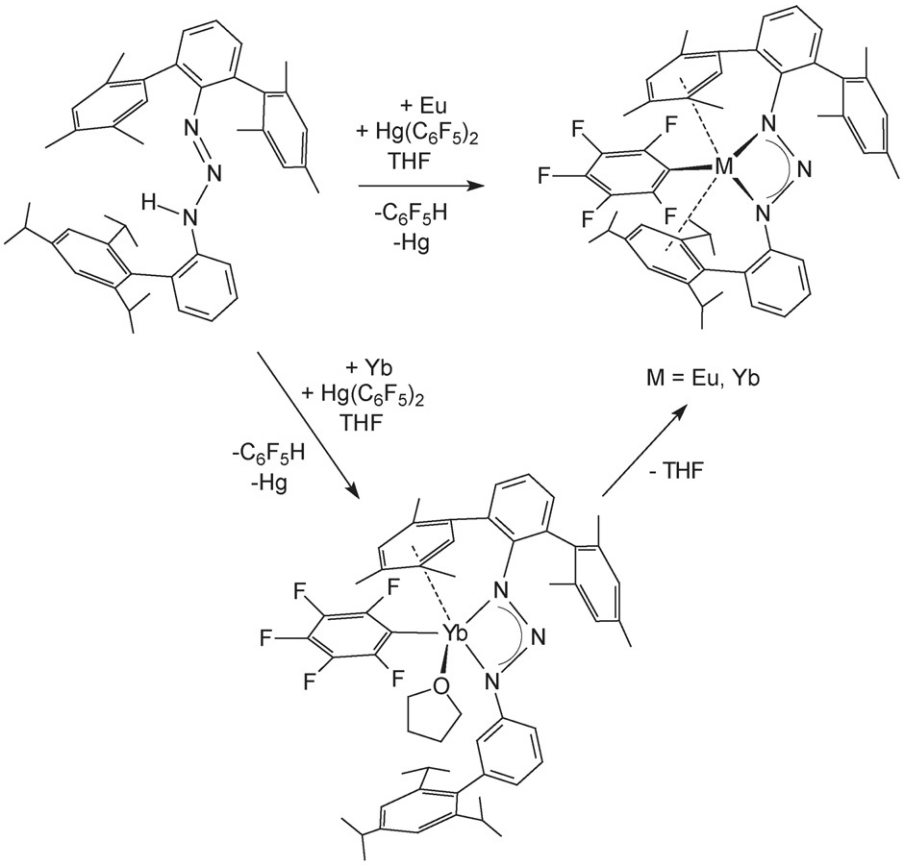

Scheme 53.

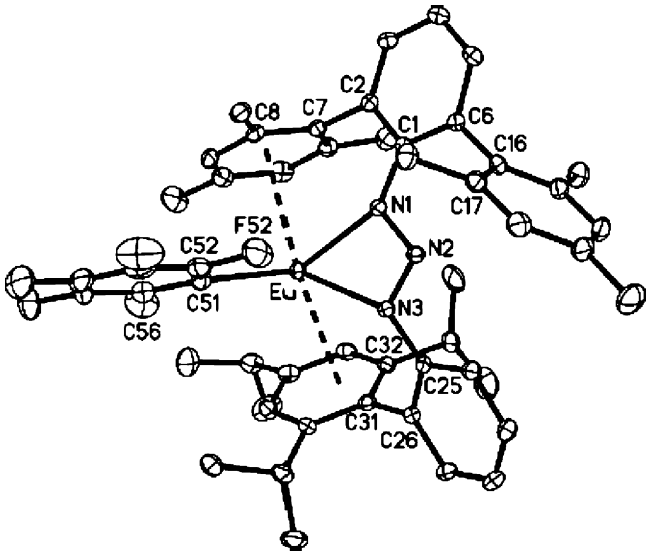

Fig. 49. Molecular structure of $[Dmp(Tph)N_3]EuC_6F_5$ [85].

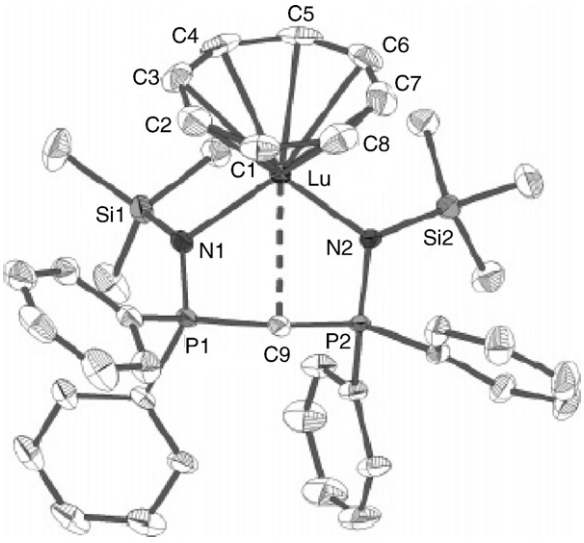

Fig. 50. Molecular structure of $(COT)Lu[CH(PPh_2NSiMe_3)_2]$ [91].

$Dmp(Tph)N_3H$ (Dmp = 2,6-(2,4,6-$Me_3C_6H_2$)$_2C_6H_3$, Tph = 2-(2,4,6-$Pr_3^iC_6H_2$)C_6H_4) with bis(pentafluorophenyl)mercury and europium or ytterbium afforded the structurally characterized unsolvated metal(II) pentafluorophenyl triazenides $[Dmp(Tph)N_3]LnC_6F_5$ or, depending on the molar ratio, the solvated complex $[Dmp(Tph)N_3]YbC_6F_5(THF)$ (Scheme 53). Fig. 49 shows the molecular structure of the unsolvated europium derivative with the additional metal–π-arene interactions [85].

2.8. Lanthanide cyclooctatetraenyl compounds

The ionization energies and electron distributions of the one-end open europium cyclooctatetraenyl clusters $Eu_n(COT)_n$ (COT = η^8-cyclooctatetraenyl, n = 1–4) have been studied using DFT calculations [86,87]. The magnetic properties of gas-phase terbium-cyclooctatetraenyl multi-decker sandwich complexes of the type $Tb_n(COT)_{n+1}$ have been measured using a Stern–Gerlach type magnetic deflection approach. Beams of $Tb_n(COT)_{n+1}$ complexes displayed one-sided deflection toward high-field, indicating that fast spin relaxation occurs within the complexes as they pass through the magnetic field [88]. In a related study, a molecular beam of europium-cyclooctatetraenyl sandwich nanowires $Eu_n(COT)_m$ was produced by a laser vaporization synthesis method. The formation of the nanowires was quantitatively revealed by photoelectron and photoionization spectroscopies of the Eu-COT species, together with supporting theoretical calculations [89]. A neutral triple-decker complex of ytterbium with tetraisopropylcyclopentadienyl ligands and a cyclooctatetraene dianion as the middle deck has been synthesized according to Scheme 54 from ytterbium metal, cyclooctatetraene, and the free pentaisopropylcyclopentadienyl radical [90].

2.8.1. Mono(cyclooctatetraenyl) lanthanide(III) compounds

A series of cyclooctatetraene bis(phosphinimino)methanide complexes of yttrium and lanthanide, $(COT)Ln[CH(PPh_2NSiMe_3)_2]$ (COT = η^8-cyclooctatetraenyl; Ln = Y, Sm, Er, Yb, Lu), have been synthesized *via* three different routes which are outlined in Scheme 55. All complexes have been structurally characterized by X-ray diffraction. The solid-state structures of these complexes show that both ligands completely shield the metal center. As a result of the steric crowding, both ligands are slightly asymmetrically attached to the metal center (Fig. 50, Ln = Lu) [91].

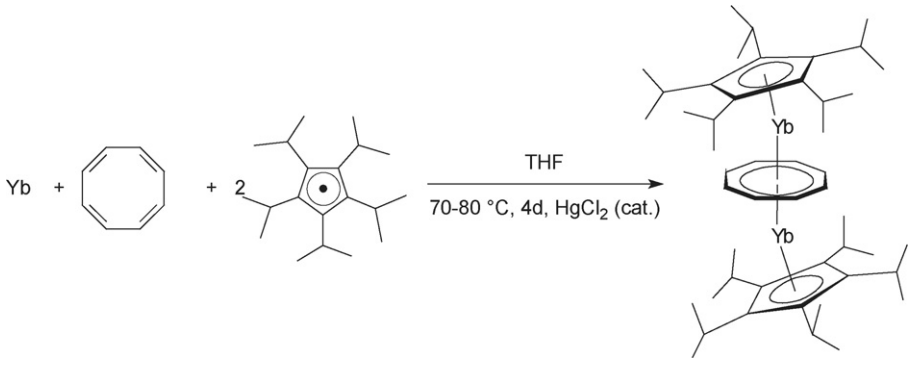

Scheme 54.

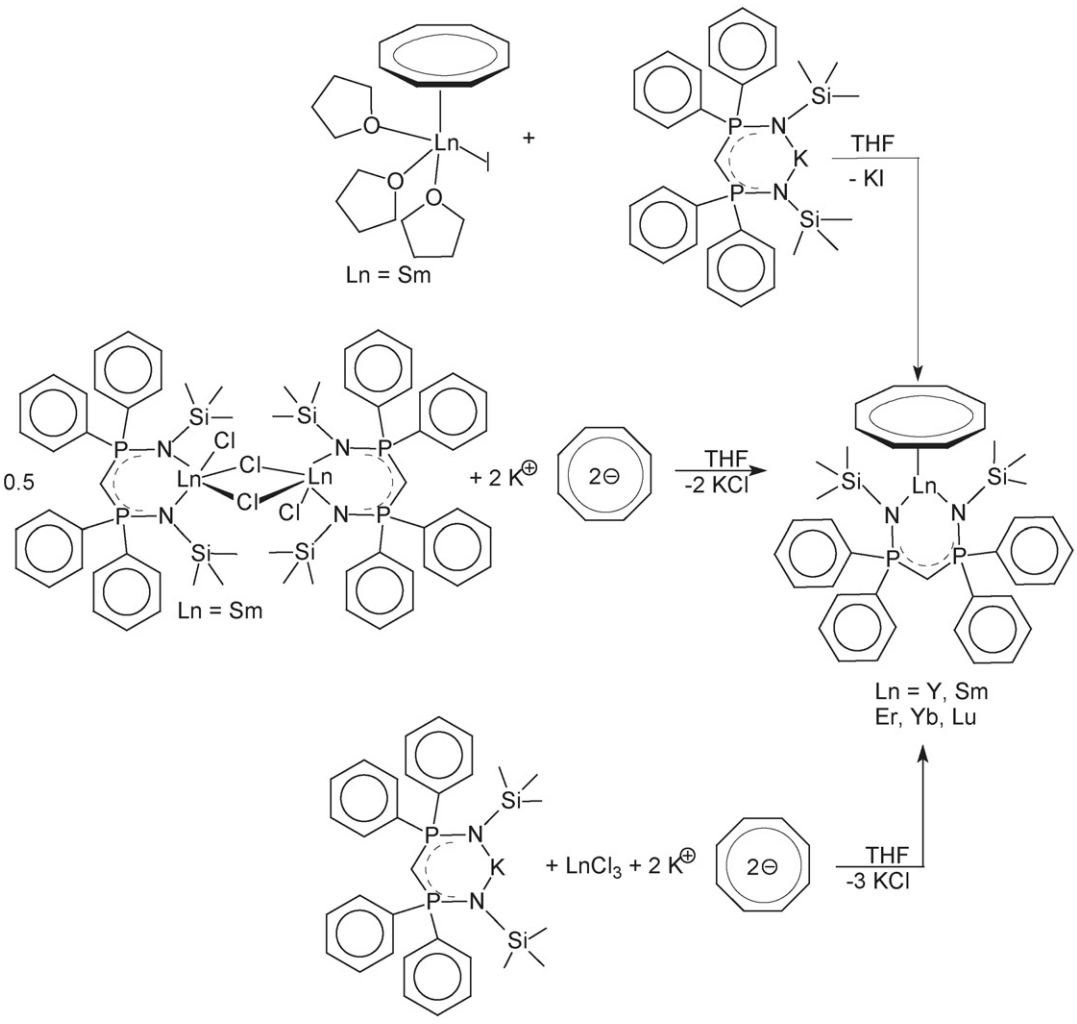

Scheme 55.

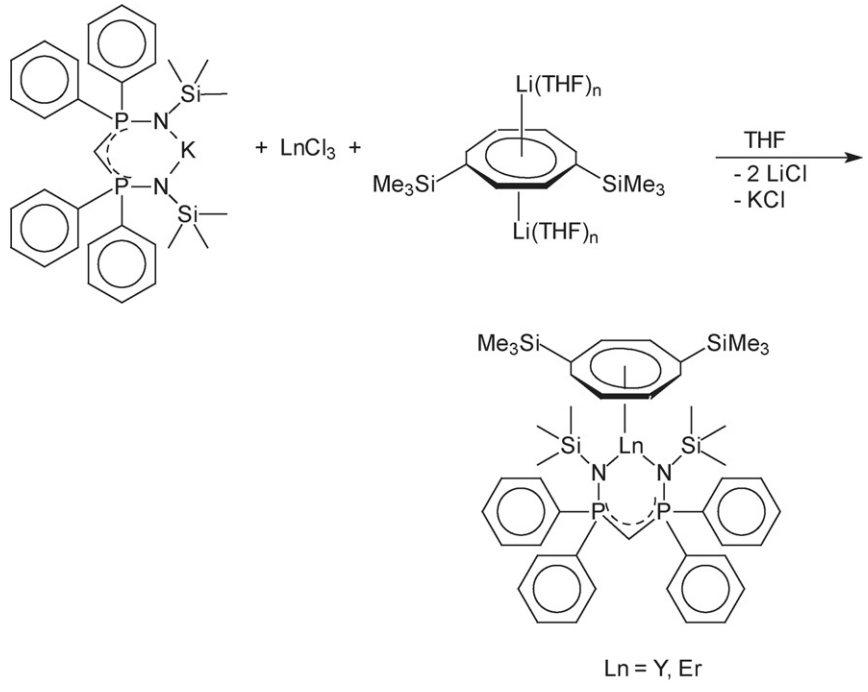

Scheme 56.

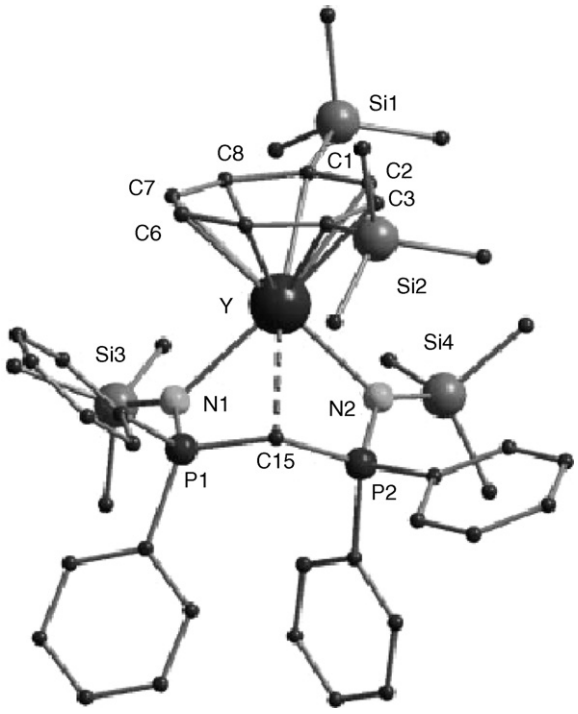

Fig. 51. Molecular structure of $[C_8H_6(SiMe_3)_2\text{-}1,4]Y[CH(PPh_2NSiMe_3)_2]$ [92].

In a closely related study, a one-pot reaction of $Li_2[C_8H_6(SiMe_3)_2\text{-}1,4]$, $LnCl_3$, and $K[CH(PPh_2NSiMe_3)_2]$ leading to the 1,4-bis(trimethylsilyl)cyclooctatetraenyl bis(phosphinimino)-methanide complexes of yttrium and erbium, $[C_8H_6(SiMe_3)_2\text{-}1,4]Ln[CH(PPh_2NSiMe_3)_2]$ (Ln = Y, Er) has been reported (Scheme 56). Both complexes have been structurally characterized by single crystal X-ray diffraction. Fig. 51 shows the molecular structure of the yttrium derivative. The solid-state structures show that the two bulky ligands cause a steric crowding around the lanthanide atom. As a result of this steric crowding both ligands are asymmetrically attached to the lanthanide atom [92].

2.8.2. *Cerocenes*

Using the original and not a newly suggested synthetic route, the tetrasilylated cerocene derivative $Ce[C_8H_6(1,4\text{-}SiMe_3)_2]_2$ (Scheme 57) has been resynthesized as an oil of deep purple color. The absorption, MCD, and luminescence spectra of this formally tetravalent organocerium compound were measured at room temperature as well as at low temperature. Especially the low-temperature spectra were found to be more consistent with a Ce^{III} compound [93].

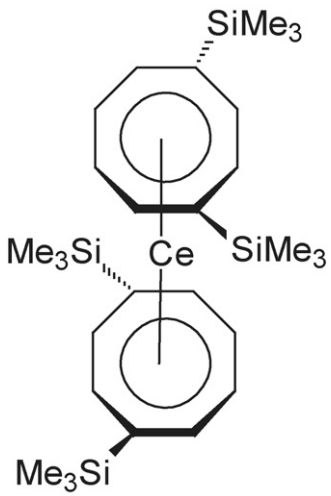

Scheme 57.

2.9. *Lanthanide metallofullerenes*

The structures of the metallofullerenes $Y_2C_2@C_{82}$ and $Y_2@C_{82}$ have been investigated by the maximum entropy method (MEM) combined with Rietveld refinement using synchrotron X-ray powder diffraction data. The cage structures obtained as C_{82} C_{3v} in this study are consistent with the structure model suggested by ^{13}C NMR spectra [94]. The ultraviolet photoelectron spectra (UPS) of $Y_2C_2@C_{82}$ and $Y_2@C_{82}$ have been measured using a synchrotron radiation light source. A difference spectrum between the UPS of $Y_2C_2@C_{82}$ and $Y_2@C_{82}$ indicates the existence of additional electrons on the cage of $Y_2@C_{82}$ [95]. In an exciting paper entitled "*Structural Determination of Metallofullerene Sc_3C_{82} Revisited: A Surprising Finding*" it was reported that the structure of Sc_3C_{82} is not $Sc_3@C_{82}$ but $Sc_3C_2@C_{80}$ containing an endohedral Sc_3C_2 unit. This finding was made possible by appropriate chemical modification of the metallofullerene cage. The analysis of the parent $Sc_3C_2@C_{80}$ proved very difficult due to the nearly free rotation of the round $Sc_3C_2@C_{80}$ units in the crystal lattice. Therefore, chemical functionalization of the $Sc_3C_2@C_{80}$ molecule by adamantylidene carbene (Ad) was carried out to obtain the cycloadduct $Sc_3C_2@C_{80}(Ad)$. Irradiation of a 1,2,4-trichlorobenzene/toluene solution of $Sc_3C_2@C_{80}$ and an excess molar amount of 2-adamantane-2,3-[3*H*]-diazirine in a degassed sealed tube at room temperature using a high-pressure mercury arc lamp (cutoff <350 nm) resulted in the formation of $Sc_3C_2@C_{80}$(A at d), which was purified by preparative HPLC. As shown clearly in the X-ray single-crystal structure (Fig. 52a), the cycloadduct $Sc_3C_2@C_{80}(Ad)$ resulted from the addition of Ad onto $Sc_3C_2@C_{80}$ and not $Sc_3@C_{82}$. This was further confirmed by the single-crystal X-ray structure analysis of the salt $[Bu^n_4N][Sc_3C_2@C_{80}]$ (Fig. 52b). Fig. 53 depicts the calculated molecular structures of $Sc_3C_2@C_{80}$ [96].

Various novel fullerenes containing exohedrally coordinated scandium have been theoretically investigated as adsorbents for high density, room temperature, ambient pressure storage of hydrogen. C_{60} or $C_{48}B_{12}$ disperse scandium atoms by charge transfer interactions to produce stable organometallic buckyballs (OBBs). A particular scandium organometallic buckyball has been found to bind as many as 11 hydrogen atoms per scandium, 10 of which are in the form of hydrogen that can be adsorbed and desorbed reversibly. In this case, the calculated binding energy is about 0.3 eV/H_2, which is ideal for use on board vehicles. The theoretical maximum retrievable H_2 storage density is ~9 wt.% [97].

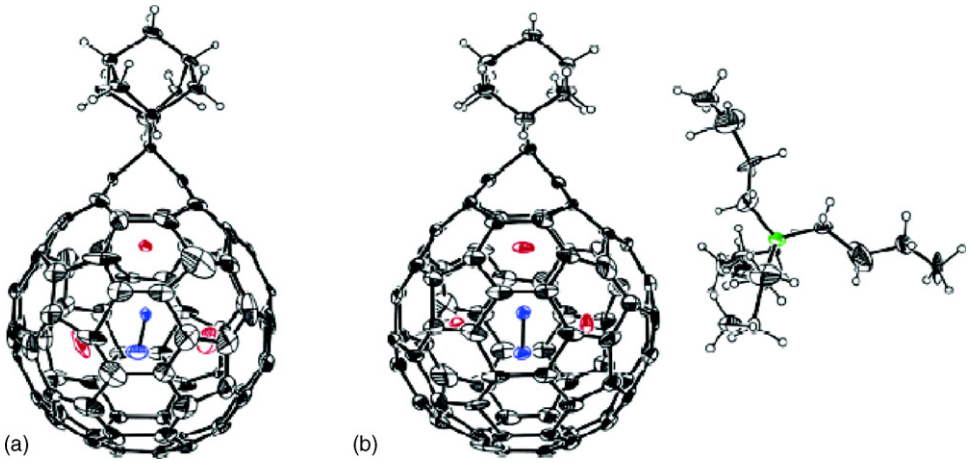

Fig. 52. Molecular structures of $Sc_3C_2@C_{80}$(Ad) (a) and $[Bu_4^nN][Sc_3C_2@C_{80}]$ (b) [96].

2.10. Heterobimetallic organolanthanide complexes

Unprecedented mixed potassium–lanthanide wheel-shaped-structured complexes containing amido and diphosphinoamido ligands have been reported in 2005. Reaction of $CpErCl_2$ with the amido compounds $KNPh_2$ and $[K(THF)_nN(PPh_2)_2]$ ($n = 1.25$ and 1.5) in THF followed by crystallization from THF/*n*-pentane (1:2) led to the hexanuclear, wheel-shaped-structured compound $[CpEr(NPh_2)_2\{N(PPh_2)_2\}_2K_2(THF)_4]_2$. As illustrated in Scheme 58, this compound and its ytterbium analogue can also be prepared in moderate yield in a one-pot reaction, in which the potassium salts $KNPh_2$ and $[K(THF)_nN(PPh_2)_2]$ as well as NaCp are reacted with anhydrous erbium or ytterbium trichloride in THF, followed by crystallization from THF/pentane. The solid-state structures of the new complexes were established by single-crystal X-ray diffraction (Fig. 54, Ln = Er). Oligomerization occurs through bridging cyclopentadienyl ligands as well as π-interactions between potassium and phenyl rings [98].

By employing the same reaction conditions as those for the Er and Yb derivatives but performing the synthesis with samarium and later optimizing the stoichiometric ratios, a coordination polymer of composition $[CpSm(NPh_2)_2\{N(PPh_2)_2\}K]_\infty$ has been obtained in moderate yield as depicted in Scheme 59 [98].

The solid-state structure of $[CpSm(NPh_2)_2\{N(PPh_2)_2\}K]_\infty$ was also established by single-crystal X-ray diffraction (Fig. 55). The compound can be regarded as an octanuclear, wheel-shaped-structured Sm_4K_4 compound, in which the potassium cations bridge the $[CpSm(NPh_2)_2\{N(PPh_2)_2\}]^-$ metalate anions. In this species too the ring is formed through bridging cyclopentadienyl ligands and π-interactions between potassium and phenyl rings. In contrast to the hexanuclear K/Er and K/Yb compounds, which consist of isolated rings, the rings in the samarium–potassium complex are connected to each other, thus forming a three-dimensional polymeric structure [98].

Heterobimetallic alkyl complexes of the types $[SmAl_2Me_8]_x$ and $[SmAl_2Et_8]_x$ have been obtained *via* a silylamide elimination reaction from $Sm[N(SiMe_3)_2]_2(THF)_2$ and excess AlR_3 (R = Me, Et). The ethyl derivatives $[LnAl_2Et_8]_x$ (Ln = Sm, Yb) react with THF, pyridine, and 1,10-phenanthroline to form the first donor adducts of homoleptic peralkylated Ln–Al heterobimetallic complexes. Fig. 56 illustrates the molecular structure of the monomeric ytterbium complex $[YbAl_2Et_8](THF)_2$ [99].

The reaction of $LnI_3(THF)_n$ (Ln = La, $n = 4$; Ln = Y, $n = 3.5$) with 3 equiv. of (allyl)MgI in THF/1,4-dioxane has been found to proceed in moderate yields to give the unexpected mixed-metal complexes $[Ln(\eta^3\text{-}C_3H_5)(\mu\text{-}C_4H_8O_2)Mg(\eta^1\text{-}C_3H_5)_2$-

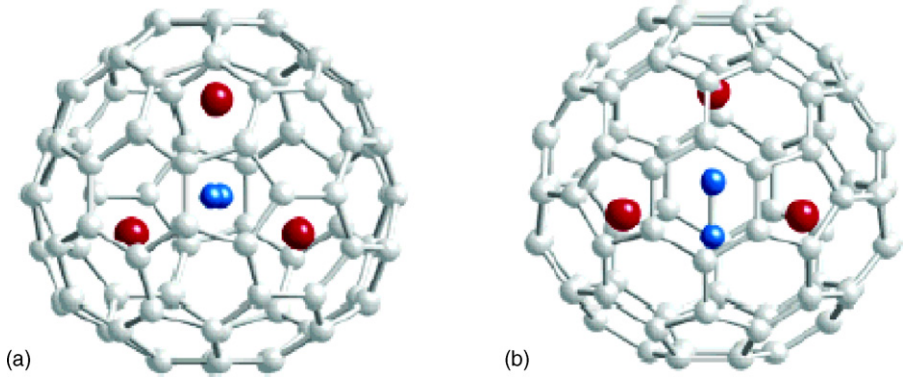

Fig. 53. Calculated molecular structures of $Sc_3C_2@C_{80}$ [96].

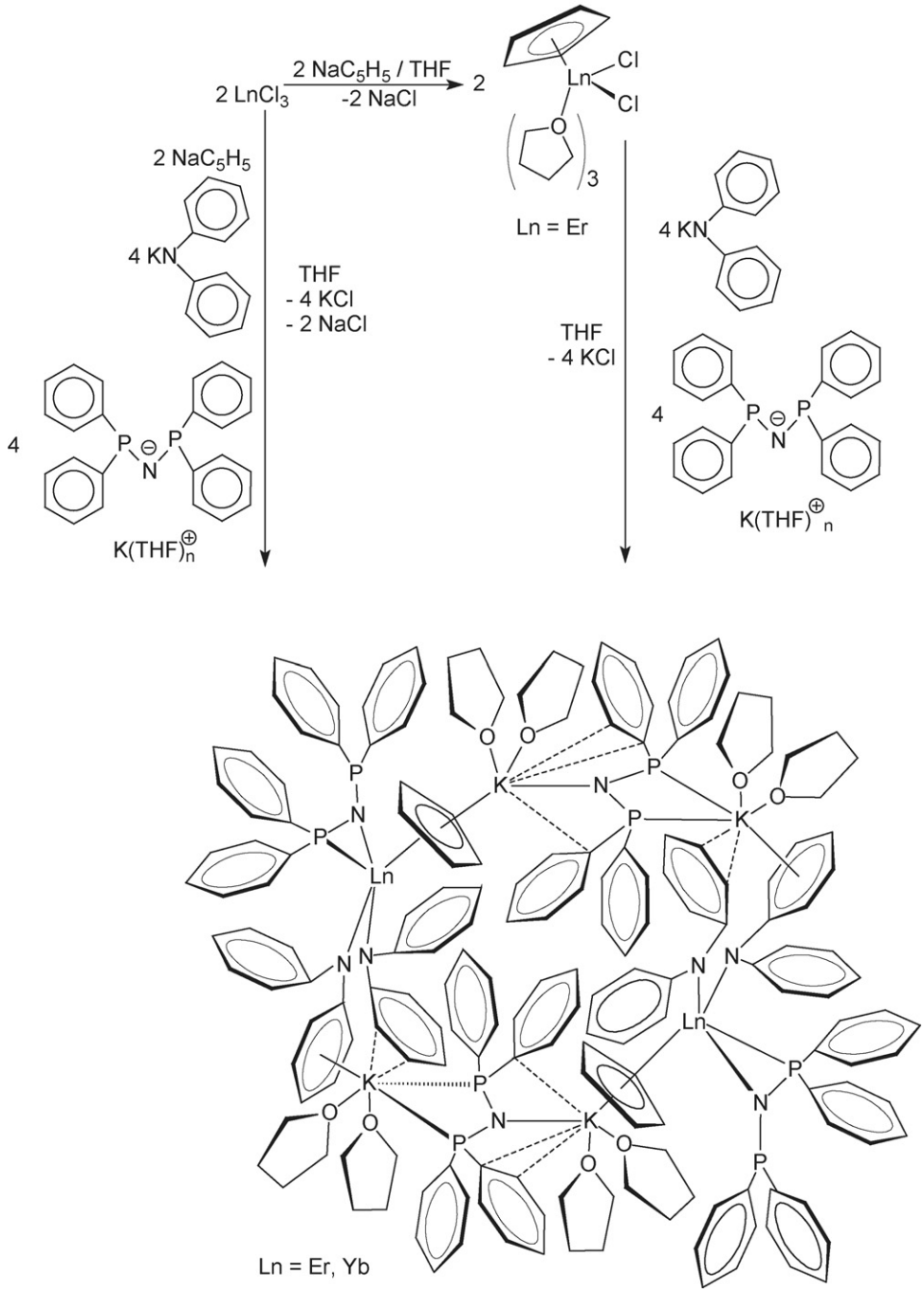

Scheme 58.

$(\mu\text{-}C_4H_8O_2)_{1.5}]_\infty$ (Ln = Y, La) (Scheme 60). By contrast, samarium triiodide gave a salt containing a new allyl-bridged anion, $[Mg(THF)_6][Sm_2(\eta^3\text{-}C_3H_5)_6(\mu\text{-}\eta^3\text{:}\eta^3\text{-}C_3H_5)]_2\cdot$toluene, while neodymium triiodide afforded $[Mg(THF)_6][Nd(\eta^3\text{-}C_3H_5)_4]_2\cdot 2THF$ under the same reaction conditions. On reaction with a mild proton acid such as the diketimine 2-(2,6-diisopropylphenyl)amino-4 - (2, 6 - diisopropylphenyl)imino-2-pentene, the allyl-bridged samarium derivative can be converted into $[Mg(THF)_6][Sm(\eta^3\text{-}C_3H_5)_4]_2\cdot 2THF$ with concomitant formation of $Sm(\eta^3\text{-}C_3H_5)_2[\kappa^2\text{-}HC(MeCNAr)_2]$ (Ar = 2,6-$C_6H_3Pr_2^i$) (*cf.* Scheme 14) [100].

As shown in Fig. 57 for the yttrium derivative (the La compound is isostructural), the solid-state structures of $[Ln(\eta^3\text{-}C_3H_5)(\mu\text{-}C_4H_8O_2)Mg(\eta^1\text{-}C_3H_5)_2(\mu\text{-}C_4H_8O_2)_{1.5}]_\infty$ (Ln = Y, La) contain distorted trigonal-bipyramidal lanthanide centers with three η^3-allyl ligands and distorted trigonal-bipyramidal magnesium centers with two η^1-bonded allyls. Both metal centers are connected by bridging 1,4-dioxane molecules building a planar polymeric network (Fig. 58) [100].

The samarium allyl complexes $[Mg(THF)_6][Sm_2(\eta^3\text{-}C_3H_5)_6(\mu\text{-}\eta^3\text{:}\eta^3\text{-}C_3H_5)]_2\cdot$toluene (red microcrystalline solid) and $[Mg(THF)_6][Sm(\eta^3\text{-}C_3H_5)_4]_2\cdot 2THF$ (red microcrystalline

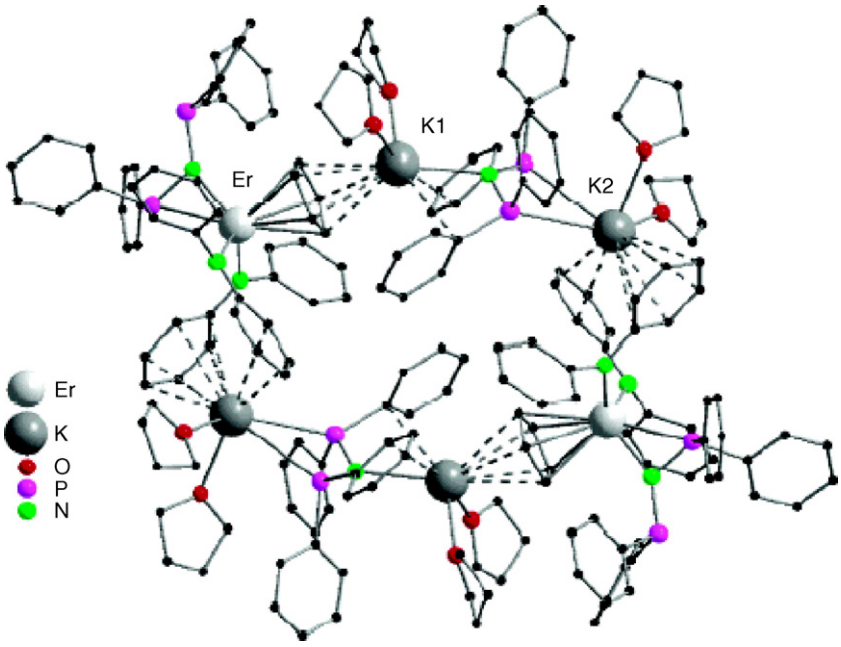

Fig. 54. Molecular structure of $[CpEr(NPh_2)_2\{N(PPh_2)_2\}_2K_2(THF)_4]_2$ [98].

slid) both consist of well-defined discrete ions in the solid-state. $[Mg(THF)_6][Sm_2(\eta^3\text{-}C_3H_5)_6(\mu\text{-}\eta^3\text{:}\eta^3\text{-}C_3H_5)]_2\cdot$toluene contains an unprecedented type of binuclear anion containing two samarium centers bridged by an η^3:η^3-allyl ligand (Fig. 59), while the anion in $[Mg(THF)_6][Sm(\eta^3\text{-}C_3H_5)_4]_2\cdot 2THF$ has distorted *pseudo*-tetrahedral geometry (Fig. 60) [100].

Addition of Al_2Me_6 to the allyl complex $[(C_5H_4)SiMe_2\text{-}(CH_2CH{=}CH_2)]_2Y(C_3H_5)$ caused the bright yellow color

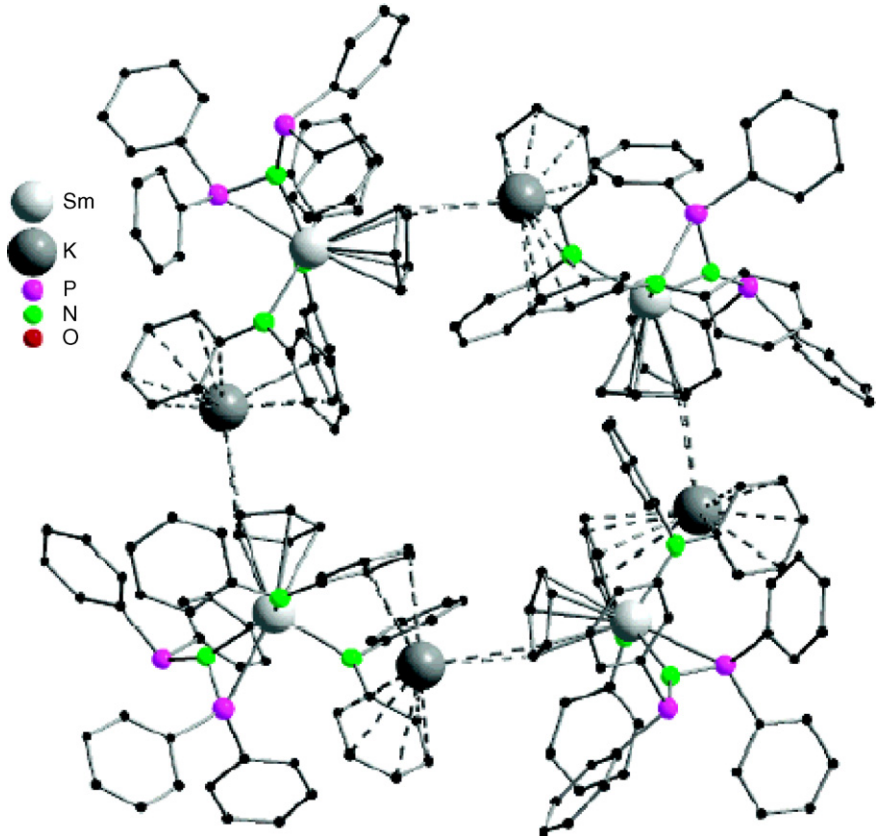

Fig. 55. Molecular structure of $[CpSm(NPh_2)_2\{N(PPh_2)_2\}K]_\infty$ [98].

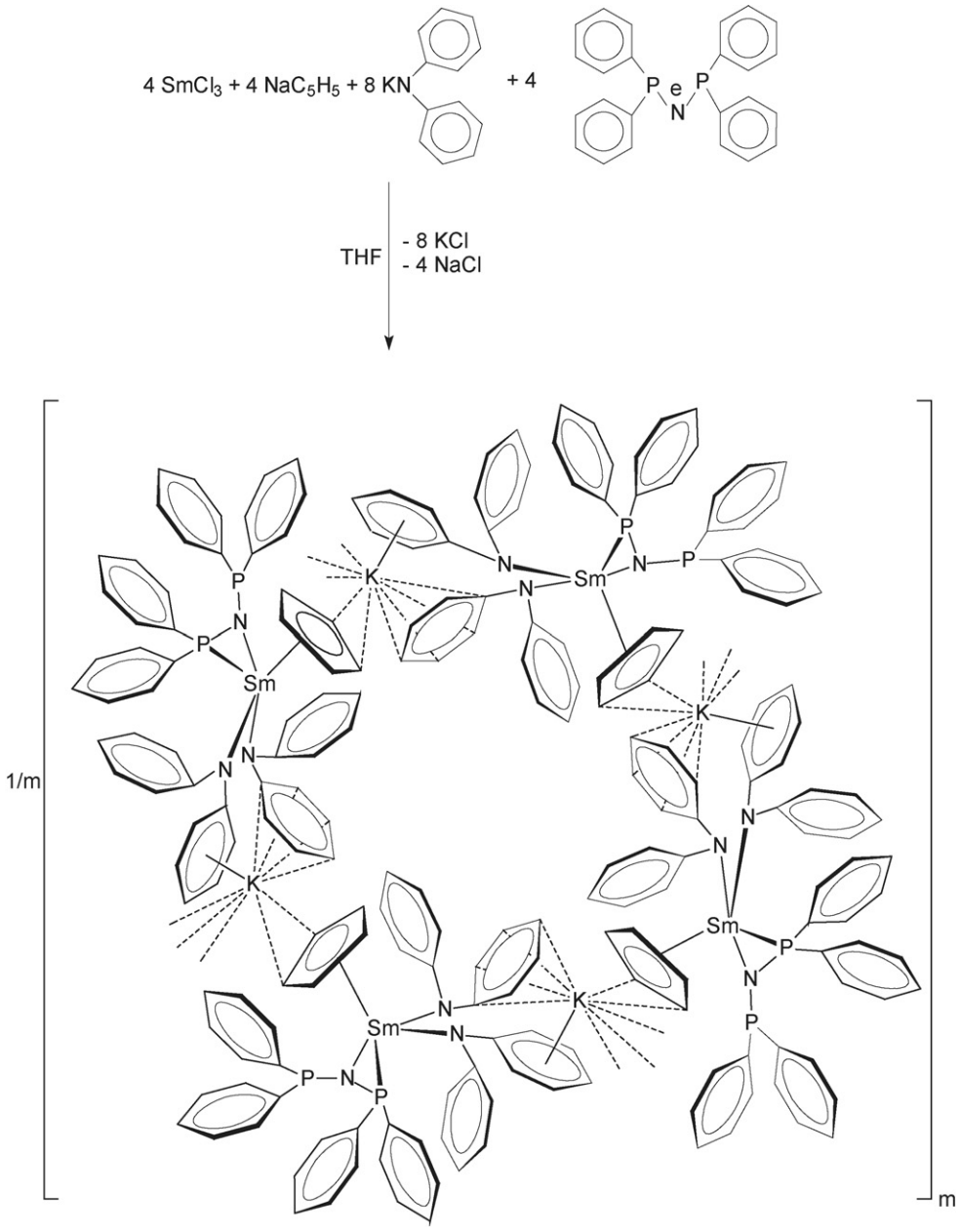

Scheme 59.

to fade to pale yellow. From the resulting solution, the heterobimetallic Y/Al complex $\{[(C_5H_4)SiMe_2(CH_2CH{=}CH_2)]_2Y[(\mu\text{-}Me)_2AlMe_2]\}_2$ was isolated in quantitative yield and definitively identified by X-ray crystallography (Scheme 61). As a result, the allyl ligand was lost as anticipated for this reaction, but a $[AlMe_4]^-$ anion was formed instead of an $[(allyl)AlMe_3]^-$ unit (Fig. 61). Evidently ligand distribution occurred in which the allyl group was completely removed from yttrium [37].

The homoleptic complexes $Ln(AlMe_4)_3$ (Ln = Y, La, Nd, Lu) have been treated with pentamethylcyclopentadiene to yield the corresponding half-sandwich complexes $Cp^*Ln(AlMe_4)_2$ in high yield and purity. NMR spectroscopic investigations revealed a highly dynamic nature of the bridging and terminal alkyl groups even at −85 °C. In the solid-state, the tetramethylaluminato ligands coordinate differently to the lanthanide center, as shown by an X-ray structure analysis of the lanthanum derivative (Fig. 62). Due to the steric unsaturation of the large lanthanum metal center, one of the aluminate ligands adopts an unusual distorted $\mu{:}\eta^3$-coordination mode, while the second ligand is bonded in the regular $\mu{:}\eta^2$-fashion [101].

The well-defined coordination environment of trivalent $Cp^*_2Ln^+$ complexes has been used to systematically examine the reaction chemistry of the lanthanide carboxylate and R_2AlCl (R = Me, Et, Bu^i) components used in the preparation of lanthanide-based diene polymerization catalysts. Each of the R_2AlCl reagents can replace a carboxylate ligand with chloride in reactions with $[Cp^*_2Sm(\mu\text{-}O_2CPh)]_2$, but instead of forming a

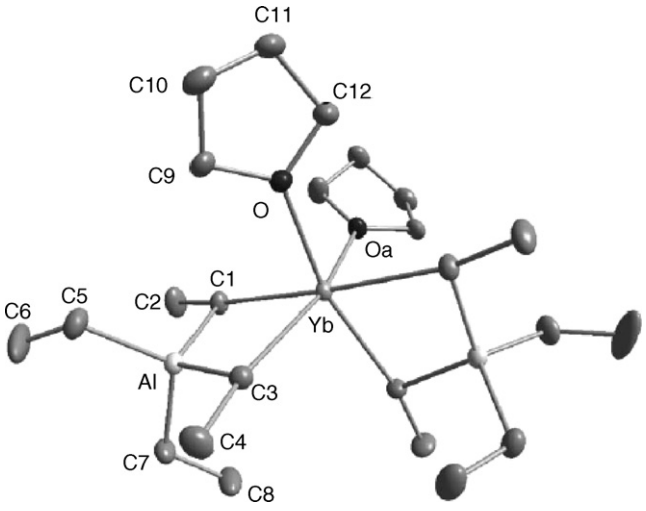

Fig. 56. Molecular structure of $[YbAl_2Et_8](THF)_2$ [99].

simple chloride complex like $[Cp^*_2SmCl]_3$, bimetallic lanthanide aluminum dichloro complexes $Cp^*_2Sm(\mu\text{-}Cl)_2AlR_2$ are generated by ligand redistribution according to Scheme 62 [102].

These bis(chloride)-bridged complexes are also readily formed from the divalent precursor $Cp^*_2Sm(THF)_2$ and R_2AlCl. However, the analogous reaction between $Cp^*_2Sm(THF)_2$ and Et_3Al afforded $Cp^*_2Sm(THF)(\mu\text{-}\eta^2\text{-}Et)AlEt_3$ (Scheme 63), which contains the first Ln(III)-(η^2-Et) linkage, a coordination mode that differentiates Et from Me. Fig. 63 depicts the molecular structure of this compound [102].

In a closely related study, the samarium carboxylate complex $[Cp^*_2Sm(\mu\text{-}O_2CPh)]_2$ was reported to react with $AlEt_3$ to form a mixture of metallocene-stabilized ethylaluminum compounds (Scheme 64), including an ethyl aluminum oxide (EAO) complex, $[Cp^*_2Sm]_2[(\mu\text{-}Et)_4Al_4Et_6O_2]$, the structure of which was determined by X-ray diffraction (Fig. 64). In addition to containing a new EAO ligand system, $[Cp^*_2Sm]_2[(\mu\text{-}Et)_4Al_4Et_6O_2]$ displays unusual $\mu\text{-}\eta^1\text{:}\eta^2$-ethyl bonding to the trivalent samarium center [103]. With $Bu_3{}^iAl$, $[Cp^*_2Sm(\mu\text{-}O_2CPh)]_2$ reacts to form a mixed-bridge samarium aluminum complex $Cp^*_2Sm(\mu\text{-}O_2CPh)(\mu\text{-}Bu^i)Al(Bu^i)_2$, that displays two different carboxylate orientations toward the metals in a single crystal [103].

The analogous reaction between $[Cp^*_2Sm(\mu\text{-}Cl)]_3$ and $AlEt_3$ generated the dimeric mixed-bridge complex $[Cp^*_2Sm(\mu\text{-}\eta^1\text{:}\eta^2\text{-}Et)(\mu\text{-}Cl)AlEt_2]_2$ (Scheme 65), a reaction that does not involve ligand redistribution [103].

As shown in Fig. 65, both methylene hydrogens and one methyl group of each of the $\mu\text{-}\eta^1\text{:}\eta^2$-Et bridges in $[Cp^*_2Sm(\mu\text{-}\eta^1\text{:}\eta^2\text{-}Et)(\mu\text{-}Cl)AlEt_2]_2$ refined into positions oriented toward samarium. Hence, the $\mu\text{-}\eta^1\text{:}\eta^2$-Et ligand functions as a polyagostic bridge between the lanthanide and aluminum [103].

The synthesis of a novel class of compounds containing a Ln–O–Al moiety has been achieved by the reaction of LAlOH(Me) (L = HC(CMeNAr)$_2$, Ar = 2,6-$Pr_2{}^iC_6H_3$) with

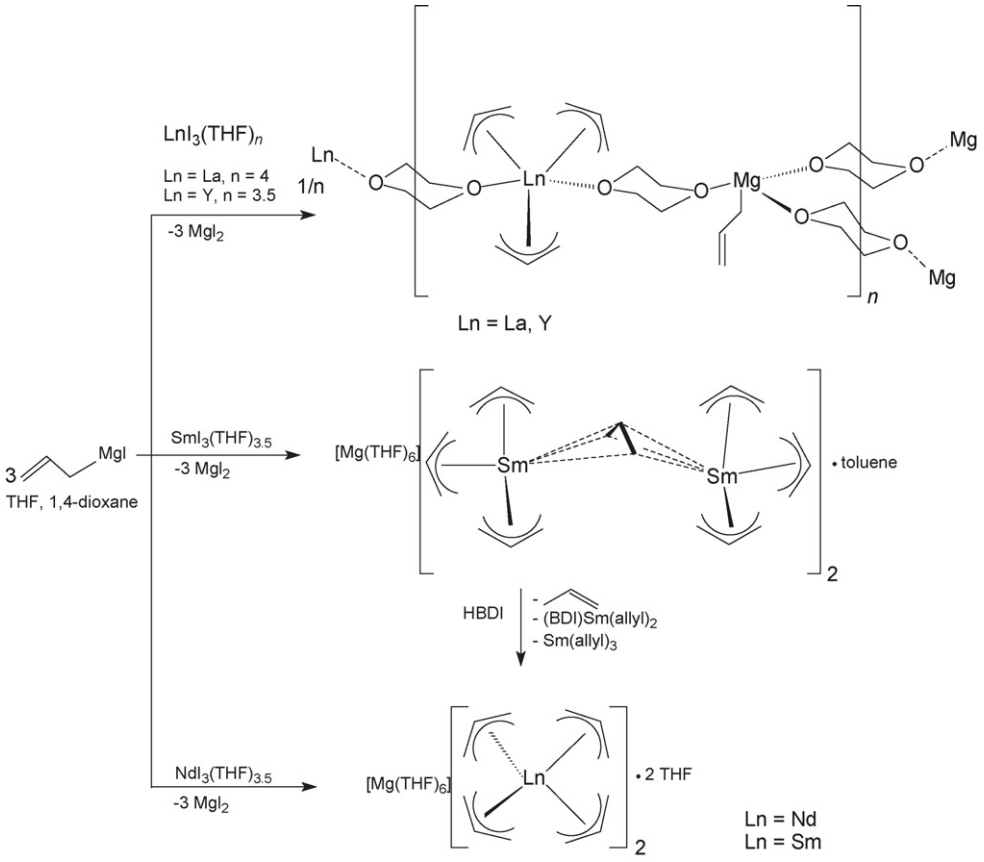

Scheme 60.

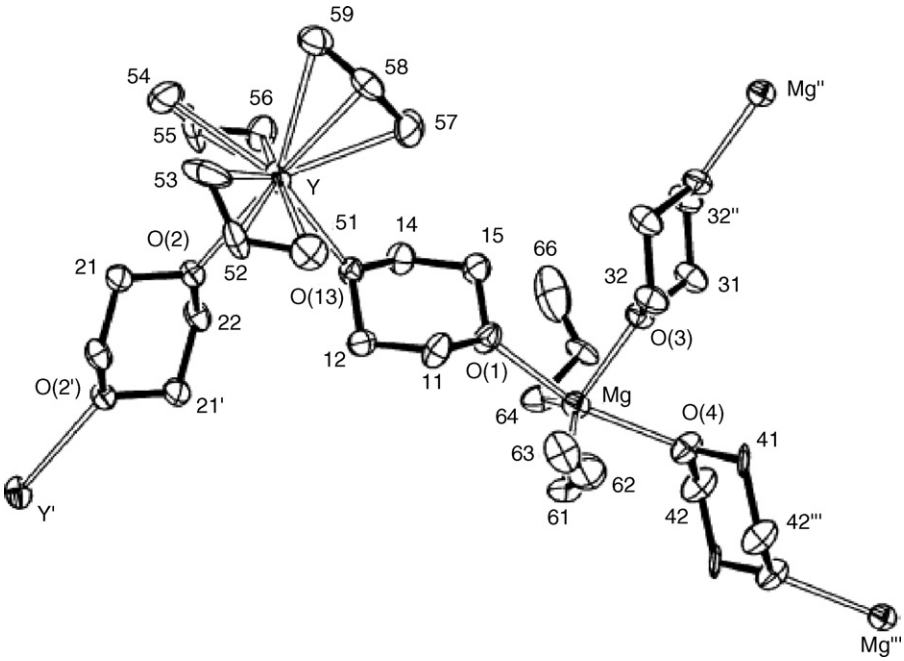

Fig. 57. View of a fragment of the planar polymer network in $[Y(\eta^3\text{-}C_3H_5)(\mu\text{-}C_4H_8O_2)Mg(\eta^1\text{-}C_3H_5)_2(\mu\text{-}C_4H_8O_2)_{1.5}]_\infty$ [100].

a series of Cp_3Ln compounds. The terminal Al–OH group shows selective reactivity, and the complexes $Cp_2Ln(THF)$–O–AlL(Me) (Ln = Dy, Er, Yb), Cp_2Yb–O–AlL(Me), and $Cp_3Ln(\mu$-OH)AlL(Me) (Ln = Sm, Dy, Er) were obtained and structurally characterized. The Ln–O–Al angles fall in the range of 151.9–169.8°. As a typical example, the molecular structure of $Cp_2Er(THF)$-O-AlL(Me) is shown in Fig. 66. The reaction of $Cp_2Yb(THF)$-O-AlL(Me) and Cp_2Yb-O-AlL(Me) with Me_3SnF in refluxing toluene unexpectedly yielded the compounds $[Cp_2Yb(\mu\text{-}OSnMe_3)]_2$ and LAl(Me)F [104].

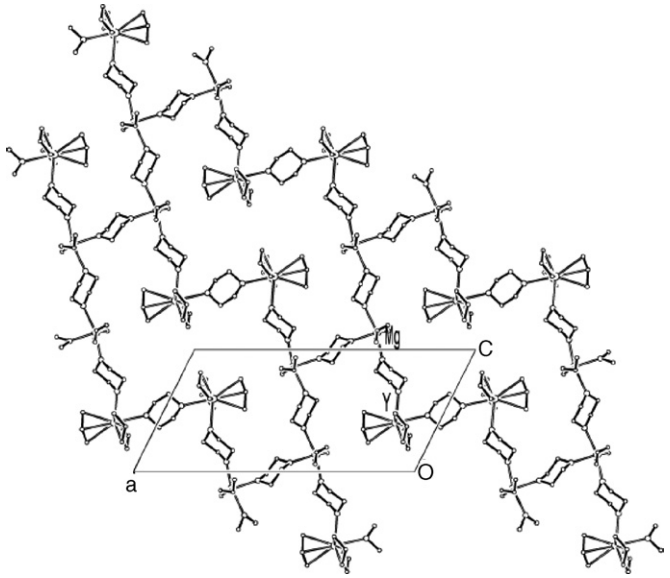

Fig. 58. Crystal structure of $[Y(\eta^3\text{-}C_3H_5)(\mu\text{-}C_4H_8O_2)Mg(\eta^1\text{-}C_3H_5)_2(\mu\text{-}C_4H_8O_2)_{1.5}]_\infty$. Projection of the planar polymeric chains down the *b*-axis [100].

2.11. Organolanthanide catalysis

2.11.1. Organolanthanide catalyzed oligomerization reactions

The acetylene cyclotrimerization reaction mediated by bare transition metals including yttrium has been studied theoretically, employing DFT in its B3LYP formulation. The complete reaction mechanism has been analyzed, identifying intermediates and transition states. The overall reaction is highly favorable from a thermodynamic point of view, and ground state transition states lie always below the energy limit represented by ground state reactants. After the activation of two acetylene molecules and formation of a bis-ligated complex, the reaction proceeds to give a metallacycle intermediate, as the alternative formation of a cyclobutadiene complex is energetically disfavored. All the examined reaction paths involve formation of a metallacycloheptatriene intermediate that in turn generates a metal–benzene adduct from which finally benzene is released [105]. Several lanthanide-imido complexes (*cf.* Scheme 20) have been shown to catalyze the cyclic trimerization of benzonitrile to form 2,4,6-triphenyl-1,3,5-triazine. A possible mechanism has been proposed [31].

2.11.2. Organolanthanide catalyzed polymerization reactions

2.11.2.1. Monoolefins (ethylene, propene, styrene, etc.). $Sc([9]aS_3)(CH_2SiMe_3)_3$, the first rare earth organometallic complex of 1,4,7-trithiacyclononane (=[9]aneS_3), has been reported to be a precursor to ethylene and α-olefin polymerization catalysts upon activation with $B(C_6F_5)_3$ or $[Ph_3C][B(C_6F_5)_4]$. These were the first cationic rare earth organometallic catalysts supported by an all-sulfur donor

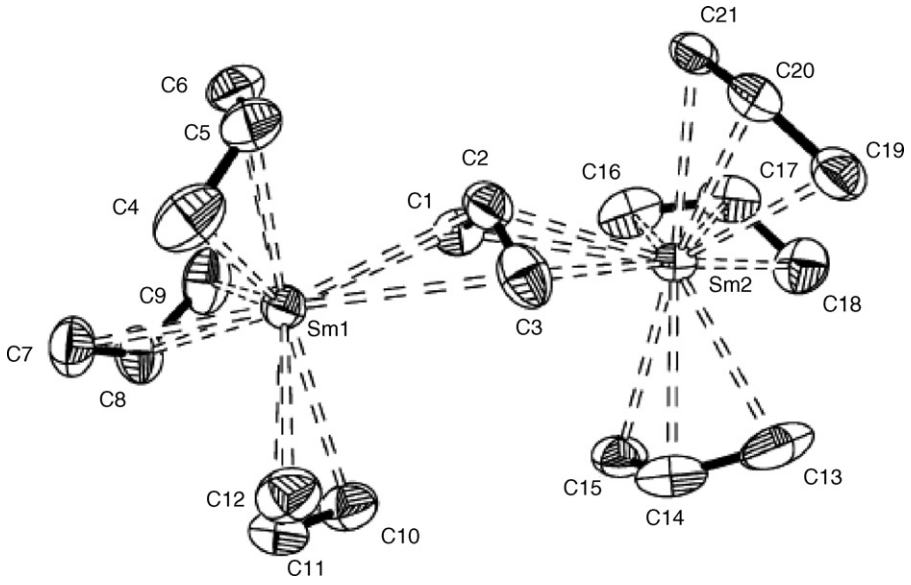

Fig. 59. Molecular structure of the anion in $[Mg(THF)_6][Sm_2(\eta^3\text{-}C_3H_5)_6(\mu\text{-}\eta^3\text{:}\ \eta^3\text{-}C_3H_5)]_2$ toluene [100].

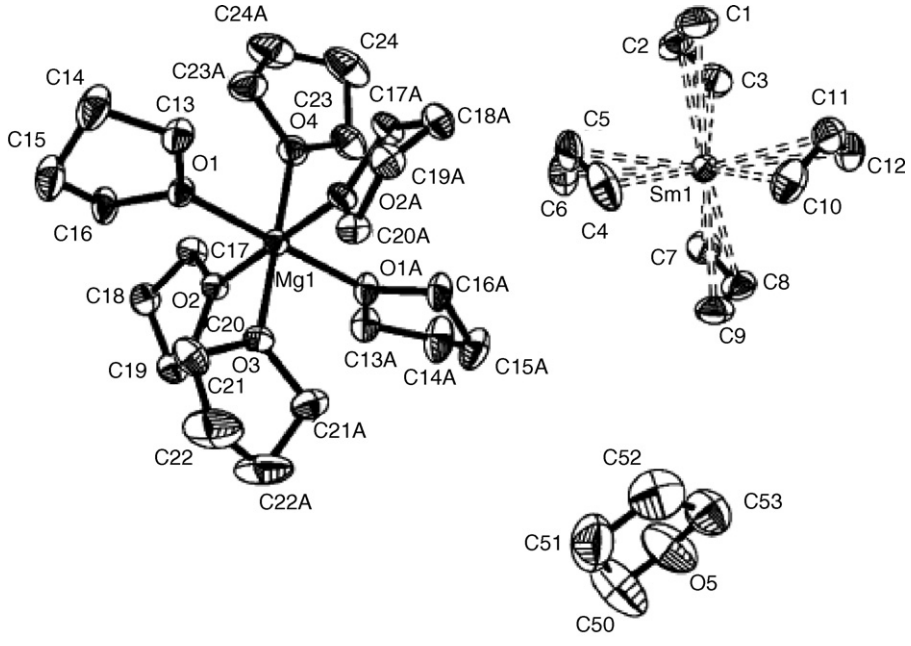

Fig. 60. Molecular structure of $[Mg(THF)_6][Sm(\eta^3\text{-}C_3H_5)_4]_2{\cdot}2THF$ [100].

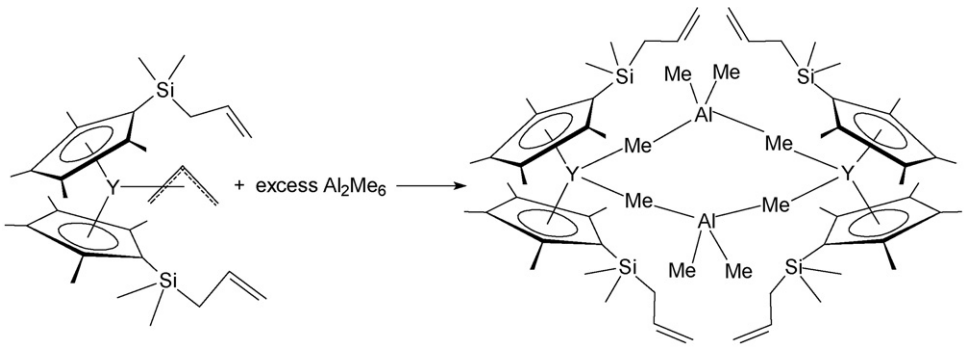

Scheme 61.

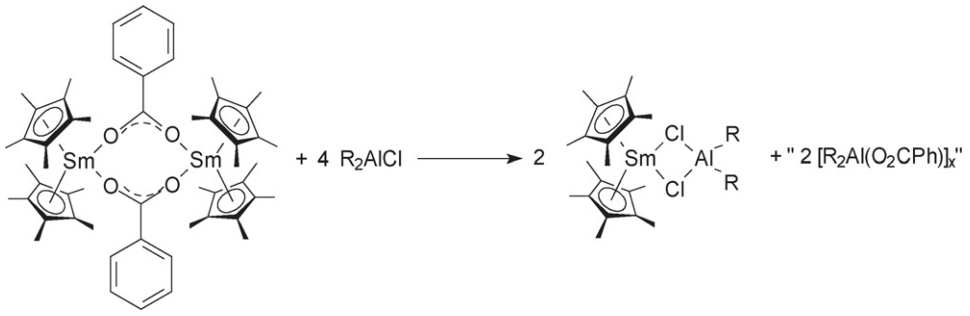

Scheme 62.

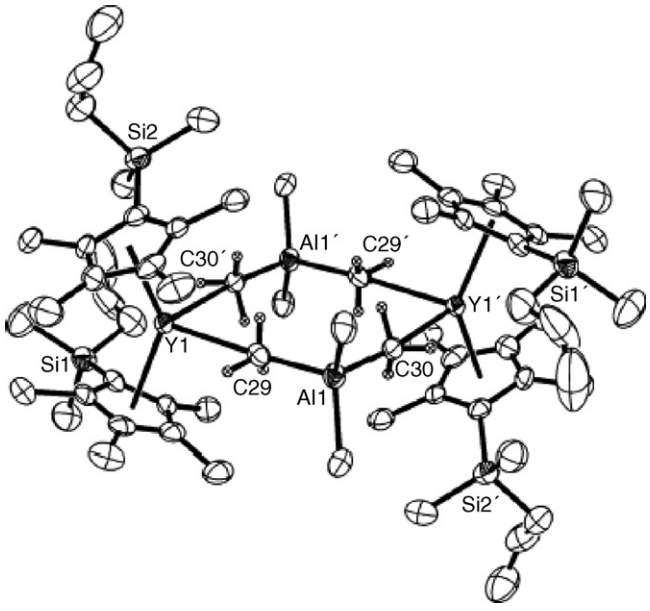

Fig. 61. Molecular structure of $\{[(C_5H_4)SiMe_2(CH_2CH{=}CH_2)]_2Y[(\mu\text{-}Me)_2AlMe_2]\}_2$ [37].

ligand [106]. The organolanthanide catalyzed synthesis of phosphine-terminated polyethylenes has been studied in detail. Primary and secondary phosphines were investigated as chain-transfer agents for this organolanthanide-mediated olefin

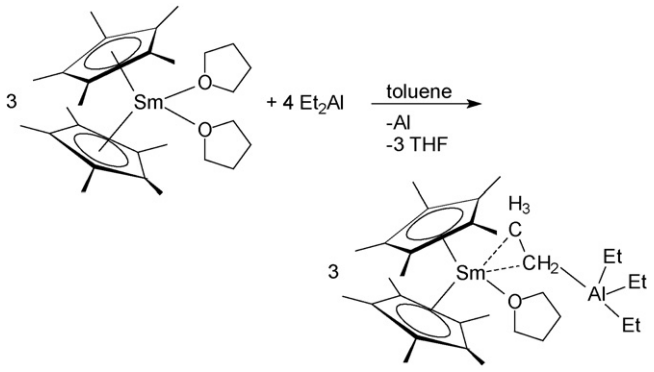

Scheme 63.

polymerization. Ethylene polymerizations were carried out with $[Cp^*_2Ln(\mu\text{-}H)]_2$ and $Cp^*_2LnCH(SiMe_3)_2$ (Ln = Y, La, Sm, Lu) precatalysts in the presence of dicyclohexyl-, diisobutyl-, diethyl-, diphenyl-, cyclohexyl- and phenylphosphine. In the presence of secondary phosphines, high polymerization activities (up to 10^7 g of polymer/(mol of Ln·atm ethylene·h)) and narrow product polymer polydispersities have been observed [54]. A dicationic scandium catalyst derived from the trialkyl complex (^{i}Pr-trisox)Sc(CH_2SiMe_2)$_3$ (*cf.* Scheme 9) has been found to be highly active in the isoselective polymerization of 1-hexene [15]. The scandium-catalyzed copolymerization of ethylene with dicyclopentadiene and terpolymerization of

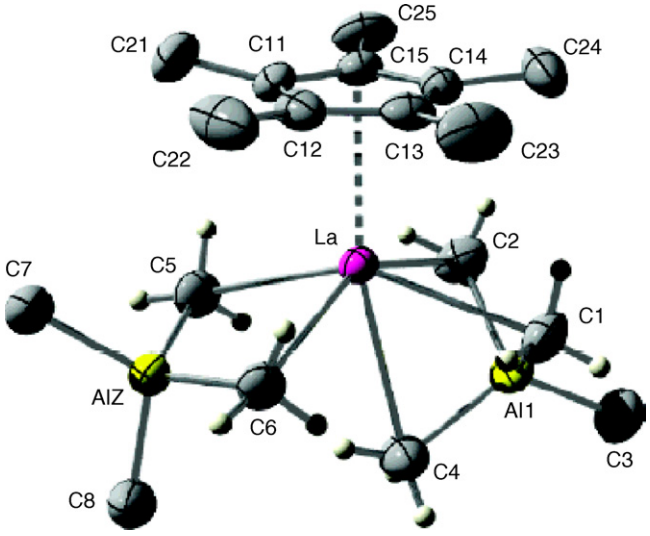

Fig. 62. Molecular structure of $Cp^*La(AlMe_4)_2$ [101].

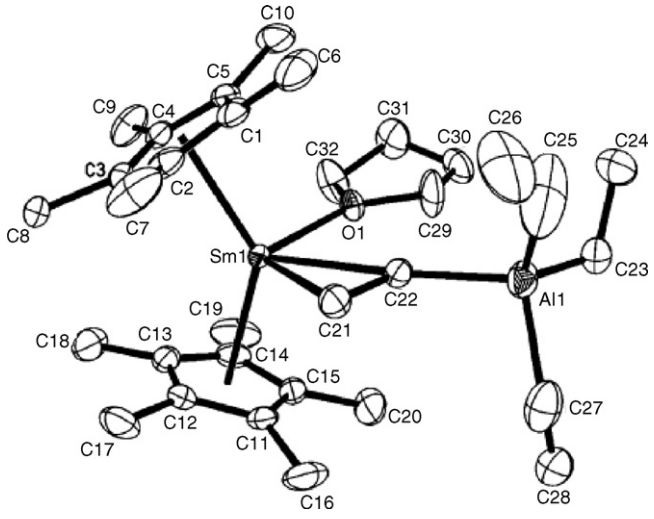

Fig. 63. Molecular structure of $Cp^*_2Sm(THF)(\mu\text{-}\eta^2\text{-}Et)AlEt_3$ [102].

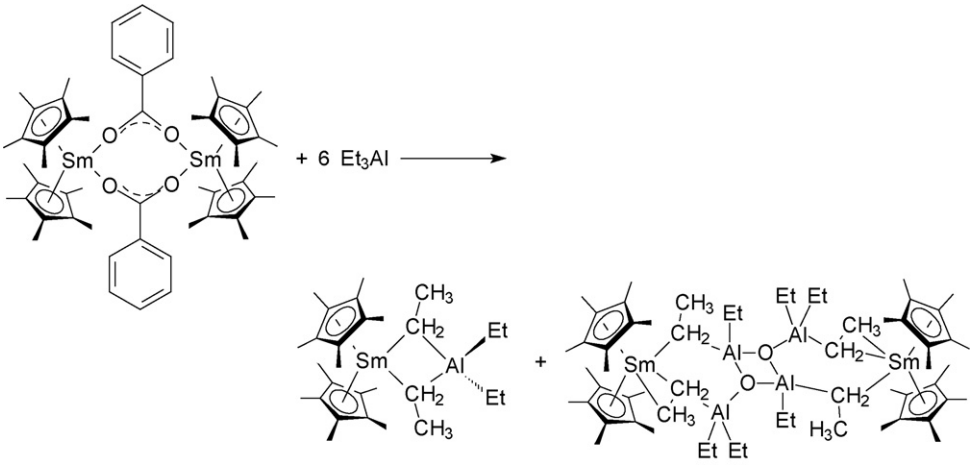

Scheme 64.

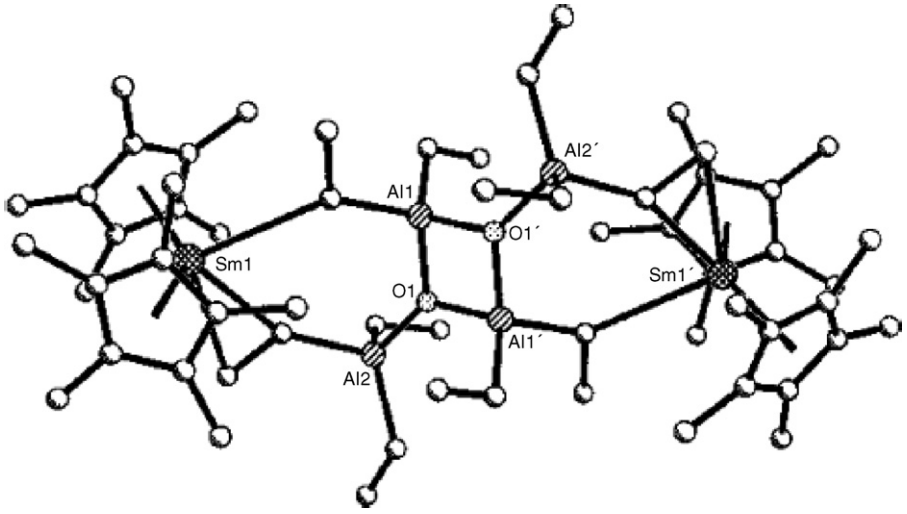

Fig. 64. Molecular structure of $[Cp^*_2Sm]_2[(\mu\text{-}Et)_4Al_4Et_6O_2]$ [103].

ethylene, dicyclopentadiene, and styrene has been investigated. These polymerizations have been achieved with excellent selectivity and activity for the first time by using a cationic half-sandwich scandium catalyst and afforded a new series of novel polymers that are difficult to be prepared with other catalyst systems. The catalyst system employed in this study was generated *in situ* by treament of $(C_5Me_4SiMe_3)Sc(CH_2SiMe_3)_2(THF)$ with 1 equiv. of $[Ph_3C][B(C_6F_5)_4]$ in toluene. As a typical example, the alternating copolymerization of ethylene with dicyclopentadiene using this catalyst system is illustrated in Scheme 66 [107].

In a closely related study the cationic half-sandwich scandium catalysts derived from $Cp'Sc(CH_2SiMe_3)_2(THF)$ ($Cp' = C_5Me_4SiMe_3$, $C_5H_3(SiMe_3)_2$-1,3, Cp^*) with 1 equiv. of

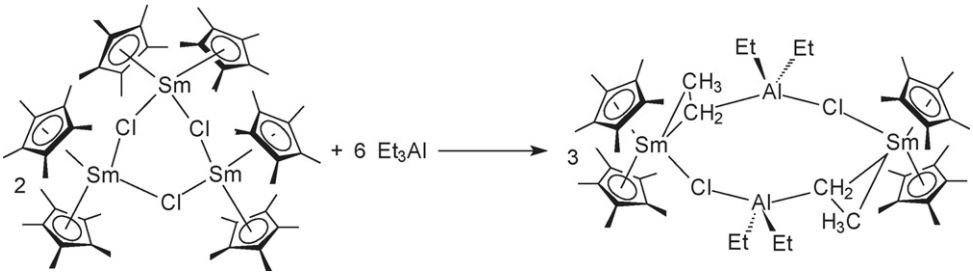

Scheme 65.

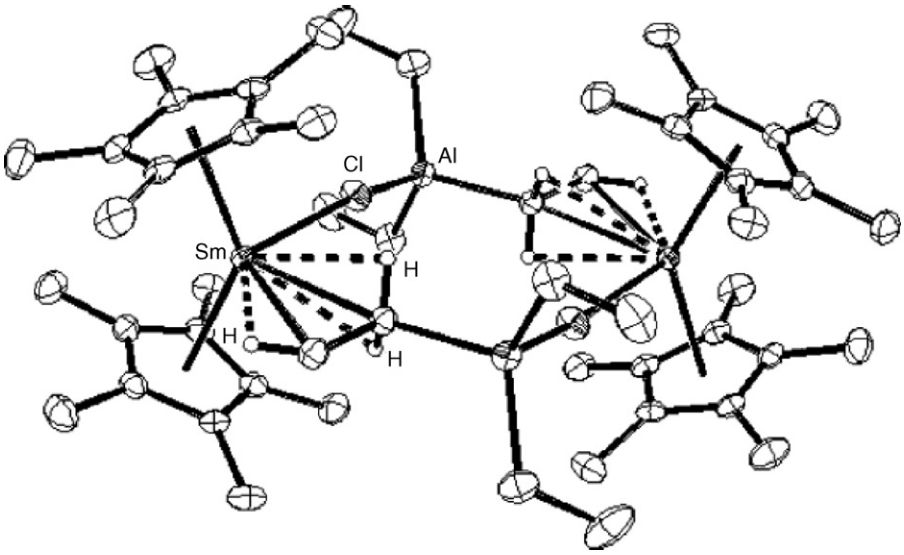

Fig. 65. Molecular structure of $[Cp^*_2Sm(\mu\text{-}\eta^1\text{:}\eta^2\text{-Et})(\mu\text{-Cl})AlEt_2]_2$ [103].

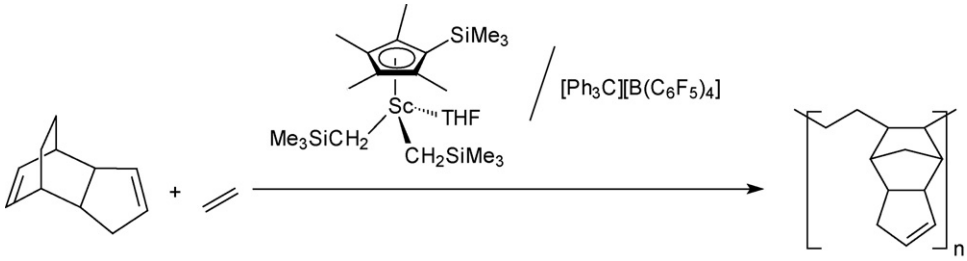

Scheme 66.

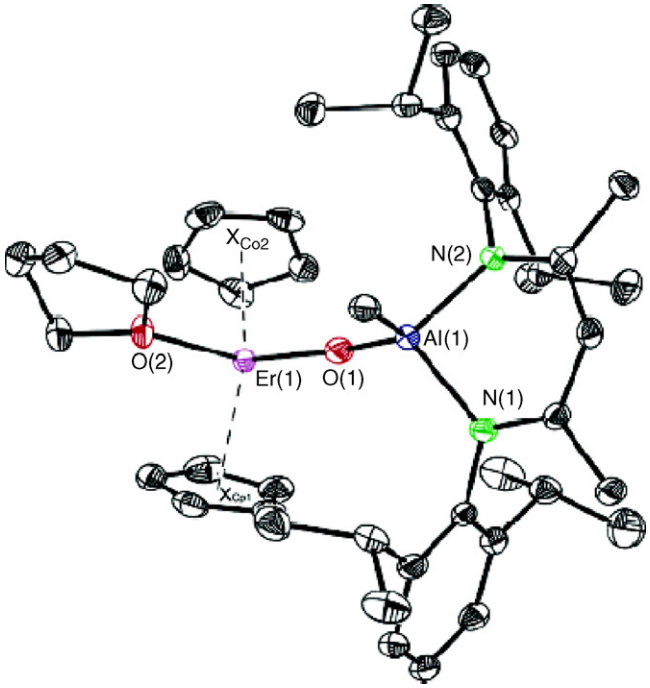

Fig. 66. Molecular structure of $Cp_2Er(THF)$-O-AlL(Me) [104].

$[Ph_3C][B(C_6F_5)_4]$ have been found to effectively catalyze the alternating ethylene–norbornene copolymerization as illustrated in Scheme 67 [29].

A detailed theoretical investigation of alternative mechanisms for chain initiation of the organolanthanide-promoted ring-opening polymerization (ROP) of 2-phenyl-1-methylenecyclopropane with an archetypical Cp_2SmH model catalyst has been published [108].

2.11.2.2. Dienes (butadiene, isoprene, etc.). Cationic methyl complexes of yttrium such as $[YMe_2(THF)_5][BPh_4]$ have been reported to catalyze the homogeneous polymerization of 1,3-butadiene and isoprene [6]. Highly stereospecific polymerization of isoprene has been achieved using neodymium borohydride complexes. In combination with stoichiometric amounts of dialkylmagnesium, $Nd(BH_4)_3(THF)_3$ and $(C_5Me_4Pr^n)Nd(BH_4)_2(THF)_2$ afford very efficient catalysts. The activity reaches 37,300 (g of polyisoprene/mol of Nd)/h. The half-metallocene gives rise to polyisoprene,

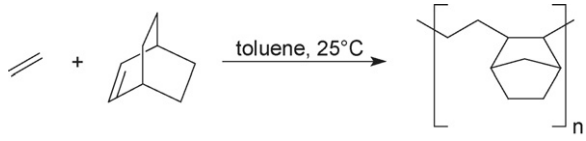

Scheme 67.

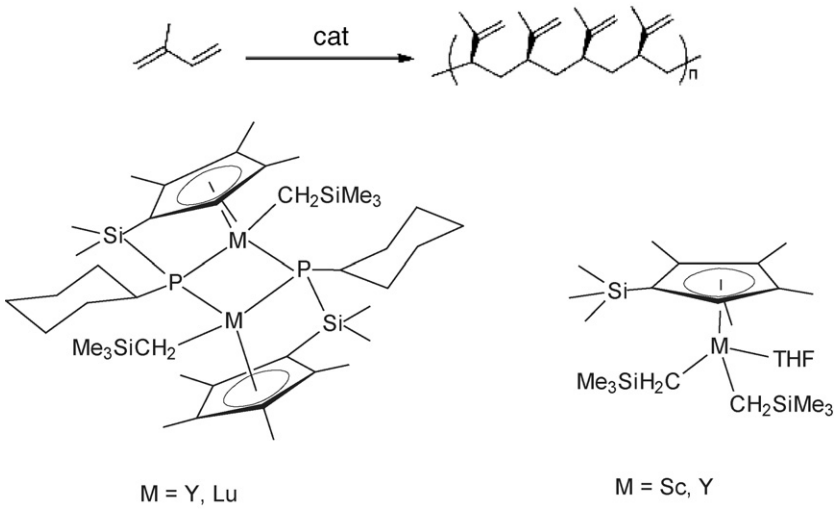

Scheme 68.

98.5% *trans*-regular, the highest content yet described for a homogeneous organometallic catalyst. NMR experiments argue for the formation of bimetallic Nd(μ-BH_4)Mg active species [109]. The alternating copolymerization of ethylene and butadiene has been achieved with the *ansa*-neodymocene catalyst [$Me_2Si(C_5H_4)(C_{13}H_8)$]NdCl ($C_{13}H_8$ = fluorenyl). This was the first time that this copolymerization has been achieved with a metallocene-based single-site catalyst. The diene was found to be mainly inserted in *trans*-1,4-configuration [110]. Unprecedented isospecific 3,4-polymerization of isoprene (Scheme 68) has been achieved by cationic rare earth metal alkyl species resulting from a binuclear precursor. The catalysts were made by *in situ* treatment of the precursors shown in Scheme 68 with [Ph_3C][$B(C_6F_5)_4$] [111].

2.11.2.3. Cyclic esters and amides (ε-caprolactone, δ-valerolactone,etc.). Several tris(allyl) and bis(allyl)(diketiminato) lanthanide complexes have been demonstrated to be highly effective single-component catalysts for the ring-opening polymerization of ε-caprolactone and *rac*-lactide. Polymer end group analysis showed that the polymerization process is initiated by allyl transfer to the monomer [24]. Reactivity studies of amine-bis(phenolate) complexes of the type [$Me_2NCH_2CH_2N\{CH_2(2\text{-}OC_6H_2Bu^t\text{-}3,5)\}_2$]LnMe(THF) (Ln = Er, Yb) showed them to be efficient initiators for the ring-opening polymerizaion of ε-caprolactone [12]. A comparison of organolanthanide complexes, Cp^*_2SmMe(THF) and (μ-PhC=C=C=CPh)[Cp^*_2Sm]$_2$, with the tin compounds $Bu^n_2Sn(OMe)_2$ and $Bu^n_2Sn(OCH_2CH_2CH_2O)$ in the preparation of random, diblock, and triblock copolymers composed of L-lactide, D,L-lactide, and cyclic carbonates, trimethylene carbonate or 2,2-dimethyltrimethylene carbonate, has been reported and the biodegradabilities of the polymers examined [112]. Lanthanide complexes containing silyl group-functionalized indenyl ligands have been reported to exhibit high catalytic activities on ε-caprolactone polymerization. The effects of temperature, substituent groups on the indenyl ligands of the complexes, and solvents on the catalytic activities have been examined [67]. The organosamarium thiolate complex [$(MeC_5H_4)_2$Sm(μ-SPh)(THF)]$_2$ has been reported to be an efficient initiator for the homo- and copolymerization of ε-caprolactone and 2,2-dimethyltrimethylenecarbonate [43].

2.11.2.4. Acrylic monomers (methylmethacrylate (MMA), acrylonitrile, etc.). A catalyst system comprising *ansa*-bis(fluorenyl)lanthanide metallocenes and nanosized sodium hydride as co-catalyst has been shown to be very active in the production of methylmethacrylate homopolymers. The observed activity was comparable to that of organolanthanide hydrides as single-component catalysts [113]. A series of *ansa*–lanthanocene complexes containing the dimethylbis[3-(1-methyl-1-phenylethyl)-2,4-cyclopentadien-1-yl]silane ligand has been tested as methylmethacrylate homopolymerization catalysts [63].

2.11.2.5. Other monomers. The mono(cyclopentadienyl)-lanthanide bis(alkyl) complexes ($C_5Me_4SiMe_3$)Ln(CH_2-$SiMe_3$)$_2$(THF) (Ln = Sc, Y, Dy, Lu) and the polyhydride complexes [($C_5Me_4SiMe_3$)Ln(μ-H)$_2$]$_4$(THF)$_x$ (Ln = Y, Lu, x = 1; Ln = Dy, x = 2) have been found to be active as single-component catalysts not only for the ring-opening homopolymerization of cyclohexene oxide (CHO), but also for the alternating copolymerization of CHO and CO_2 yielding the corresponding polycarbonates (Scheme 69) [30].

2.11.3. Organolanthanide catalyzed hydrosilylation reactions

Organolanthanide catalyzed cyclization-silylation of nitrogen-containing polyunsaturated systems allows access to core structures commonly found in naturally occurring alkaloids. In this context, nitrogen-containing dienes with various

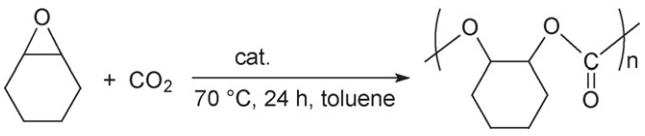

Scheme 69.

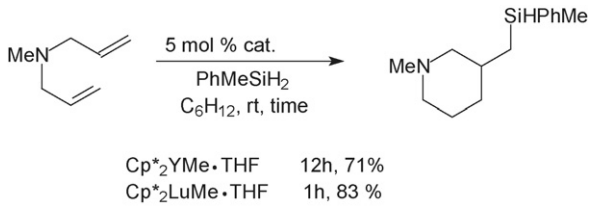

Scheme 70.

substitution patterns have been investigated. A prototypical reaction is illustrated in Scheme 70. The method was found to be most successful for substrates with terminal alkenes. Cyclization upon pendant 1,1-disubstituted olefins was not realized under various conditions. Interestingly, sterically hindered sulfonamides, which were previously believed to render the catalyst inactive, were actually compatible with the catalyst, thus affording the cyclized products after prolonged reaction times. Variations using fused ring systems have also been investigated [114].

2.11.4. Organolanthanide catalyzed hydroamination reactions

Hultzsch et al. have published a short review entitled "Non-metallocene rare earth metal catalysts for the diastereoselective hydroamination of aminoalkenes". The synthesis and catalytic activity of non-metallocene lanthanide complexes based on diamidoamine, biphenolate and binaphtholate ligands have been summarized in this article [13].

The complete catalytic reaction course for the organolanthanide-mediated intramolecular hydroamination/cyclization of (4E,6)-heptadiene-1-amine by a prototypical achiral $Cp^*_2La[CH(SiMe_3)_2]$ precatalyst has been thoroughly investigated employing a gradient-corrected DFT method [115]. In a similar manner, the hydrophosphination/cyclization of a prototypical phosphinoalkene, $H_2P(CH_2)_3CH{=}CH_2$, catalyzed by $Cp_2LaCH(SiMe_3)_2$, has been analyzed using density functional theory methods, and the results have been compared/contrasted to analogous hydroamination/cyclization processes. The reaction was found to proceed in two discrete steps: (1) cyclization *via* C=C insertion into the Cp_2La-P(phosphido) linkage to form La–C and C–P bonds and (2) subsequent La–C protonolysis (Scheme 71). The insertion of the alkene fragment into the Cp_2La-P(phosphido) bond is approximately thermoneutral and proceeds *via* a highly organized, seven-membered, chairlike cyclic transition state. The resulting cyclopentylmethyl complex then undergoes turnover-limiting but exothermic protonolysis to yield a phosphine-phosphido complex, the likely resting state of the catalyst [116].

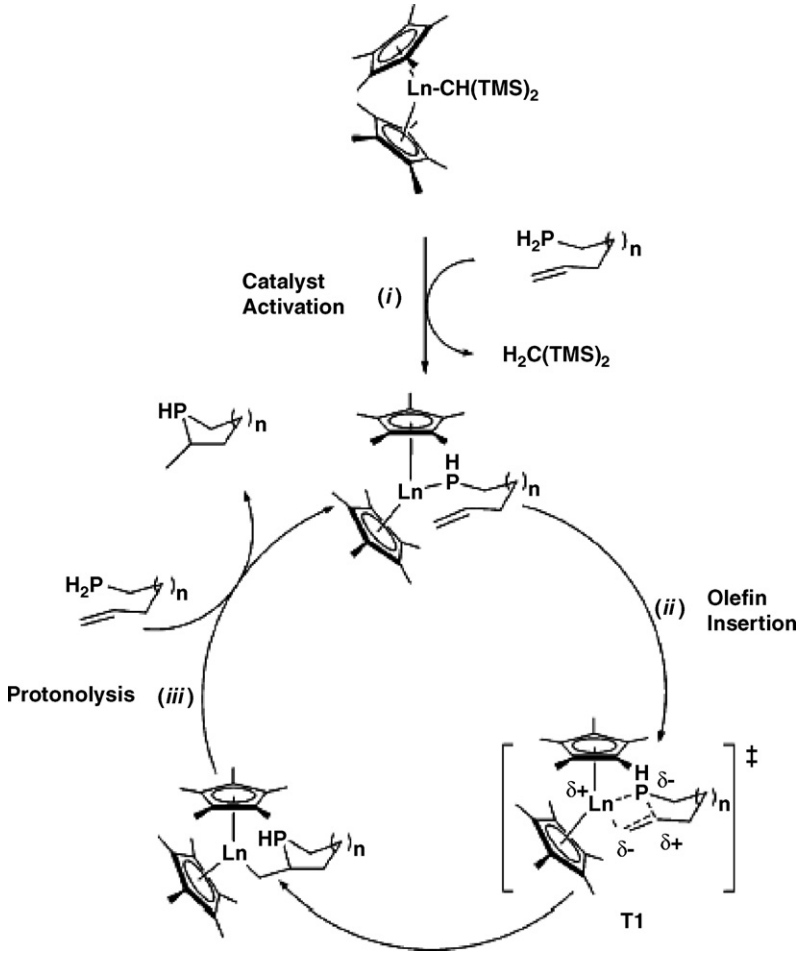

Scheme 71. Proposed catalytic cycle for the organolanthanide catalyzed cyclohydrophosphination of phosphinoalkenes [116].

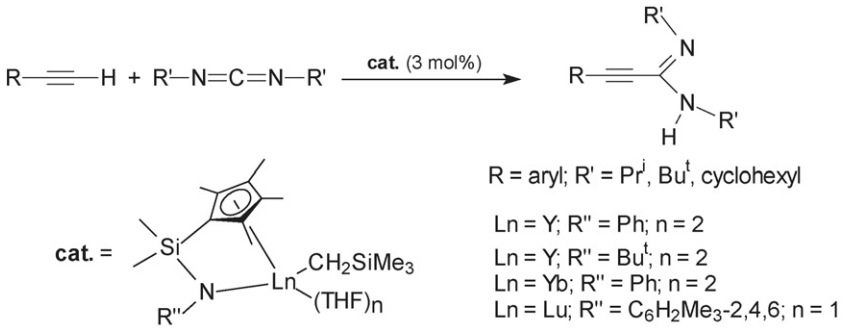

Scheme 72.

In a closely related theoretical study the complete catalytic reaction course for the organolanthanide mediated intermolecular hydroamination of 1,3-butadiene and *n*-propylamine by an archetypical $[Me_2Si(C_5Me_4)_2]NdCH(SiMe_3)_2$ precatalyst has been investigated by employing a reliable gradient-corrected DFT method [117].

2.11.5. Other organolanthanide catalyzed reactions

The compound $[Me_2Si(C_5Me_4)_2]ScMe$ has been reported to be a catalyst for the addition of methane across the double bond of secondary terminal olefins [65].

Two anhydrous, dimeric samarium(III) complexes bearing a bulky μ-alkoxide (diphenylmethoxide) ligand and different tetradentate Schiff bases have been shown to catalyze the epoxidation of 1,3-diphenylpropenone (chalcone) [118]. Treatment of the mesoporous silicate SBA-15 with $Sm[N(SiMe_3)_2]_3$ led to formation of a novel organolanthanide/inorganic hybrid material $[SBA\text{-}15]Sm[N(SiMe_3)_2]_x$ *via* abstraction of $N(SiMe_3)_2$ by terminal silanol groups and subsequent surface silylation. The hybrid material was shown to be a promising catalyst for the Tishchenko reaction, which is one of the most attractive transformations of aldehydes [119]. A series of *ansa*-bis(fluorenyl)lanthanide metallocenes has been shown to be very active Lewis acidic catalysts for the cyanosilylation of prochiral aldehydes and ketones with Me_3SiCN giving cyanotrimethylsilyl ethers with >99% conversion of the starting materials [120,121]. The catalytic addition of terminal alkynes to carbodiimides has been achieved with the half-sandwich complexes $[Me_2Si(C_5Me_4)(NR'')]Ln(CH_2SiMe_3)(THF)$ (Ln = Y, Yb, Lu) as illustrated in Scheme 72. The reaction leads to an almost quantitative formation of propiolamidine derivatives [32].

2.12. Organolanthanides in organic synthesis

Applications of samarium reagents in organic synthesis have been reviewed by Liu and Zhang under the title: "New progress in the application of samarium reagent to organic synthesis". The following aspects have been considered in this account: (1) studies on organic reactions promoted by samarium diiodide; (2) the direct use of metallic samarium in organic synthesis; (3) the application of other samarium reagents such as samarium triiodide and organosamarium species (e.g. allylsamarium bromide) in organic reactions [122].

2.13. Organolanthanides in materials science

A number of dysprosium alkoxides, some of them involving π-arene coordination, have been used as Dy dopants in lead zirconium titanate (PZT) thin films in order to add improved fatigue-resistance characteristics [83]. Gadolinium oxide thin films have been deposited on Si(1 0 0) by atomic layer deposition (ALD) using as precursor $(MeC_5H_4)_3Gd$ together with water. At 250 °C the uniform films obtained from this organogadolinium precursor showed almost an ideal stoichiometry with low impurity contents (*e.g.* 0.5 at.% of C). X-ray diffraction data indicated that the Gd_2O_3 films were crystalline with cubic C-type structure when deposited even at 150 °C [123]. Organometallic tris(methylcyclopentadienyl)erbium and water have been successfully exploited as precursors for the atomic layer deposition (ALD) of Er_2O_3 thin films. Deposition studies were carried out in the temperature range 175–450 °C, where Si(1 0 0) and soda-lime glass were used as substrates. The deposited Er_2O_3 films were smooth and very uniform, and contained only low concentrations of carbon and hydrogen as impurities [124].

3. Actinides

3.1. Actinide carbonyls

The coordination and bonding of equatorial carbonyl ligands with the uranyl dication, $[UO_2]^{2+}$, has been studied using density functional theory with relativistic effective core potentials. Newly predicted ground-state structures of $[UO_2(CO)_5]^{2+}$ have been reported [125]. The reaction of the coordinatively unsaturated tris(aryloxide) uranium(III) complex U(L) (L = 1,4,7-tris(3,5-di-*tert*-butyl-2-hydroxybenzylate)-1,4,7-triazacyclononane) with carbon monoxide has been investigated. Exposure of a degassed pentane solution of U(L) to CO (1 atm) resulted in a gradual color change from red-brown to light brown. Solvent evaporation to dryness and recrystallizaion from benzene afforded brown hexagonal

crystals. An X-ray crystal structure determination revealed the presence of the unprecedented μ-isocarbonyl-bridged, mixed-valent diuranium species (L)U–CO–U(L) [126].

3.2. Actinide hydrocarbyls

Laser-ablated thorium atoms have been reported to react with methyl fluoride to give the thorium methylidene complex CH_2=ThHF as the major product observed and trapped in solid argon. Infrared spectroscopy, isotopic substitution, and density functional theoretical frequency calculations confirmed the identification of this methylidene complex. The homologous CH_2=ThHCl and CH_2=ThHBr were obtained in a similar manner from methyl chloride and methyl bromide, respectively [127]. The derivative chemistry of a heteroleptic monoalkyl uranium complex supported by the hydrotris(3,5-dimethylpyrazolyl)borate ligand has been investigated. Insertion of benzonitrile and acetonitrile into the U–C bond of $U(Tp^{Me_2})Cl_2(CH_2SiMe_3)$ ($Tp^{Me_2} = HB(3,5-Me_2pz)_3$) afforded the ketimide komplexes $U(Tp^{Me_2})Cl_2[NC(R)(CH_2SiMe_3)]$ (R = Ph, Me) [128]. Novel uranium bis(alkyls) have been synthesized with the use of different diamido ether ancillary ligands. A typical reaction sequence is outlined in Scheme 73 [129].

The synthesis of two tetravalent uranium alkoxide-carbene complexes has been reported, golden-colored UIL_3 and emerald green UL_4, where L = $OCMe_2CH_2$[1-C(NCHCHNPr^i)] (Scheme 74). The latter shows dynamic behavior in solution at room temperature, and the crystal structure of UL_4 shows that one carbene group remains uncoordinated (Fig. 67). The unbound *N*-heterocyclic carbene group can be trapped by a range of reagents such as 16-valence-electron metal carbonyl fragments and BH_3 moieties, forming, for example, $UL_3(\mu\text{-}L)W(CO)_5$, $UL_2(\mu\text{-}L)_2Mo(CO)_4$, and $UL_n(L\text{-}BH_3)_{4-n}$ (n = 1–4). This reactivity demonstrates the potential for these hemilabile electropositive metal–carbene complexes to participate in the bifunctional activation of small molecules [130].

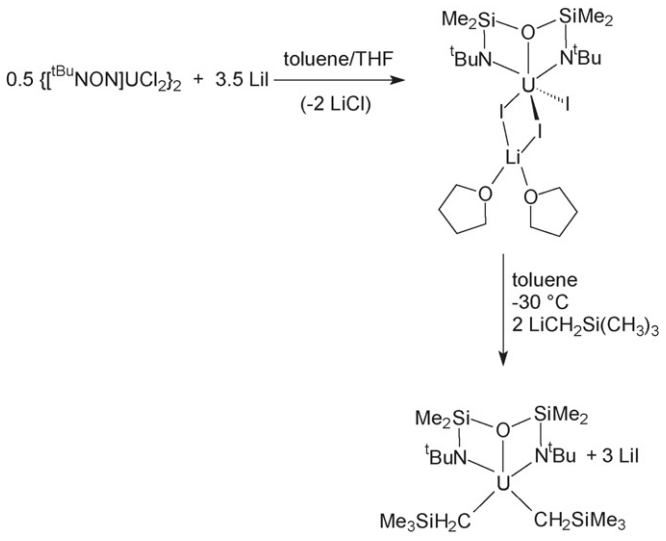

Scheme 73. ([^{tBu}NON] = $(Bu^tNSiMe_2)_2O^{2-}$).

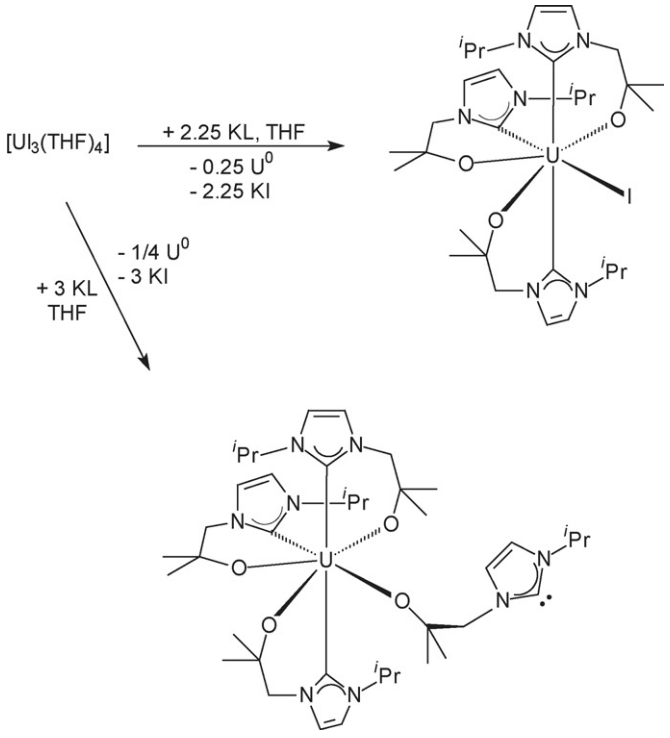

Scheme 74.

3.3. Actinide cyclopentadienyl compounds

3.3.1. Cp_3An and Cp_3AnL compounds

The mono and bis(cyclopentadienyl) compounds $(C_5H_4Bu^t)UI_2$ and $(C_5H_4Bu^t)_2UI$ were formed in THF by comproportionation reactions of $U(C_5H_4Bu^t)_3$ and UI_3L_4 (L = THF or py) in the molar ratio of 1:2 and 2:1, respectively, while treatment of $UI_3(py)_4$ with one or two molar equivalents of $Li(C_5H_4Bu^t)$ in THF afforded the $(C_5H_4Bu^t)UI_2$ and $[(C_5H_4Bu^t)_2UI_2]^-$ complexes, respectively. The X-ray crystal structures of $(C_5H_4Bu^t)UI_2(py)_3$ (dark blue crystals,

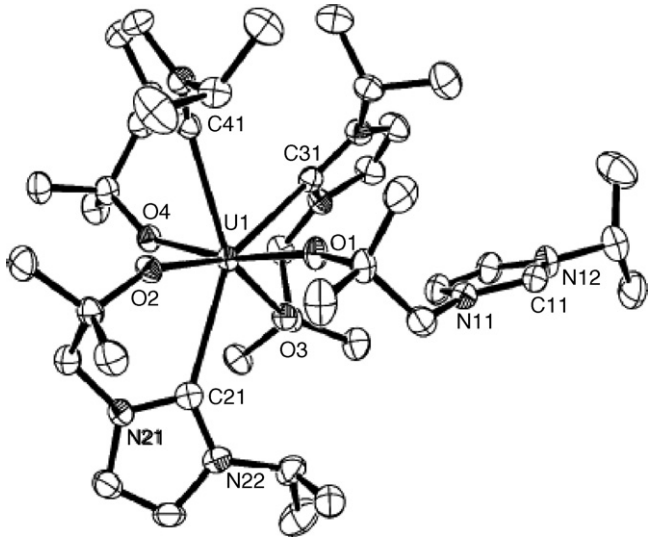

Fig. 67. Molecular structure of UL_4 (L = $OCMe_2CH_2$[1-C(NCHCHNPr^i)]) [130].

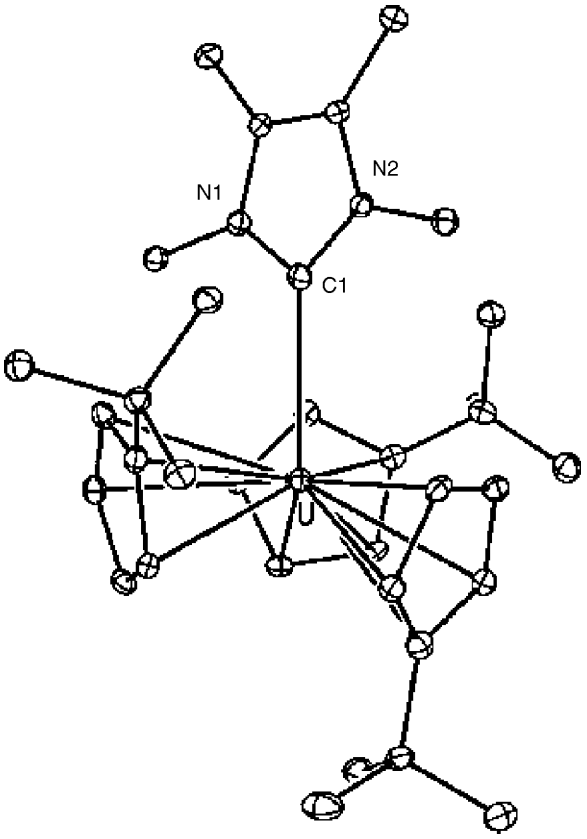

Fig. 68. Molecular structure of $(C_5H_5Bu^t)_3U(C_3Me_4N_2)$ [57].

78% yield) and $(C_5H_4Bu^t)_2UI(py)_2$ (dark green crystals, 75% yield) have been determined [27]. In the presence of one molar equivalent of the heterocyclic carbene $C_3Me_4N_2$ (=tetramethylimidazolylidene) the trivalent metallocene $U(C_5H_5Bu^t)_3$ is readily and quantitatively transformed in toluene into its carbene adduct $(C_5H_5Bu^t)_3U(C_3Me_4N_2)$, which crystallizes from this solvent as dark brown crystals in 98% yield. This was the first example of an organometallic uranium(III) complex containing a heterocyclic carbene ligand. Its molecular structure is illustrated in Fig. 68 [57].

Several uranium(III) compounds supported by the hydrotris(3,5-dimethylpyrazolyl)borate ligand ($= Tp^{Me_2}$) have been synthesized and characterized, including an organometallic mono(cyclopentadienyl) derivative. Metathesis of $(Tp^{Me_2})_2UI$ with NaCp yielded $(\kappa^3\text{-}Tp^{Me_2})(\kappa^2\text{-}Tp^{Me_2})UCp$ as a dark green solid in 76% yield. Thermolysis of this compound at 160 °C resulted in oxidation of the metal center and redistribution of the ligands, giving $Cp_3U(dmpz)$, pyrazabole, and $(Tp^{Me_2})U(dmpz)_3$ (dmpz = 3,5-pyrazole) [131]. The formally anionic complex $(C_5Me_4H)_2UMe_2K$ provides entry into unsolvated bis(tetramethylcyclopentadienyl)U(III) chemistry. Treatment of this complex with 2 equiv. of $[Et_3NH][BPh_4]$ led to formation of the trivalent cationic complex $[(C_5Me_4H)_2U][(\mu\text{-}Ph)_2BPh_2]$ (Scheme 75), which has a structure differing from that of $[Cp^*_2U][(\mu\text{-}Ph)_2BPh_2]$ in that one arene ring in $[(C_5Me_4H)_2U][(\mu\text{-}Ph)_2BPh_2]$ approaches the uranium ion in an η^6 mode and the other in an η^1 orientation (Fig. 69) [132].

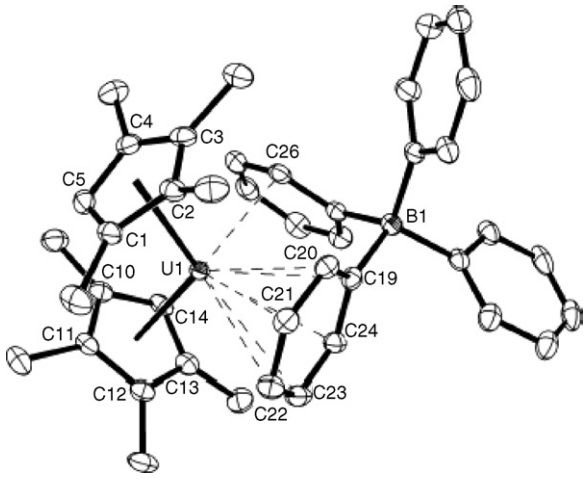

Fig. 69. Molecular structure of $[(C_5Me_4H)_2U][(\mu\text{-}Ph)_2BPh_2]$ [132].

It was reported that $(C_5Me_4H)_3U$ can be prepared in high yield either from unsolvated UI_3 or from the THF solvate $UI_3(THF)_4$ by treatment with 3 equiv. of $K(C_5Me_4H)$. Pure $(C_5Me_4H)_3U$ forms a brown-green powder [133].

3.3.2. $CpAnX_3$, Cp_2AnX_2 and Cp_3AnX compounds

Although bis(pentamethylcyclopentadienyl)uranium metallocene chemistry has been extensively explored, relatively little is known about the reactivity of the bis(tetramethylcyclopentadienyl) analogues. An important starting material, $(C_5Me_4H)_2UCl_2$, has been prepared *via* two different synthetic routes, either by treatment of $(C_5Me_4H)_3UCl$ with $HgCl_2$ (82% yield) or from UCl_4 and $(C_5Me_4H)MgCl(THF)$ in a 1:2 molar ratio (78% yield) [133]. It was also shown that $(C_5Me_4H)_2UCl_2$ reacts with MeLi to form the methyl complexes $(C_5Me_4H)_2UClMe$ and $(C_5Me_4H)_2UMe_2$, both of which were

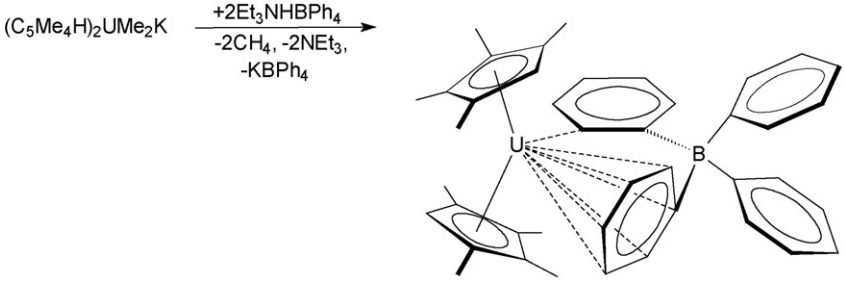

Scheme 75.

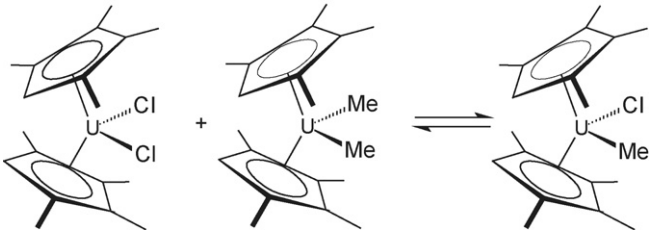

Scheme 76.

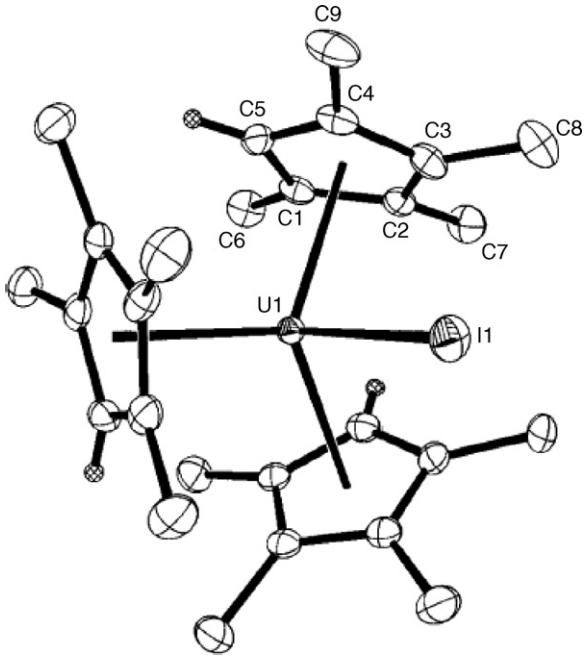

Fig. 70. Molecular structure of $(C_5Me_4H)_3UI$ [133].

characterized by X-ray crystallography. $(C_5Me_4H)_2UClMe$ can also be synthesized by ligand redistribution between $(C_5Me_4H)_2UCl_2$ and $(C_5Me_4H)_2UMe_2$ (Scheme 76) [132].

Other tetramethylcyclopentadienyl uranium(IV) complexes include $(C_5Me_4H)_3UCl$ and $(C_5Me_4H)_3UI$, which can be obtained by allowing $U(C_5Me_4H)_3$ to react with either Bu^tCl, PhCl, or $HgCl_2$ for the chloride or PhI or HgI_2 for the iodide. The molecular structure of $(C_5Me_4H)_3UI$ has been determined by X-ray diffraction (Fig. 70) [133].

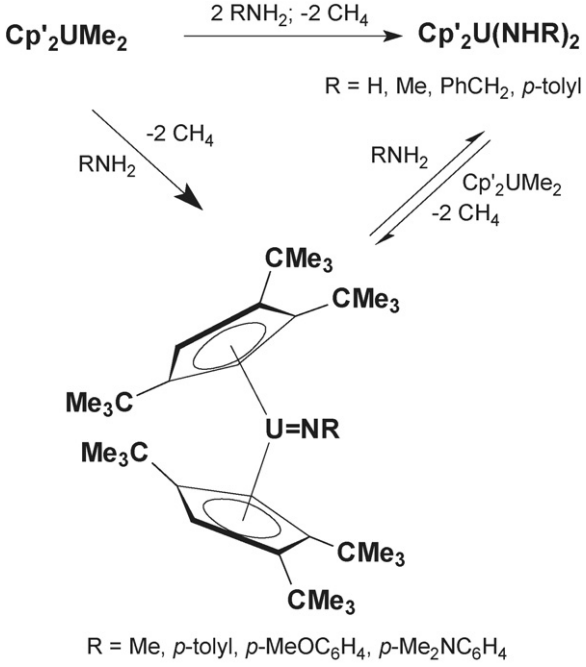

Scheme 78.

Attempts to make unsolvated bis(tetramethylcyclopentadienyl) U(III) complexes with the tethered olefin ligand $[(C_5Me_4)SiMe_2(CH_2CH{=}CH_2)]^-$ by allowing $K[(C_5Me_4)SiMe_2(CH_2CH{=}CH_2)]$ to react with $UI_3(THF)_4$ led to the formation of $[(C_5Me_4)SiMe_2(CH_2CH{=}CH_2)]_2UI(THF)$ (Scheme 77). Although solvated, this compound readily loses THF and is the first example of an actinide complex that contains a tethered olefin functionality [132].

The uranium metallocenes $[C_5H_3(EMe_3)_2\text{-}1,3]_2UMe_2$ (E = C, Si) react with NH_3 to give the dimers $[\{C_5H_3(EMe_3)_2\text{-}1,3\}_2U(\mu\text{-}NH)]_2$, but with *p*-toluidine to give the monomeric diamides $[C_5H_3(EMe_3)_2\text{-}1,3]_2U(NH\text{-}p\text{-}tolyl)_2$. The uranium metallocene $[C_5H_2(Bu^t)_3\text{-}1,2,4]_2UMe_2$ reacts with RNH_2 to yield $[C_5H_2(Bu^t)_3\text{-}1,2,4]_2U(NHR)_2$ (R = Me, CH_2Ph, *p*-tolyl), which have been isolated as crystalline solids. In benzene solution these diamides are in equilibrium with $[C_5H_2(Bu^t)_3\text{-}1,2,4]_2U{=}NR$, which can be isolated pure when R is Me or *p*-tolyl (Scheme 78), and the primary amine [134].

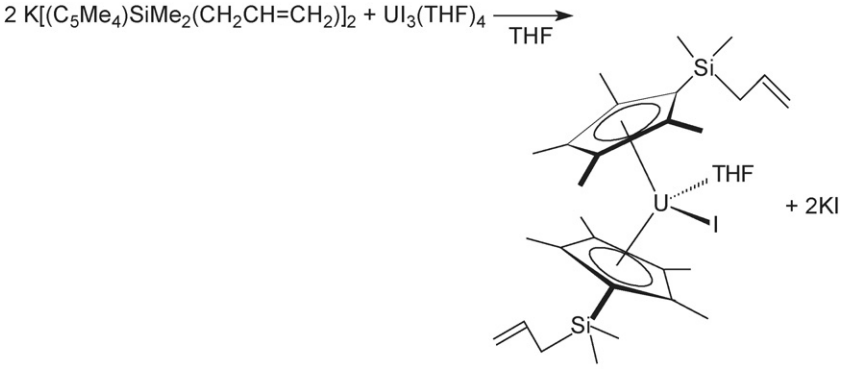

Scheme 77.

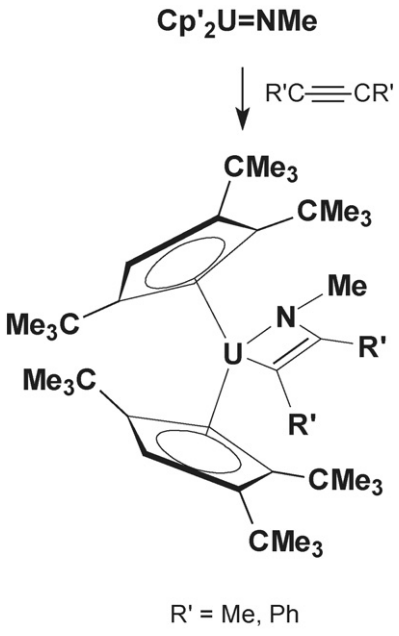

Scheme 79.

The monomeric imide $[C_5H_2(Bu^t)_3\text{-}1,2,4]_2U{=}NMe$ reacts with $R'C{\equiv}CR'$ to yield the cycloaddition products $[C_5H_2(Bu^t)_3\text{-}1,2,4]_2U[N(Me)C(R'){=}C(R')]$ ($R' = Me$, Ph) as illustrated in Scheme 79 [134].

In a related study the remarkable base-free bis(1,2,4-tri-*tert*-butylcyclopentadienyl)uranium oxide Cp'_2UO ($Cp' = C_5H_2(Bu^t)_3\text{-}1,2,4$) has been prepared. In this context the derivative chemistry of the starting material, $[C_5H_2(Bu^t)_3\text{-}1,2,4]_2UCl_2$, has also been investigated. These reactions are summarized in Scheme 80 [135].

Reduction of $[C_5H_2(Bu^t)_3\text{-}1,2,4]_2UCl_2$ in the presence of 2,2′-bipyridine and sodium naphthalide afforded the dark green metallocene complex $Cp'_2U(bipy)$, which reacts with *p*-tolyl azide or pyridine N-oxide to give $Cp'_2U{=}N(p\text{-tolyl})$ or $Cp'_2U(O)(py)$, respectively (Scheme 81). The Lewis acid BPh_3 precipitates $Ph_3B(py)$ and gives the base-free oxo complex Cp'_2UO, which crystallizes from pentane as red-brown microcrystals. This compound behaves as a nucleophile with Me_3SiX (Scheme 81, X = Cl, Br, CN, N_3, OSO_2CF_3), but it does not exhibit cycloaddition behavior with acetylenes, suggesting that the polar resonance structure $Cp'_2U^+{-}O^-$ dominates the double-bond resonance structure $Cp'_2U{=}O$ [135].

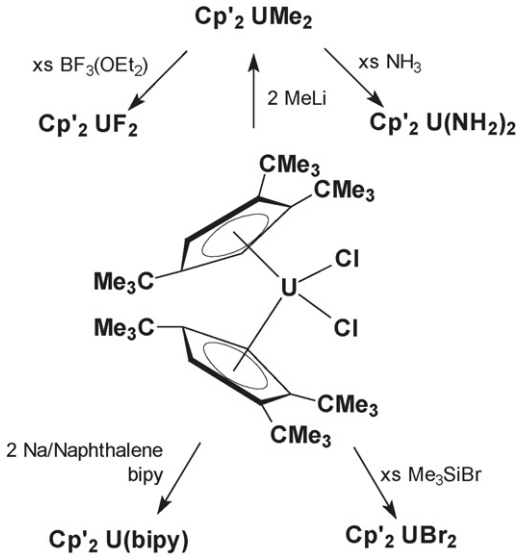

Scheme 80.

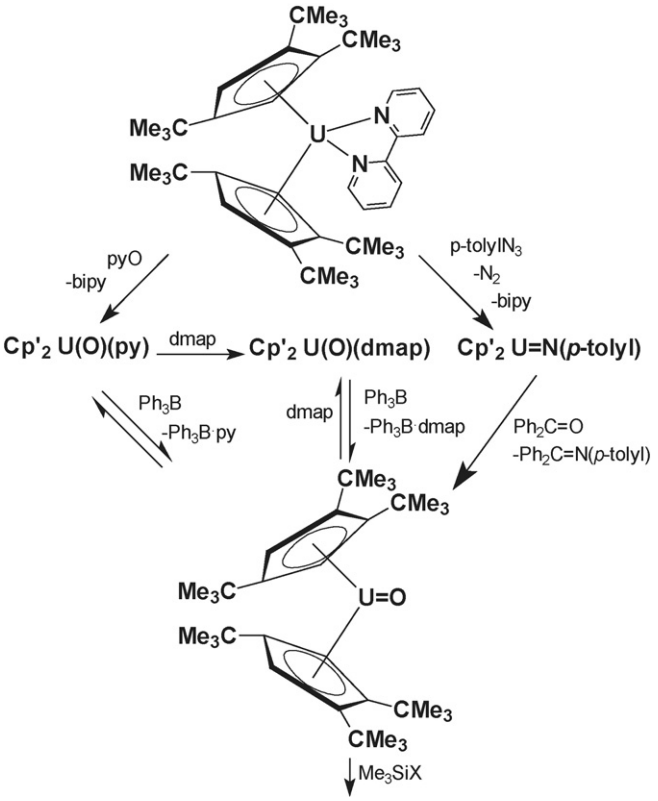

Scheme 81.

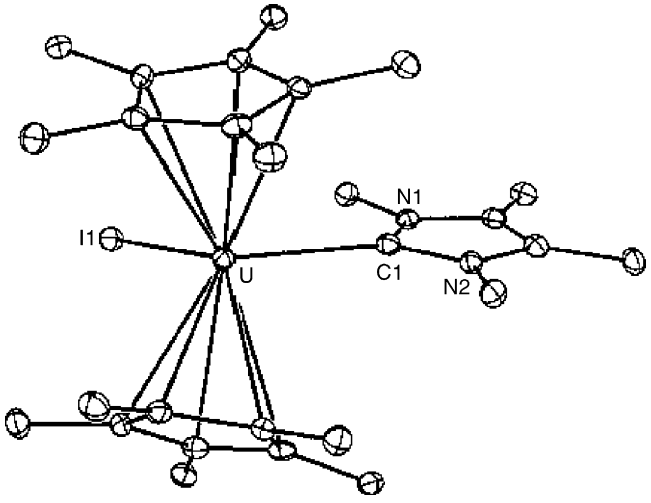

Fig. 71. Molecular structure of $Cp^*_2UI(C_3Me_4N_2)$ [57].

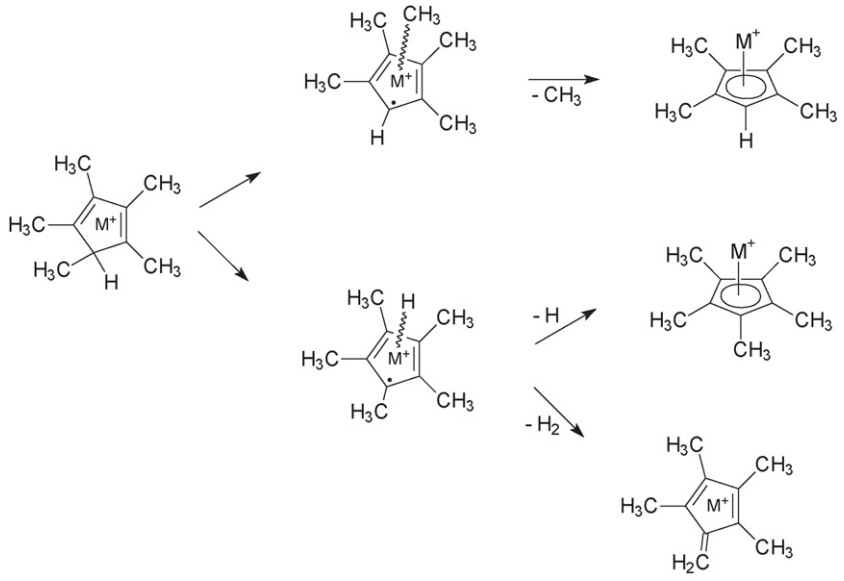

Scheme 82.

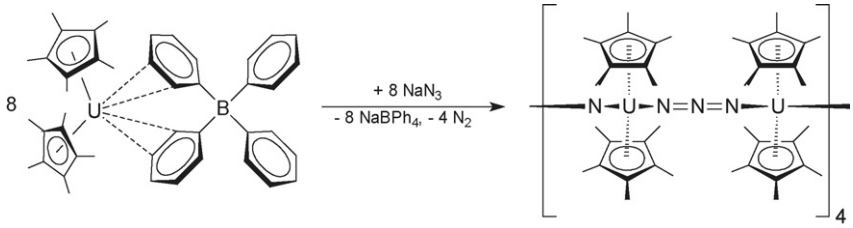

Scheme 83.

3.3.3. Pentamethylcyclopentadienyl compounds

3.3.3.1. Cp^*AnX_2 and Cp^*_2AnX compounds. Treatment of $Cp^*_2UI(py)$ (py = pyridine) with one mole equivalent of 2,2′-bipyridine (=bipy) in THF gave the adduct $Cp^*_2UI(bipy)$, which was transformed into $Cp^*_2U(bipy)$ by Na(Hg) reduction. Similar reaction of $Cp^*_2UI(py)$ with one mole equivalent 2,2′:6′,2″-terpyridine (=terpy) afforded the ionic adduct $[Cp^*_2U(terpy)]I$, which could also be reduced to the neutral complex $Cp^*_2U(terpy)$ by sodium amalgam [53]. Reduction of $Cp^*_2U(dddt)$ with Na(Hg) or addition of Na_2dddt to $Cp^*_2U(\mu\text{-}Cl)_2Na(THF)_x$ in the presence of 18-crown-6 gave the first uranium(III) dithiolene compound, $[Na(18\text{-crown-}6)(THF)_2][Cp^*_2U(dddt)]$ (dddt = 5,6-dihydro-1,4-dithiin-2,3-dithiolato) [52]. Addition of one molar equivalent of the heterocyclic carbene $C_3Me_4N_2$ (=tetramethylimidazolylidene) to $Cp^*_2UI(py)$ in toluene led to the immediate substitution of the pyridine ligand to give the carbene complex $Cp^*_2UI(C_3Me_4N_2)$, which was isolated as dark green crystals in 70% yield. The metal coordination geometry is the familiar *pseudo*-tetrahedral arrangement found in the series of complexes Cp^*_2AnXL (Fig. 71) [57].

3.3.3.2. Mono(pentamethylcyclopentadienyl) actinide(IV)-compounds. Reactions of the monopositive actinide ions An^+ with pentamethylcyclopentadiene, HCp^*, have been studied by mass spectrometry. This was the first study of the An^+/HCp^* reaction for $An^+ = Am^+$, Cm^+, Bk^+, Cf^+, and Es^+. Each of the actinide ions reacted with HCp^* to produce $[AnCp^*]^+$ (+H), as well as additional products. Both Cf^+ and Es^+ have previously been found to be inert toward most alkenes, but efficiently reacted with HCp^* to induce (1) H-loss and $[AnCp]^+$; (2) H_2-loss and $[An(C_5Me_4CH_2)]^+$, and (3) CH_3-loss and $[An(C_5Me_4H)]^+$ (An = Cf, Es). The proposed pathways are illustrated in Scheme 82. These were the first organoeinsteinium complexes derived from activation of an organic substrate. Secondary products included $[Cp^*_2An]^+$ (An = Am, Cm, Bk, Cf, Es), the compositions of which correspond to the metallocene sandwich complexes [136].

3.3.3.3. Bis(pentamethylcyclopentadienyl) actinide(IV)-, (V)-, and (VI)-compounds. The most exciting achievement in organoactinide chemistry in 2005 was the synthesis of molecular octauranium rings with alternating nitride and azide bridges. Several 24-membered uranium nitrogen rings, $(UNUN_3)_4$,

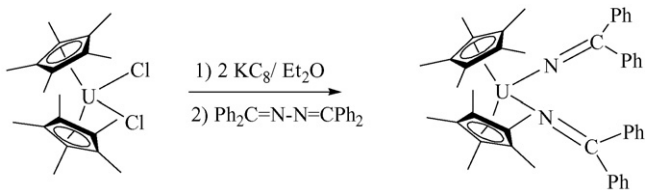

Scheme 84.

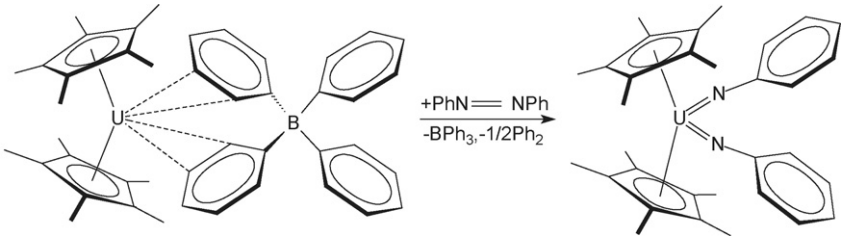

Scheme 85.

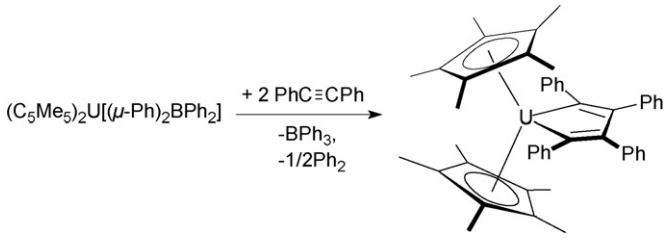

Scheme 86.

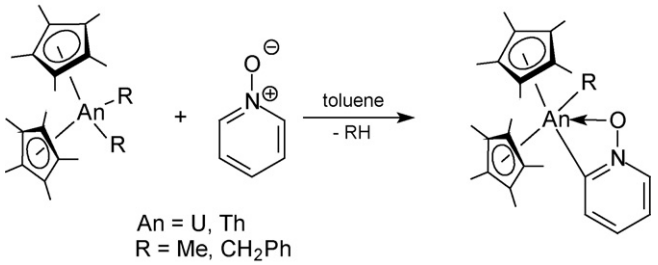

Scheme 87.

have been synthesized by reduction of sodium azide with the tetraphenylborate derivatives $[(C_5Me_4R)_2U][(\mu\text{-}Ph)_2BPh_2]$ (R = H, Me). Scheme 83 illustrates the reaction with the Cp^* precursor. The nanometer-sized rings contain unusual UNU nitride linkages that have short U–N distances within the double-bond range [137].

A toluene slurry of $UI_4(C{\equiv}NPh)_4$ treated with 2.2 equiv. of $Cp^*MgCl(THF)$ provided $Cp^*_2UI_2(N{\equiv}CPh)$ in low yields. A single-crystal X-ray structure determination showed that the iodide ligands in $Cp^*_2UI_2(N{\equiv}CPh)$ are in a rare *cis*-configuration with an acute I–U–I angle of 83.16(7)° [138]. Electronic absorption and resonance-enhanced Raman spectra have been recorded for the uranium(IV) ketimido complexes $Cp^*_2U{-}[N{=}C(Ph)(R)]_2$ (R = Me, Ph, CH_2Ph), which had been previously synthesized according to Scheme 84. The products have been found to be surprisingly unreactive and display unusual electronic properties. The physical properties and chemical stability of these complexes already suggested higher U–N bond order owing to significant ligand to metal π-bonding in the uranium ketimido interactions. The observations of both charge-transfer transitions and resonance enhancement of Raman vibrational bands in the more recent study are exceedingly rare for tetravalent actinide complexes and reflect the strong bonding interactions between the uranium 5*f*/6*d* orbitals and those on the ketimido ligands [139,140].

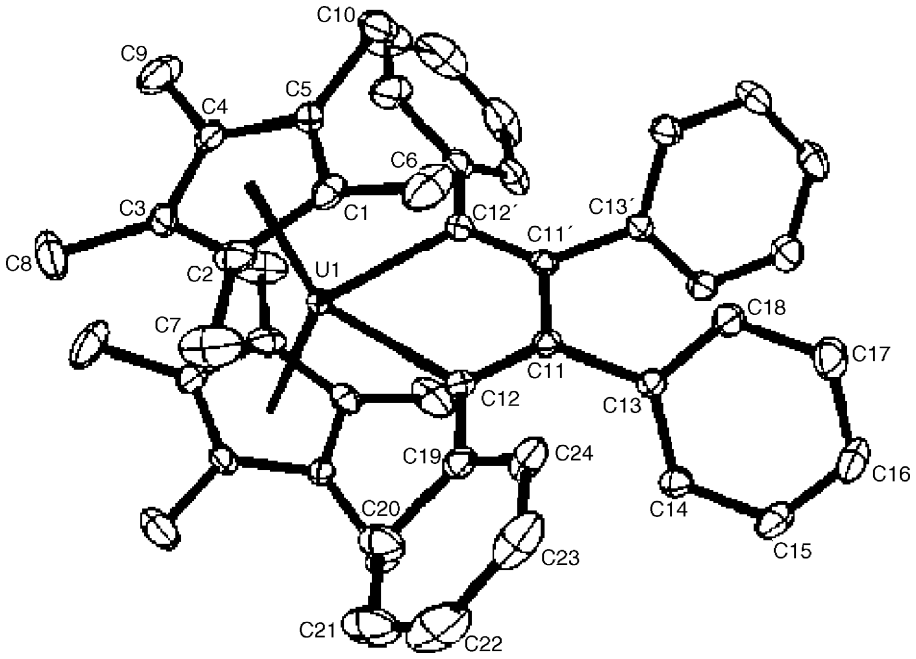

Fig. 72. Molecular structure of $Cp^*_2U(C_4Ph_4)$ [141].

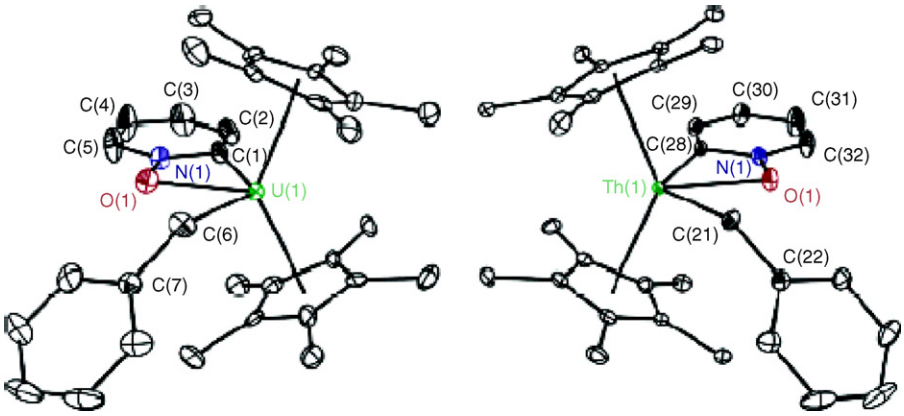

Fig. 73. Molecular structure of $Cp^*_2U(CH_2Ph)[\eta^2\text{-}(O,C)\text{-}ONC_5H_4]$ (left) and $Cp^*_2Th(CH_2Ph)[\eta^2\text{-}(O,C)\text{-}ONC_5H_4]$ (right) [142].

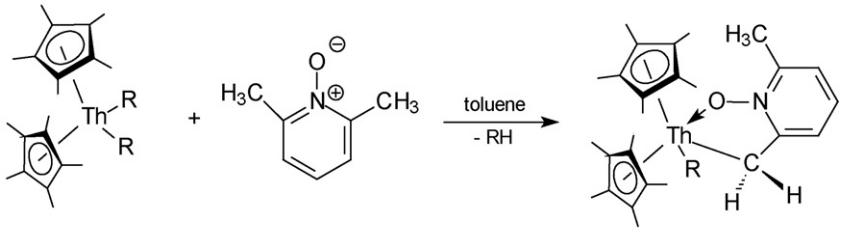

R = Me, CH_2Ph

Scheme 88.

Examination of the reactivity of $[Cp^*_2U][(\mu\text{-}Ph)_2BPh_2]$ as a "blank" for comparison with the four- and eight-electron reductive chemistry of the sterically crowded Cp^*_3U and $[Cp^*_2U](C_6H_6)$ complexes revealed that the tetraphenylborate complex surprisingly functions as a four-electron reductant by combining $[BPh_4]^{1-}$ and U(III) reduction. All three complexes cleave the N=N bond in PhN=NPh to form the bis(organoimido) U(VI) complex $Cp^*_2U(NPh)_2$ (Scheme 85), and they also reduce PhC≡CPh to form $Cp^*_2U(C_4Ph_4)$ (Scheme 86). The latter has been structurally characterized by X-ray diffraction, confirming the presence of a localized metallacyclopentadiene structure (Fig. 72) [141].

An unusual case of C–H activation with uranium(IV) and thorium(IV) bis(alkyl) complexes has been discovered for pyridine N-oxide. As shown in Scheme 87, addition of 1 equiv. of pyridine N-oxide to a toluene solution of the uranium(IV) bis(alkyl) complexes $Cp^*_2UR_2$ (R = Me, CH_2Ph) unexpectedly resulted in activation of an sp^2 hybridized C–H bond, with loss of alkane and formation of novel cyclometalated pyridine N-oxide complexes in greater than 70% yield. The same reactions could be carried out with the analogous thorium(IV) bis(alkyls). The molecular structures of two representative examples have been determined by X-ray diffraction (Fig. 73) [142].

This chemistry is not limited to sp^2 hybridized C–H bonds. As depicted in Scheme 88, reaction of 1 equiv. of 2,6-lutidine N-oxide with the Th(IV) bis(alkyls) at room temperature afforded the cyclometalated complexes in 70–80% yield, whereas the analogous uranium(IV) complexes did not form even at elevated temperatures. Fig. 74 illustrates the molecular structures of both thorium complexes [142].

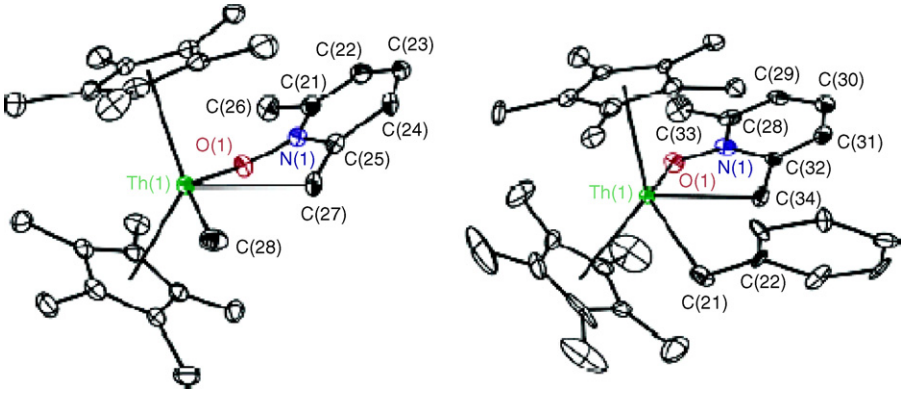

Fig. 74. Molecular structure of $Cp^*_2Th(Me)[\eta^2\text{-}(O,C)\text{-}ONC_5H_2(Me)CH_2]$ (left) and $Cp^*_2Th(CH_2Ph)[\eta^2\text{-}(O,C)\text{-}ONC_5H_2(Me)CH_2]$ [142].

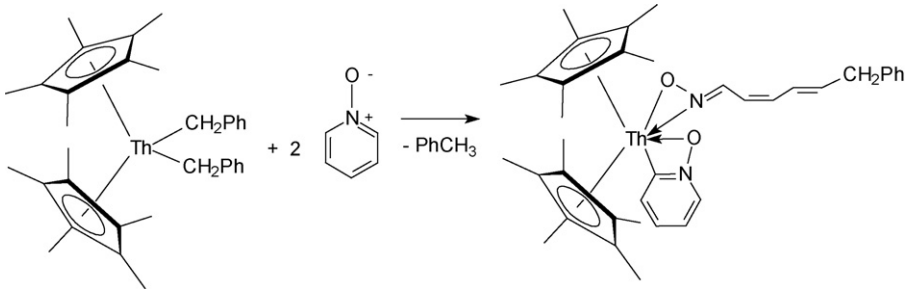

Scheme 89.

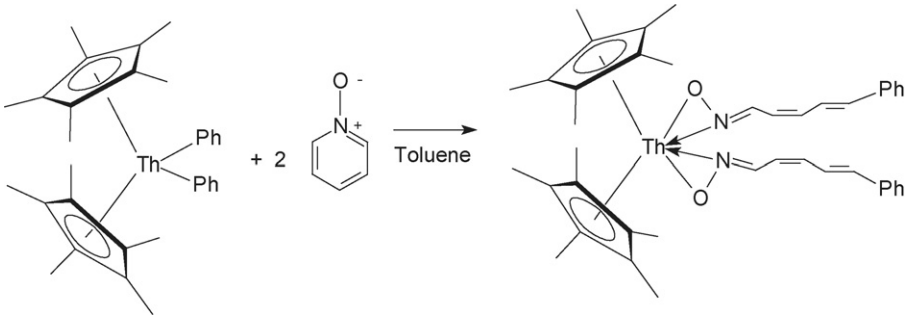

Scheme 90.

These results have demonstrated that U(IV) and Th(IV) bis(alkyl) complexes readily activate both sp^2 and sp^3 hybridized C–H bonds in pyridine N-oxides, providing rare examples of C–H activation chemistry mediated by actinide metal centers [142]. Later it was discovered that the reactions between the thorium bis(hydrocarbyls) $Cp^*_2UR_2$ (R = CH_2Ph, Ph) take yet a different course when 2 equiv. of pyridine N-oxide are employed. As illustrated in Scheme 89, the reaction of $Cp^*_2Th(CH_2Ph)_2$ with 2 equiv. of pyridine N-oxide (pyNO) at ambient temperature unexpectedly resulted in facile C–N bond cleavage and ring-opening of pyNO to give the first thorium oximate complex as an orange-brown solid in 77% isolated yield. The product contains both a cyclometallated η^2-(O,C)-pyNO and an oximate linkage resulting from the ring-opening of a second pyNO molecule [143].

Similar addition of 2 equiv. of pyNO to a toluene solution of $Cp^*_2ThPh_2$ at ambient temperature afforded the novel bis(oximate) complex $Cp^*_2Th[\eta^2$-(O,N)-ON=CH-$(CH=CH)_2Ph]_2$ as a brown solid in 67% isolated yield (Scheme 90). It is remarkable, that in this case *two* pyNO ring systems are dissected by *one* thorium metal center. Fig. 75 depicts the molecular structure of the bis(oximate) product [143].

Treatment of $Cp^*_2UCl_2$ with Na_2dddt in THF afforded the "ate" complex Cp^*_2UCl(dddt)$Na(THF)_2$, and the salt-free compound Cp^*_2U(dddt) could be extracted from the initial product with toluene (dddt = 5,6-dihydro-1,4-dithiin-2,3-dithiolato) [52].

3.3.3.4. Tris(pentamethylcyclopentadienyl) actinide(IV) compounds. An atom- and time-efficient synthetic route to sterically crowded organoactinide complexes of the type Cp^*_3UX (X = Cl, Me) involving the *in situ*-formation of borate salts has been reported. Addition of BPh_3 to Cp^*_2UMeCl followed by KCp^* has been found to provide a greatly improved synthesis of Cp^*_3UCl that presumably proceeds through an intermediate $[Cp^*_2UCl][MeBPh_3]$ borate salt. Sterically highly crowded Cp^*_3UCl has been isolated according to Scheme 91 as a red powder in >90% yield [144].

In the analogous reaction system involving $Cp^*_2UMe_2$, BPh_3, and KCp^* the formation of the borate intermediate,

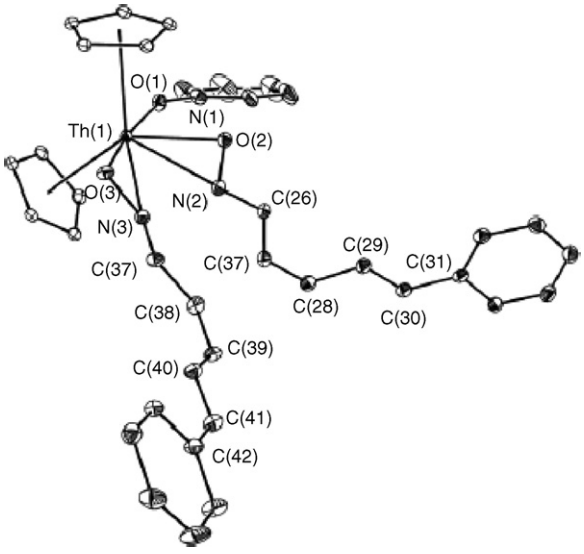

Fig. 75. Molecular structure of $Cp^*_2Th[\eta^2$-(O,N)-ON=CH-$(CH=CH)_2Ph]_2$ [143].

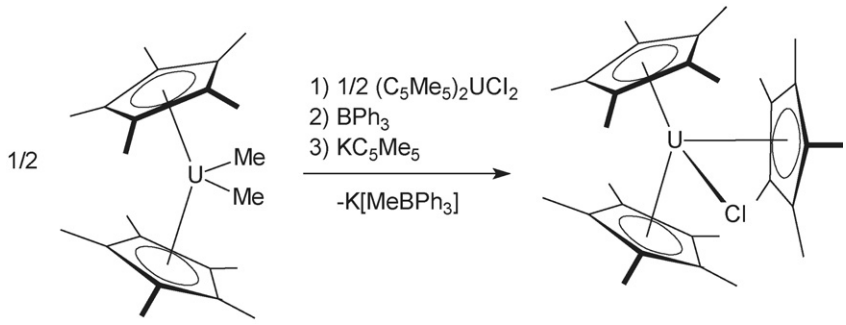

Scheme 91.

$[Cp^*_2UMe][MeBPh_3]$, was confirmed by variable-temperature NMR spectroscopy and by X-ray crystallography of the THF adduct (Fig. 76). The crystal structure of this compound consists of well separated ions [144].

Addition of KCp^* instead of THF to the *in situ* generated $[Cp^*_2UMe][MeBPh_3]$ salt at room temperature in benzene precipitated white solids and left a red solution from which Cp^*_3UMe was isolated in 66% yield (Scheme 92). The identity of Cp^*_3UMe was established by X-ray crystallography (Fig. 77). The U–C(Me) distance in this highly sterically crowded molecule is 2.66(2) Å [144].

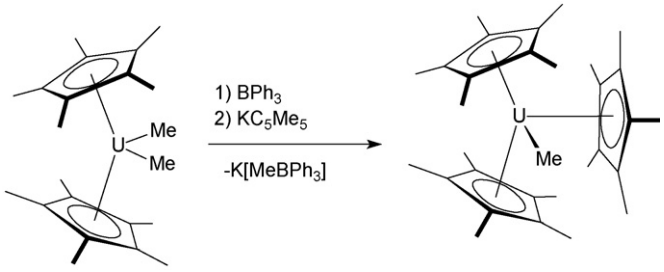

Scheme 92.

3.3.4. Compounds with heteroatom five-membered ring ligands

Reactions of *in situ*-generated potassium salts of the dipyrroles $Me_2C(C_4H_3NH)_2$ and $MePhC(C_4H_3N)_2$ with $ThCl_4(DME)_2$ has been reported to afford the corresponding homoleptic salt-like species $\{[K_2(DME)][Th\{Me_2C(C_4H_3N)_2\}_3]\}_n$ and $[K_2(DME)][Th\{MePhC(C_4H_3N)_2\}_3]$, respectively [145]. The complex $[Li(THF)_4][\{1,3\text{-}[2,6\text{-}Pr^i_2C_6H_3N]_2(CH_2)_3\}_2ThCl]$, containing two chelating amide ligands, was prepared *via* straightforward halogen replacement of $ThCl_4(DME)$ with the dilithium salt of 1,3-

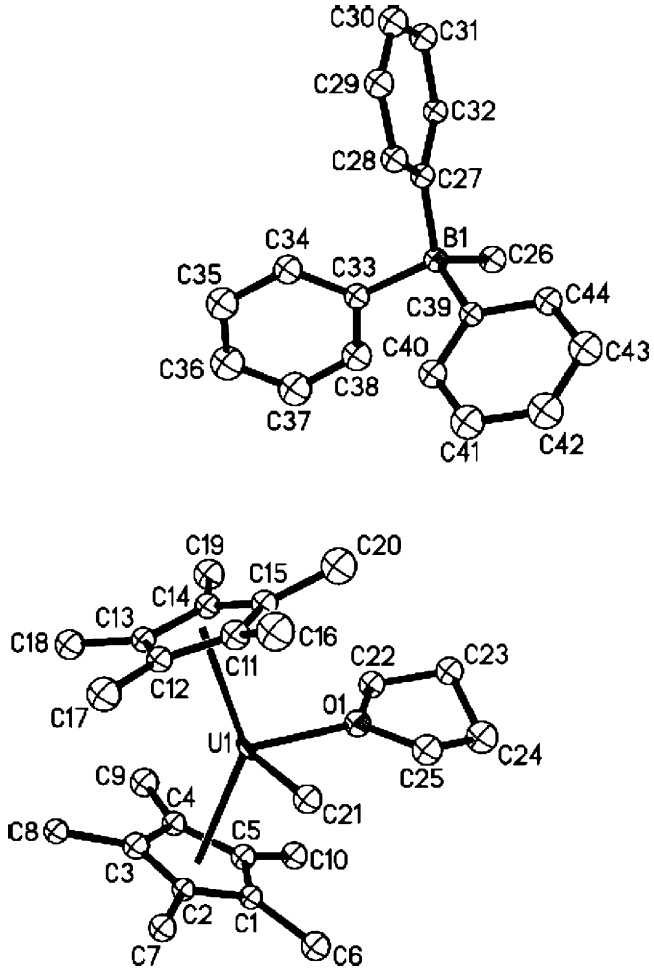

Fig. 76. Molecular structure of $[Cp^*_2UMe(THF)][MeBPh_3]$ [144].

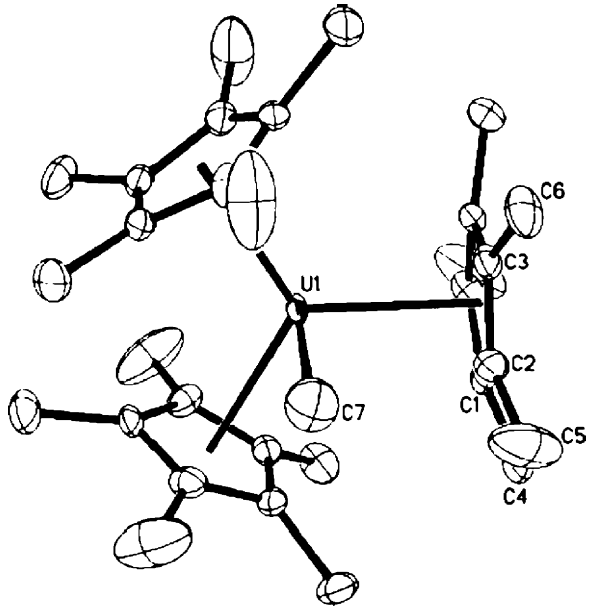

Fig. 77. Molecular structure of Cp^*_3UMe [144].

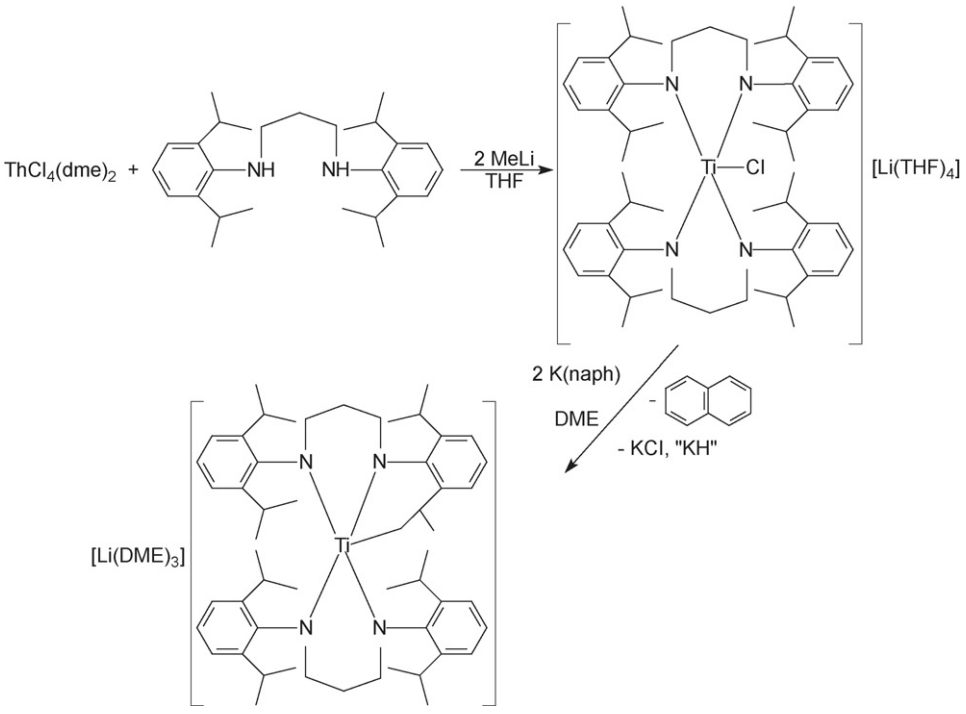

Scheme 93.

[2,6-$Pr_2^iC_6H_3NH]_2(CH_2)_3$ (Scheme 93). Attempts to reduce this species were carried out with K(naphthalenide), affording an intermediate dark colored solution that slowly discolored and yielded colorless crystals of the tetravalent metallacyclic complex $[Li(DME)_3][Th\{1,3\text{-}[2,6\text{-}Pr_2^iC_6H_3N]_2(CH_2)_3\}\{1,3\text{-}[2\text{-}Pr^i\text{-}6\text{-}(CH_2CHCH_2)C_6H_3N]_2(CH_2)_3\}]$. In this species, one hydrogen group was eliminated to form a metallacyclic structure [146].

3.4. Actinide arene complexes

Gas phase actinide benzene complexes of the type $U(C_6H_6)_n^+$ ($n = 1$–3) and $UO_m(C_6H_6)^+$ ($m = 1$, 2) have been produced by laser vaporization and studied with UV (355 nm) laser photodissociation. The $n = 1$ complex dissociates to form U^+, $U(C_2H_2)^+$ and $U(C_4H_2)^+$ *via* ligand elimination and ligand decomposition channels. The $n = 2$ and 3 complexes fragment down to the $n = 1$ complexes, losing intact neutral benzene molecules. The $UO_m(C_6H_6)^+$ ($m = 1$, 2) complexes eliminate intact neutral benzene ligands with no further fragmentation. These photodissociation trends indicate that bare uranium cations are more reactive than uranium oxide ions [147].

References

[1] C. Koukounas, S. Kardahakis, A. Mavridis, J. Chem. Phys. 123 (2005) 074372.
[2] L. Jiang, Q. Xu, J. Am. Chem. Soc. 127 (2005) 42.
[3] I. Vidal, S. Melchor, J.A. Dobado, J. Chem. Phys. A 109 (2005) 7500.
[4] H.M. Dietrich, G. Raudaschl-Sieber, R. Anwander, Angew. Chem. 117 (2005) 5437;
H.M. Dietrich, G. Raudaschl-Sieber, R. Anwander, Angew. Chem. Int. Ed. 44 (2005) 5303.
[5] S. Harder, Organometallics 24 (2005) 373.
[6] S. Arndt, K. Beckerle, P.M. Zeimentz, T.S. Spaniol, J. Okuda, Angew. Chem. 117 (2005) 7640;
S. Arndt, K. Beckerle, P.M. Zeimentz, T.S. Spaniol, J. Okuda, Angew. Chem. Int. Ed. 44 (2005) 7473.
[7] C.S. Tredget, S.C. Lawrence, B.D. Ward, R.G. Howe, A.R. Cowley, P. Mountford, Organometallics 24 (2005) 3136.
[8] B.R. Elvidge, S. Arndt, P.M. Zeimentz, T.P. Spaniol, J. Okuda, Inorg. Chem. 44 (2005) 6777.
[9] P.B. Hitchcock, M.F. Lappert, A.V. Protchenko, Chem. Commun. (2005) 951.
[10] P.G. Hayes, W.E. Piers, M. Parvez, Organometallics 24 (2005) 1173.
[11] C. Cui, A. Shafir, J.A.R. Schmidt, A.G. Oliver, J. Arnold, Dalton Trans. (2005) 1387.
[12] Y. Yao, M. Ma, X. Xu, Y. Zhang, Q. Shen, W.-T. Wong, Organometallics 24 (2005) 4014.
[13] K.C. Hultzsch, D.V. Gribkov, F. Hampel, J. Organomet. Chem. 690 (2005) 4441.
[14] C.L. Boyd, T. Toupance, B.R. Tyrrell, B.D. Ward, C.R. Wilson, A.R. Cowley, P. Mountford, Organometallics 24 (2005) 309.
[15] B.D. Ward, S. Bellemin-Laponnaz, L.H. Gade, Angew. Chem. 117 (2005) 1696;
B.D. Ward, S. Bellemin-Laponnaz, L.H. Gade, Angew. Chem. Int. Ed. 44 (2005) 1668.
[16] S.T. Liddle, P.L. Arnold, Organometallics 24 (2005) 2597.
[17] P.L. Arnold, S.T. Liddle, Chem. Commun. (2005) 5638.
[18] P.B. Hitchcock, Q. Huang, M.F. Lappert, M. Zhou, Dalton Trans. (2005) 2988.
[19] M.T. Gamer, M. Rastätter, P.W. Roesky, A. Steffens, M. Glanz, Chem. Eur. J. 11 (2005) 3165.
[20] T.K. Panda, A. Zulys, M.T. Gamer, P.W. Roesky, J. Organomet. Chem. 690 (2005) 5078.
[21] J. Pilme, B. Silvi, M.E. Alikhani, J. Phys. Chem. A 109 (2005) 10028.
[22] P. Redondo, C. Barrientos, A. Largo, J. Phys. Chem. A (2005) 8594.
[23] C.K. Simpson, R.E. White, C.N. Carlson, D.A. Wrobleski, C.J. Kuehl, T.A. Croce, I.M. Steele, B.L. Scott, V.G. Young Jr., T.P. Hanusa, A.P. Sattelberger, K.D. John, Organometallics 24 (2005) 3685.
[24] L.F. Sánchez-Barba, D.L. Hughes, S.M. Humphrey, M. Bochmann, Organometallics 24 (2005) 3792.

[25] V. Lorenz, H. Görls, S.K.-H. Thiele, J. Scholz, Organometallics 24 (2005) 797.
[26] F. Nief, B.T. de Borms, L. Ricard, D. Carmichael, Eur. J. Inorg. Chem. (2005) 637.
[27] T. Mehdoui, J.-C. Berthet, P. Thuéry, M. Ephritikhine, Dalton Trans. (2005) 1263.
[28] Y. Yao, X. Xu, B. Liu, Y. Zhang, Q. Shen, W.-T. Wong, Inorg. Chem. 44 (2005) 5133.
[29] X. Li, J. Baldamus, Z. Hou, Angew. Chem. 117 (2005) 984;
X. Li, J. Baldamus, Z. Hou, Angew. Chem. Int. Ed. 44 (2005) 962.
[30] D. Cui, M. Nishiura, Z. Hou, Macromolecules 38 (2005) 4089.
[31] D. Cui, M. Nishiura, Z. Hou, Angew. Chem. 117 (2005) 981;
D. Cui, M. Nishiura, Z. Hou, Angew. Chem. Int. Ed. 44 (2005) 959.
[32] W.-X. Zhang, M. Nishiura, Z. Hou, J. Am. Chem. Soc. 127 (2005) 16788.
[33] J. Wang, Y. Yao, J. Cheng, X. Pang, Y. Zhang, Q. Shen, J. Mol. Struct. 743 (2005) 229.
[34] Y. Luo, J. Baldamus, O. Tardif, Z. Hou, Organometallics 24 (2005) 4362.
[35] D.L. Clark, J.C. Gordon, P.J. Hay, R. Poli, Organometallics 24 (2005) 5747.
[36] A.C. Boccia, F. Grisi, R. Centore, A. Tuzi, Acta Cryst. E61 (2005) m1449.
[37] W.J. Evans, S.A. Kozimor, J.C. Brady, B.L. Davis, G.W. Nyce, C.A. Seibel, J.W. Ziller, R.J. Doedens, Organometallics 24 (2005) 2269.
[38] L. Maron, E.L. Werkema, L. Perrin, O. Eisenstein, R.A. Andersen, J. Am. Chem. Soc. 127 (2005) 279.
[39] E.L. Werkema, E. Messines, L. Perrin, L. Maron, O. Eisenstein, R.A. Andersen, J. Am. Chem. Soc. 127 (2005) 7781.
[40] J. Zhang, X. Zhou, R. Cai, L. Weng, Inorg. Chem. 44 (2005) 716.
[41] J. Zhang, L. Ma, R. Cai, L. Weng, X. Zhou, Organometallics 24 (2005) 738.
[42] L. Ma, J. Zhang, R. Cai, Z. Chen, L. Weng, X. Zhou, J. Organomet. Chem. 690 (2005) 4926.
[43] H. Li, Y. Yao, C. Yao, H. Sheng, Q. Shen, J. Polymer Sci. 43 (2005) 1312.
[44] Y. Li, C. Pi, J. Zhang, X. Zhou, Z. Chen, L. Weng, Organometallics 24 (1982).
[45] X. Zhou, M. Zhu, L. Zhang, Z. Zhu, C. Pi, Z. Pang, L. Weng, R. Cai, Chem. Commun. (2005) 2342.
[46] W.J. Evans, D.S. Lee, M.A. Johnston, J.W. Ziller, Organometallics 24 (2005) 6393.
[47] J. Miyazaki, Y. Yamada, J. Mol. Struct. 734 (2005) 115.
[48] M.C. Cassani, M.J. Davies, P.B. Hitchcock, M.F. Lappert, Inorg. Chim. Acta 358 (2005) 1595.
[49] J.M. Veauthier, E.J. Shelter, C.J. Kuehl, A.E. Clark, B.L. Scott, D.E. Morris, R.L. Martin, J.D. Thompson, J.L. Kiplinger, K.D. John, Inorg. Chem. 44 (2005) 5911.
[50] K.A. Tupper, T. Don Tilley, J. Organomet. Chem. 690 (2005) 1689.
[51] W.J. Evans, K.A. Miller, D.S. Lee, J.W. Ziller, Inorg. Chem. 44 (2005) 4326.
[52] M. Roger, L. Belkhiri, P. Thuéry, T. Arliguie, M. Fourmigué, A. Boucekkine, M. Ephritikhine, Organometallics 24 (2005) 4940.
[53] T. Mehdoui, J.-C. Berthet, P. Thuéry, L. Salmon, E. Rivière, M. Ephritikhine, Chem. Eur. J. 11 (2005) 6994.
[54] A.M. Kawaoka, T.J. Marks, J. Am. Chem. Soc. 127 (2005) 6311.
[55] W.J. Evans, J.M. Perotti, J.W. Ziller, J. Am. Chem. Soc. 127 (2005) 3894.
[56] W.J. Evans, J.M. Perotti, J.W. Ziller, J. Am. Chem. Soc. 127 (2005) 1068.
[57] T. Mehdoui, J.-C. Berthet, P. Thuéry, M. Ephritikhine, Chem. Commun. (2005) 2860.
[58] M.W. Pouwkamp, P.H.M. Budzelaar, J. Gercama, I.D.H. Morales, J. de Wolf, A. Meetsma, S.I. Troyanov, J.H. Teuben, B. Hessen, J. Am. Chem. Soc. 127 (2005) 14310.
[59] A.D. Sadow, T.D. Tilley, J. Am. Chem. Soc. 127 (2005) 643.
[60] W.J. Evans, J.M. Perotti, J.W. Ziller, Inorg. Chem. 44 (2005) 5820.
[61] W.J. Evans, S.A. Kozimor, J.W. Ziller, Inorg. Chem. 44 (2005) 7960.
[62] W.J. Evans, J.M. Perotti, S.A. Kozimor, T.M. Champagne, B.J. Davis, G.W. Nyce, C.H. Fujimoto, R.D. Clark, M.A. Johnston, J.W. Ziller, Organometallics 24 (2005) 3916.
[63] X.-M. Xie, J.-L. Huang, Chin. J. Chem. 23 (2005) 85.
[64] M. Schultz, C.D. Sofield, M.D. Walter, R.A. Andersen, New. J. Chem. 29 (2005) 919.
[65] F.-G. Fontaine, T.D. Tilley, Organometallics 24 (2005) 4340.
[66] E. Kirillov, J.-Y. Saillard, J.-F. Carpentier, Coord. Chem. Rev. 249 (2005) 1221.
[67] Y. Wu, S. Wang, C. Qian, W. Sheng, M. Xie, G. Yang, Q. Feng, L. Zhang, X. Tang, J. Organomet. Chem. 690 (2005) 4139.
[68] G.R. Giesbrecht, J.C. Gordon, D.L. Clark, B.L. Scott, Appl. Organomet. Chem. 19 (2005) 98.
[69] J. Wang, M.J. Gardiner, Chem. Commun. (2005) 1589.
[70] K. Müller-Buschbaum, C.C. Quitmann, Z. Kristallogr. 220 (2005) 158.
[71] X. Zhu, W.-K. Wong, W.-K. Lo, W.-Y. Wong, Chem. Commun. (2005) 1022.
[72] J. Wang, M.G. Gardiner, B.W. Skelton, A.H. White, Organometallics 24 (2005) 815.
[73] M.-S. Cheung, H.-S. Chan, Z. Xie, Organometallics 24 (2005) 4468.
[74] M.-S. Cheung, H.-S. Chan, S. Bi, Z. Lin, Z. Xie, Organometallics 24 (2005) 4333.
[75] M.-S. Cheung, H.-S. Chan, Z. Xie, Organometallics 24 (2005) 4207.
[76] (a) F. Rabilloud, J. Chem. Phys. 122 (2005) 134303;
(b) M. Aubert-Frécon, F. Rabilloud, A.R. Allouche, D. Rayane, R. Antoine, M. Broyer, P. Dugourd, Chem. Phys. Lett. 405 (2005) 422.
[77] H.J. Xiang, J. Yang, J.G. Hou, Q. Zhu, Los Alamos National Laboratory, Preprint Archive, Condens. Matter. 2005, 1–9 (arXivcondmat/0511417).
[78] R. Zhang, A. Dinca, K.J. Fisher, D.R. Smith, G.D. Willett, J. Phys. Chem. A 109 (2005) 157.
[79] J. Yuasa, T. Suenobu, S. Fukuzumi, J. Phys. Chem. A 109 (2005) 9356.
[80] J. Collin, J.-C. Daran, O. Jacquet, E. Schulz, A. Trifonov, Chem. Eur. J. 11 (2005) 3455.
[81] A.V. Vlasov, T.I. Shabatina, A.Y. Ivanov, G.G. Sheina, A.V. Nemukhin, G.B. Sergeev, Mendeleev Commun. 15 (2005) 10.
[82] C.C. Quitmann, K. Müller-Buschbaum, Z. Anorg. Allg. Chem. 631 (2005) 350.
[83] T.J. Boyle, S.D. Bunge, P.G. Clem, J. Richardson, J.T. Dawley, L.A.M. Ottley, M.A. Rodriguez, B.A. Tuttle, G.R. Avilucea, R.G. Tissot, Inorg. Chem. 44 (2005) 1588.
[84] G.B. Deacon, C.M. Forsyth, P.C. Junk, Chem. Eur. J. 11 (2005) 817.
[85] S.-O. Hauber, M. Niemeyer, Inorg. Chem. 44 (2005) 8644.
[86] R. Takegami, N. Hosoya, J.-I. Suzumura, K. Yada, A. Nakajima, S. Yabushita, Chem. Phys. Lett. 403 (2005) 169.
[87] R. Takegami, N. Hosoya, J.-I. Suzumura, K. Yada, A. Nakajima, S. Yabushita, J. Phys. Chem. A 109 (2005) 2476.
[88] K. Miyajima, M.B. Knickelbein, A. Nakajima, Polyhedron 24 (2005) 2341.
[89] N. Hosoya, R. Takegami, J.-I. Suzumura, K. Yada, K. Koyasu, K. Miyajima, M. Mitsui, M.B. Knickelbein, S. Yabushita, A. Nakajima, J. Phys. Chem. A 109 (2005) 9.
[90] M.D. Walter, G. Wolmershäuser, H. Sitzmann, J. Am. Chem. Soc. 127 (2005) 17494.
[91] T.K. Panda, A. Zulys, M.T. Gamer, P.W. Roesky, Organometallics 24 (2005) 2197.
[92] T.K. Panda, P. Benndorf, P.W. Roesky, Z. Anorg. Allg. Chem. 631 (2005) 81.
[93] H.-D. Amberger, H. Reddmann, F.T. Edelmann, J. Organomet. Chem. 690 (2005) 2238.
[94] E. Nishibori, S. Narioka, M. Sakata, M. Takata, T. Inoue, H. Shinohara, Toyota Kenkyu Hokoku 58 (2005) 167.
[95] S. Hino, N. Wanita, K. Iwasaki, D. Yoshimura, T. Akachi, T. Inoue, Y. Ito, T. Sugai, H. Shinohara, Phys. Rev. B 72 (2005) 195424.
[96] Y. Liduka, T. Wakahara, T. Nakahodo, T. Tsuchiya, A. Sakuraba, Y. Maeda, T. Akasaka, K. Yoza, E. Horn, T. Kato, M.T.H. Liu, N. Mizorogi, K. Kobayashi, S. Nagase, J. Am. Chem. Soc. 127 (2005) 12500.
[97] Y. Zhao, Y.-H. Kim, A.C. Dillon, M.J. Heben, S.B. Zhang, Phys. Lett. Rev. 94 (2005) 155504.
[98] M.T. Gamer, P.W. Roesky, Inorg. Chem. 44 (2005) 5963.
[99] M.G. Schrems, H.M. Dietrich, K.W. Törnroos, R. Anwander, Chem. Commun. (2005) 5922.

[100] L.F. Sánchez-Barba, D.L. Hughes, S.M. Humphrey, M. Bochmann, Organometallics 24 (2005) 5329.
[101] H.M. Dietrich, C. Zapilko, E. Herdtweck, R. Anwander, Organometallics 24 (2005) 5767.
[102] W.J. Evans, T.M. Champagne, D.G. Giarikos, J.W. Ziller, Organometallics 24 (2005) 570.
[103] (a) W.J. Evans, T.M. Champagne, J.W. Ziller, Organometallics 24 (2005) 4882;
(b) W.J. Evans, T.M. Champagne, J.W. Ziller, Chem. Commun. (2005) 5925.
[104] J. Chai, V. Jancik, S. Singh, H. Zhu, C. He, H.W. Roesky, M. Noltemeyer, N.S. Hosmane, J. Am. Chem. Soc. 127 (2005) 7521.
[105] M. Martinez, M. del Carmen Michelini, I. Rivalta, N. Russo, E. Sicilia, Inorg. Chem. 44 (2005) 9807.
[106] C.S. Tredget, F. Bonnet, A.R. Cowley, P. Mountford, Chem. Commun. (2005) 3301.
[107] X. Li, Z. Hou, Macromolecules 38 (2005) 6767.
[108] S. Tobisch, Chem. Eur. J. 11 (2005) 3113.
[109] F. Bonnet, M. Visseaux, A. Pereira, D. Barbier-Baudry, Macromolecules 38 (2005) 3162.
[110] J. Thuilliez, V. Monteil, R. Spitz, C. Boisson, Angew. Chem. 117 (2005) 2649;
J. Thuilliez, V. Monteil, R. Spitz, C. Boisson, Angew. Chem. Int. Ed. 44 (2005) 2593.
[111] L. Zhang, Y. Luo, Z. Hou, J. Am. Chem. Soc. 127 (2005) 14562.
[112] Y. Nakayama, H. Yasuda, K. Yamamoto, C. Tsutsumi, R. Jerome, P. Lecomte, React. Funct. Polym. 63 (2005) 95.
[113] X.-M. Xie, J.-L. Huang, Chin. J. Chem. 23 (2005) 85.
[114] G.A. Molander, J.A.C. Romero, Tetrahedron 61 (2005) 2631.
[115] S. Tobisch, J. Am. Chem. Soc. 127 (2005) 11979.
[116] A. Motta, I.L. Fragalà, T.J. Marks, Organometallics 24 (2005) 4995.
[117] S. Tobisch, Chem. Eur. J. 11 (2005) 6372.
[118] S.A. Schuetz, E.A. Bowman, C.M. Silvernail, V.W. Day, J.A. Belot, J. Organomet. Chem. 690 (2005) 1011.
[119] Y. Chen, Z. Zhu, J. Zhang, J. Shen, X. Zhou, J. Organomet. Chem. 690 (2005) 3783.
[120] L. Mei, J. Mol. Catal. A: Chem. 227 (2005) 183.
[121] L. Mei, M.H. Zhu, Synth. Commun. 35 (2005) 2615.
[122] Y.-J. Liu, Y.-M. Zhang, Huaxue Xuebao 63 (2005) 341.
[123] J. Niinistö, N. Petrova, M. Putkonen, L. Niinistö, K. Arstila, T. Sajavaara, J. Cryst. Growth 285 (2005) 191.
[124] J. Päiväsaari, J. Niinistö, K. Arstila, K. Kukli, M. Putkonen, L. Niinistö, Chem. Vap. Depos. 11 (2005) 415.
[125] J.L. Sonnenberg, P.J. Hay, R.L. Martin, B.E. Bursten, Inorg. Chem. 44 (2005) 2255.
[126] I. Castro-Rodriguez, K. Meyer, J. Am. Chem. Soc. 127 (2005) 11242.
[127] J.T. Lyon, L. Andrews, Inorg. Chem. 44 (2005) 8610.
[128] M. Silva, M.A. Antunes, M. Dias, Â. Domingos, I. Cordeiro dos Santos, J. Marçalo, N. Marques, Dalton Trans. (2005) 3353.
[129] K.C. Jantunen, F. Haftbaradaran, M.J. Katz, R.J. Batchelor, G. Schatte, D.B. Leznoff, Dalton Trans. (2005) 3083.
[130] P.L. Arnold, A.L. Blake, C. Wilson, Chem. Eur. J. 11 (2005) 6095.
[131] M.A. Antunes, M. Dias, Â. Domingos, I. Cordeiro dos Santos, N. Marques, J. Takats, Polyhedron 24 (2005) 3038.
[132] W.J. Evans, S.A. Kozimor, W.R. Hillman, J.W. Ziller, Organometallics 24 (2005) 4676.
[133] W.J. Evans, S.A. Kozimor, J.W. Ziller, A.A. Fagin, M.N. Bochkarev, Inorg. Chem. 44 (2005) 3993.
[134] G. Zi, L.L. Blosch, L. Jia, R.A. Andersen, Organometallics 24 (2005) 4602.
[135] G. Zi, L. Jia, E.L. Werkema, M.D. Walter, J.P. Gottfriedsen, R.A. Andersen, Organometallics 24 (2005) 4251.
[136] J.K. Gibson, R.G. Haire, Organometallics 24 (2005) 119.
[137] W.J. Evans, S.A. Kozimor, J.W. Ziller, Science 309 (1835).
[138] A.E. Enriquez, B.L. Scott, M.P. Neu, Inorg. Chem. 44 (2005) 7403.
[139] R.E. Da Re, K.C. Jantunen, J.T. Golden, J.L. Kiplinger, D.E. Morris, J. Am. Chem. Soc. 127 (2005) 682.
[140] A.E. Clark, R.L. Martin, P.J. Hay, J.C. Green, K.C. Jantunen, J.L. Kiplinger, J. Phys. Chem. A (2005) 5481.
[141] W.J. Evans, S.A. Kozimor, J.W. Ziller, Chem. Commun. (2005) 4681.
[142] J.A. Pool, B.L. Scott, J.L. Kiplinger, J. Am. Chem. Soc. 127 (2005) 1338.
[143] J.A. Pool, B.L. Scott, J.L. Kiplinger, Chem. Commun. (2005) 2591.
[144] W.J. Evans, S.A. Kozimor, J.W. Ziller, Organometallics 24 (2005) 3407.
[145] A. Athimoolam, S. Gambarotta, I. Korobkov, Can. J. Chem. 83 (2005) 832.
[146] A. Athimoolam, S. Gambarotta, I. Korobkov, Organometallics 24 (1996).
[147] E.D. Pillai, K.S. Molek, M.A. Duncan, Chem. Phys. Lett. 405 (2005) 247.